Scuffing Under Starved Lubrication Conditions

H. K. Yoon and C. Cusano

ACRC TR-147 January 1999

For additional information:

Air Conditioning and Refrigeration Center
University of Illinois
Mechanical & Industrial Engineering Dept.
1206 West Green Street
Urbana, IL 61801

(217) 333-3115

Prepared as part of ACRC Project 82
Compressor—Lubrication, Friction and Wear
C. Cusano, Principal Investigator

The Air Conditioning and Refrigeration Center was founded in 1988 with a grant from the estate of Richard W. Kritzer, the founder of Peerless of America Inc. A State of Illinois Technology Challenge Grant helped build the laboratory facilities. The ACRC receives continuing support from the Richard W. Kritzer Endowment and the National Science Foundation. The following organizations have also become sponsors of the Center.

Amana Refrigeration, Inc.
Brazeway, Inc.
Carrier Corporation
Caterpillar, Inc.
Chrysler Corporation
Copeland Corporation
Delphi Harrison Thermal Systems
Eaton Corporation
Frigidaire Company
General Electric Company
Hill PHOENIX
Hussmann Corporation
Hydro Aluminum Adrian, Inc.
Indiana Tube Corporation
Lennox International, Inc.
Modine Manufacturing Co.
Peerless of America, Inc.
The Trane Company
Thermo King Corporation
Visteon Automotive Systems
Whirlpool Corporation
York International, Inc.

For additional information:

Air Conditioning & Refrigeration Center
Mechanical & Industrial Engineering Dept.
University of Illinois
1206 West Green Street
Urbana IL 61801

217 333 3115

ABSTRACT

A few among many otherwise highly successful lubricated sliding components fail catastrophically and without warning. This sudden mode of failure is often called scuffing. The phenomenon of scuffing has been known for many years and numerous attempts have been made to understand its processes and mechanisms. There is still, however, a general lack of agreement concerning the processes leading up to scuffing. One of the main reasons for this is that the detailed mechanisms of scuffing are not well understood. The main purpose of this study is to obtain a better understanding of the scuffing processes and material failure mechanisms under starved lubrication conditions.

The research focuses on two major goals. The first is to examine the scuffing behavior of 52100 steel shoes/390-T6 Al plate contacts under starved lubrication conditions. The evaluation is based on a shoe-on-disc geometry which approximately simulates the swashplate/shoe contacts in an automotive swashplate compressor. All tests are conducted in a high pressure tribometer (HPT) under R134a environment with a base polyalkylene glycol (PAG) lubricant. The effects of degree of lubricant starvation, sliding velocity, geometry of contact, surface topography, a tin coating, and socket geometry supporting the shoe are evaluated. The second goal is to study the processes and mechanisms of the scuffing phenomenon also under starved lubrication conditions. A pin-on-disc geometry is used to examine the effect of materials, lubricant/refrigerant mixtures and loading history on scuffing. The transition behavior of a 390-T6 Al pin sliding against a 1018 carburized steel disc is also examined. To better understand the processes and failure mechanisms of scuffing, the scuffed surfaces and subsurfaces are examined. Based on the experimental observations, a hypothesis and its corresponding criterion for scuffing under starved lubrication conditions are proposed. According to this hypothesis, scuffing is caused by the formation of macroscopic adhesions leading to bulk material failure due to plastic shearing.

TABLE OF CONTENTS

LIST OF TABLES

LIST OF FIGURES

CHAPTER 1

INTRODUCTION

1.1 Background

A few among many otherwise highly successful lubricated sliding components fail catastrophically and without warning. This sudden mode of failure is often called scuffing. The phenomenon of scuffing has been known for many years and numerous attempts have been made to define it. In the literature, scuffing is described as a collapse of lubricant films [1-6], desorption of physically or chemically adsorbed films [7,8], breakdown of the oxide layers [9], local thermal expansion of the asperities [10,11], plastic flow of the asperities [12-14], accumulation of wear debris at the sliding contact interface [15,16], and subsurface material failure [17]. The variation between these definitions reflects a general lack of agreement concerning the processes leading up to and during scuffing. However, there seems to be an agreement on only one characteristic feature of the scuffing process. This is the formation of macroscopically large areas of exposed bare metal unprotected by surface films. The contact of these areas eventually results in the formation of cold welds on the sliding surfaces. This aspect of scuffing has led to the development of the most widely used definition of scuffing, which is given by the Organization of Economic Cooperation and Development (OECD). Based on the OECD, scuffing is defined as *"localized damage caused by the occurrence of solid-phase welding between sliding surfaces without local surface melting"* [18].

Scuffing occurs in many mechanical components where sliding exists. Gears, cams and followers, piston rings and cylinder pairs, splines, sleeve bearings and parts of swash and wobble plate compressors are representative examples. Scuffing can be determined by various manifestations. In practice, when scuffing occurs, there is a sudden rise in friction force accompanied by increased noise, vibration and operating temperature. A sharp increase in friction is almost invariably observed when scuffing occurs. This is the reason why the coefficient of friction is the most widely used indicator of scuffing in laboratory tests. The

scuffed surfaces appear as if they had been welded at discrete points and this feature forms the basis of the definition of scuffing as already noted. Severe wear and plastic deformation are often observed on the damaged surface. In the worst case, this leads to seizure which is the complete stopping of motion. A typical scuffed surface is shown in Fig. 1.1 for a swashplate/shoe contact in a swashplate compressor.

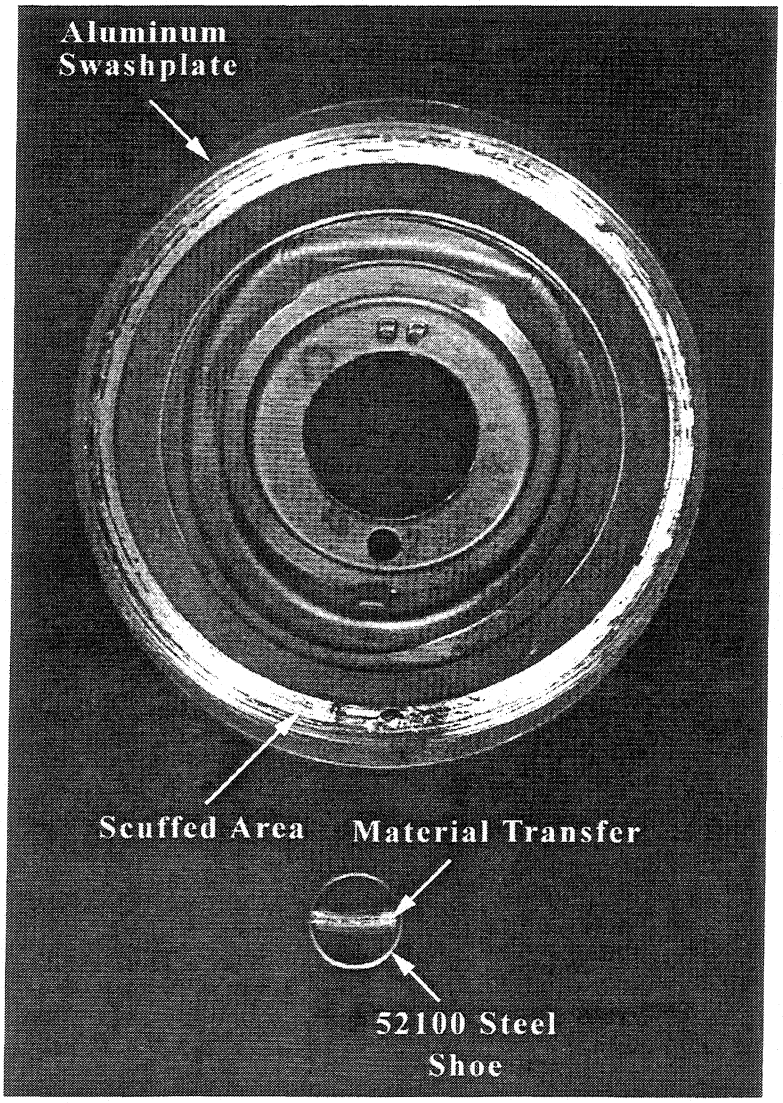

Fig. 1.1 - Typical scuffing failure of a swashplate/shoe contact

Usually, scuffing damage is so severe that the part must be replaced. This is the reason why a large number of studies have been devoted to this phenomenon. Most of these studies, however, are phenomenological in nature. Due to the catastrophic nature of scuffing failures, a better understanding of the scuffing mechanism as well as predictive models are needed to improve the reliability of mechanical components.

Scuffing is a very broad and complex phenomenon because it is affected by many factors. Among the more important of these factors are contact stress, sliding velocity and environmental temperature. The scuffing process is also strongly affected by additional factors such as materials, geometry of contact, morphology of contacting surfaces, mechanical, thermal and chemical properties of the bodies in contact, availability plus properties of the lubricant, and the chemical composition of the environment. These various factors often make the study of scuffing very complex. Mainly due to this complexity, a large number of hypotheses have been proposed in the literature. Some of the more important of these hypotheses will be described in the following section.

1.2 Literature Review

1.2.1 Scuffing Hypotheses

Serious studies on scuffing began more than 60 years ago. Researchers in several different disciplines have proposed numerous scuffing hypotheses. However, none of the existing hypotheses and criteria for scuffing can explain adequately all the experimental results and observations. In this section, some of the important scuffing hypotheses are briefly described. A more detail description of each hypothesis will be given in Chapter 6, where they are evaluated based on the experimental data obtained.

The earliest and the most widely known theory of scuffing was proposed by Blok in 1937 [19]. He proposed that scuffing would occur if the surface temperature in the contact area exceeded a certain critical value. This temperature consists of two components. The first component is the bulk temperature of the material and the second is the flash

temperature (the instantaneous local increase of temperature at the two rubbing surfaces as they pass through the contact zone). The critical temperature hypothesis was based on experimental studies of gear lubrication. These studies showed that gears, lubricated by straight mineral oils, scuffed when the temperature of the surface reaches approximately 150 °C. Initially, Blok did not suggest an explicit reason for what this temperature might represent, but this finding coincided with a major development in the field of tribology, which revealed the important role of adsorbed molecular layers of the lubricants in reducing friction and wear. This has led to the development of a subsequent hypothesis proposed by Askwith, Cameron and Crouch [20]. This hypothesis, which is based on the Langmuir's adsorption theory, relates the critical temperature of scuffing to desorption of the surface active agent in the lubricating oil. The hypothesis suggests that scuffing occurs when the layer of polar molecules adsorbed on the surfaces becomes critically depleted or disoriented. Extension of the above hypothesis has been proposed by Lee and Cheng [21] to account for the effect of lubricant pressure on the adsorption and desorption of surface active agents. They proposed a temperature-pressure theory for scuffing. This theory predicts the breakdown point of the adsorbed surface film as a function of the hydrodynamically generated pressure and the surface temperature.

An alternative hypothesis relating scuffing to some critical thermal condition is the critical frictional power intensity hypothesis [22]. The criterion used in this hypothesis is the ratio of the generated frictional power to the nominal area of contact. This hypothesis is based on the experimental observation that scuffing often occurs along the curves described by $PV = constant$ relationship, where P and V are the contact pressure and the sliding velocity, respectively. This relationship also approximately corresponds to a constant surface temperature condition. The competitive oxide formation/destruction hypothesis [9] and the thermal instability hypothesis [10,11] are recently developed thermal criteria. The former hypothesis states that a critical temperature condition will be reached when the rates of oxide formation and destruction become equal. If the destruction rate is higher than the formation

rate, large areas of bare metal will be exposed and scuffing will occur. The thermal instability hypothesis also relates scuffing to a critical temperature condition reached at the surface. The suggested mechanism responsible for scuffing is asperity expansion. When an asperity encounters the counterface it heats up and expands, which leads to a more severe loading, resulting in further heating and expansion. If this process becomes unstable, which is determined by an excessive increase in frictional heating at the sliding contact, scuffing will occur.

In 1949, the concept of elastohydrodynamic lubrication (EHL) was developed by Grubin [23]. He managed to incorporate both the elastic deformation of the solids and the viscosity-pressure characteristics of the lubricant in analyzing the inlet region of lubricated non-conformal contacts. Since then, EHL has been an area of intensive research and has also been used as a tool to study scuffing. In a hypothesis proposed by Dyson [24], scuffing was explained as a collapse of the hydrodynamic and elastohydrodynamic films. Dyson's model states that scuffing occurs when insufficient fluid pressure is generated in the inlet of the contact to develop a macro-EHL film. This hypothesis was further developed by Cheng et al. [25,26] and Houpert et al. [4] to account for the effects of micro-EHL on an asperity level.

The major problem with the hypotheses described above is that the effects of the mechanical properties of the contacting surfaces are not taken into account. These properties play a major role in the scuffing process. It is well known that a large amount of surface and subsurface plastic flow is present at scuffing. Therefore, hypotheses relating scuffing to plastic flow or strain [12-14, 27] have also received much attention. An early attempt to relate plastic flow to scuffing is the plasticity index criterion, originally proposed by Greenwood and Williamson [12]. It was postulated that scuffing will occur when the plasticity index given by:

$$\psi = (E'/H)\sqrt{\sigma/\beta} \tag{1.1}$$

reaches some critical value. In this equation $E' = \left[\left(1-\upsilon_1^2\right)/E_1 + \left(1-\upsilon_2^2\right)/E_2\right]^{-1}$ is the equivalent elastic modulus of the interacting bodies where E_1, E_2 and υ_1, υ_2 are Young's modulii and Poisson's ratios of each bodies, respectively, H is the hardness of the softer material, β is the average asperity tip radius, and σ is the composite surface roughness of the two bodies in contact. This hypothesis was supported by some experimental results obtained in the work of Hirst and Hollander [13]. However, the results from Park and Ludema [28] suggest that the correlation between scuffing and plasticity index is weak. Xue and Ludema [29] have hypothesized that a critical amount of accumulated plastic strain in the sliding surface can cause scuffing. From this hypothesis, scuffing failure is related to the damage in the surface caused by extensive plastic deformation. Another study from Kim and Ludema [30] relates scuffing to low cycle subsurface fatigue. In this study, the results show a strong correlation between the low cycle fatigue properties of the materials and number of cycles of repeated sliding to failure. Recently, the critical subsurface stress hypothesis was introduced by Somi Reddy and coworkers [17,31] to describe the large-scale subsurface failure of aluminum-silicon alloys, which is observed at scuffing under dry sliding conditions. This hypothesis suggests that scuffing occurs if the shear stress at a critical depth under the surface exceeds the temperature-dependent shear strength of the material at this depth. Sheiretov et al. [32,33] have examined the scuffing behavior of aluminum/steel contacts under dry sliding conditions. Based on the experimental observations, it was hypothesized that the accumulation of plastic deformation and fatigue damage in the subsurface is responsible for scuffing.

Other hypotheses for scuffing proposed in the literature are the critical contact pressure [34], and the accumulation of wear debris hypotheses [15,16]. The critical contact pressure hypothesis contradicts most of the experimental results on scuffing. Debris can contribute to scuffing by causing the lubricant starvation [15], or by forming large agglomerates between the sliding contacts [16]. However, the role of debris is very system

dependent. From the hypotheses described above, the more widely accepted are based on the critical temperature, the EHL collapse and the critical surface and/or subsurface plastic deformation.

1.2.2 Factors Which Affect Scuffing

Although many scuffing hypotheses have been proposed over the past sixty years, there are still no universal specifications available on how to prevent scuffing of lubricated surfaces. It is believed that there is a safe regime of operating conditions to prevent scuffing, but this regime is not easily quantified. Beyond this regime, permanent damage occurs and the component becomes inoperable. Practical experience accumulated throughout the years, with some widely used engineering materials and lubricants, has helped to outline the safe regimes of operation for some components. This safe regime is believed to be extended by increasing lubricant supply if the contact is starved, by using the proper additives in the lubricant, by improving the surface finish, by surface coatings and by proper material selection. As a secondary issue and yet one of the more importance, scuffing can be improved by a proper run-in procedure. In this section, some of the variables which affect scuffing and its prevention are discussed to provide a perspective on the state of knowledge of the scuffing process.

Pressure, Velocity and Temperature

As previously noted, parameters such as contact pressure, speed and temperature are considered to be the major influencing factors which affect scuffing. Therefore, numerous scuffing studies in the past have focused on these operating variables. A large-scale study on scuffing was reported in the 1970's by the International Research Group (IRG) of Wear of Engineering Materials. The IRG program was designed to examine the failure mechanism of thin film lubrication of sliding concentrated steel contacts [35-41]. Within this group, Czichos [35,36] and Begelinger and de Gee [37-39] made significant progress in understanding the conditions for failure of lubricated surfaces. They found that the load carrying capacity

decreases with increasing temperature and sliding velocity. The latter suggests that the thickness of the fluid films decreased as sliding velocity increases, contrary to predictions based on isothermal elastohydrodynamic calculations. A transition map between adequately lubricated and inadequately lubricated operation of steel contacts was developed over ranges of applied load and sliding velocity as shown in Fig. 1.2. The transition map has three characteristic regions. In region I, partial or full elastohydrodynamic (EHD) lubrication condition exists, therefore, a relatively low coefficient of friction and wear rate are obtained. In region II, thin film lubrication has failed but the steel surfaces are still protected by a boundary lubricant film. Finally, in region III, the surfaces are no longer protected by any lubricant films and severe adhesive wear occurs leading to scuffing failure.

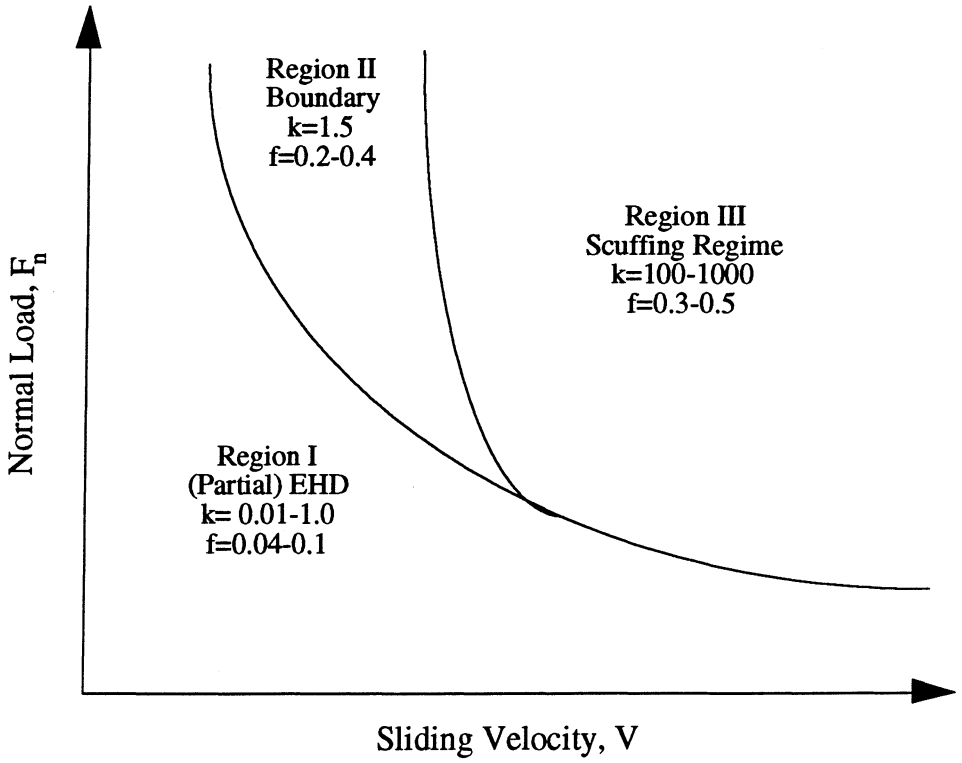

Fig. 1.2 - Schematic form of IRG transition diagram for constant oil bath temperature

k: wear rate (10^{-6} mm^3/Nm), f: coefficient of friction, Ref [38]

The concept of a failure surface for lubricated concentrated contacts was proposed in terms of a critical load-velocity-temperature relation given by [35]:

$$F_n{}^a V^b T^c = C = \text{constant} \qquad (0 < a,b,c < 1) \tag{1.2}$$

where F_n, V and T are normal load, sliding velocity and bulk oil temperature, respectively. The constants a, b, and c reflect the relative influence of these parameters. Unfortunately, this relationship can only be applied in the limited range of conditions and geometries studied.

Among the variables studied in the IRG program was contact geometry. Good agreement between results obtained by Czichos [35] on a four-ball machine and by Begelinger and de Gee [37] on a pin-on-ring machine indicated that different geometries showed similar trends.

Lubricant Additives

It is well known that additives in the lubricant affect scuffing. Bollani [40] examined the effects of extreme pressure (EP) additives on the scuffing behavior of sliding steel contacts using a pin-on-ring machine. He found that, at low speeds (up to 1 m/s), a relatively large increase in scuffing load is obtained with the additives, however, the increase in scuffing load is very small at higher speeds. Föhl and Uetz [41] investigated the influence of surface temperature on seizure, wear and reaction layer formation on soft iron with elementary sulfur in the lubricant using a pin-on-disc machine. The seizure load decreases, and the wear rate and sulfur reaction rate increases with increasing temperature.

Surface Topography

Much research [13,27,42-43] has been devoted to examine the influence of surface topography on scuffing failure. Surface roughness affects the magnitudes of the real area of contact, the local contact pressures and temperatures which, in turn, affects the scuffing process. Ludema [27], in a review of scuffing, emphasizes the importance of the influence of surface asperities on scuffing. Hirst and Hollander [13] have indicated that scuffing of sliding

isotropic steel surfaces, under boundary lubricated conditions, is controlled by two surface topography parameters: the composite RMS roughness σ and correlation distance β^*. Their results were represented by the boundaries separating the safe and unsafe regions in a σ-β^* plane. They proposed that scuffing is associated with the onset of plastic flow of asperity tips. Recently, Nivatvongs et al. [42] have conducted a series of experiments with a ball-on-flat test apparatus. Their results supported the view that scuffing failure, under boundary lubricated and low-sliding velocity conditions (0.04-0.8 mm/s), is caused by asperity plastic deformation. Recently, Patching et al. [43] have examined the scuffing performance of conventionally ground and superfinished hardened steel disks operating at sliding speeds of up to 26 m/s and lubricated with a gas turbine engine oil. It is shown that superfinishing gives a significant increase in the load at which scuffing occurs. Frictional traction was found to be significantly lower for the superfinished disks in the loading stages preceding scuffing failure.

Materials and Metallurgical Aspects

It is also well known that scuffing is strongly dependent on the materials used in the sliding contact pair. However, little systematic work has been done on the influence of materials on the scuffing process. In general, there are three commonly stated criteria for scuff resisting materials: (a) The materials should not readily adhere together when unprotected by interposing films (a concept sometimes referred to as the compatibility of metal pairs), (b) as a corollary to (a), similar materials should not slide against each other, and (c) two phase materials are superior to single phase materials.

In the past, most scuffing studies have focused on steel components such as gears, cams and followers, and piston ring/cylinder pairs [44,45]. A literature review on the materials and metallurgical aspect of piston ring scuffing was conducted by Scott et al. [46]. In this paper, the role of microstructure of steel and cast iron, surface treatments and metallographic changes in service and their effect on scuffing are outlined. However, specific connection of scuffing resistance with mechanical properties of metals was not described.

Gregory [47] found that, in steels, ferrite promotes scuffing, cementite in pearlite retards scuffing, and tempered martensite has an intermediate effect.

Since aluminum alloys are increasingly being used in many tribological applications, recently, scuffing studies of these alloys have also been increasing. The main focus has been on the optimization of the metallurgical composition, the microstructure, and the method of fabrication of the alloys. Tiwari et al. [48] found that, under boundary lubrication conditions, the scuffing resistance of all the leaded aluminum alloys (10-50 % Pb) tested is higher than that of the base alloys. Under dry sliding conditions, the friction coefficient generally decreases and the scuffing load increases with increasing lead concentration up to 25 % Pb. Ni and Cheng [49] found that, for silicon particle size ranging from 1-5 μm, the scuffing resistance of Al-Pb-Si bearings increases as the Si particle size increased. In a latter paper [50], Ni and Cheng proposed that the melting and depletion of tin in aluminum-tin bearings are the failure mechanism for these alloys. Recently, Barber et al. [51] have conducted tests with 390 Al-Si alloys to determine the effects of silicon particle size and etching on scuff and wear resistance. It was shown that the amount of near-surface silicon and the oxide films formed during the rubbing process are important conditions for improving the scuffing resistance of these alloys.

Surface Coatings

One approach to the prevention or minimization of scuffing has been the use of some form of surface coating or other surface treatments on the sliding components. Coatings have been widely used in tribological applications mainly to reduce friction and wear. A general review of surface treatments to enhance the frictional behavior of metals in rubbing contact has been presented by Bradley [52]. However, not many coatings to improve the scuff resistance of materials have been developed or studied. Some of the more common coatings used are chromium, tin and molybdenum. Scuff resistance of piston rings with chromium plating has been studied by Braendel [53]. It is known that the improvement in scuff resistance is due to the relatively high melting point and hardness of chromium plating. Tin

coating has also been widely used in many sliding components such as in piston rings in aero-engines and in swashplates of an automotive air conditioning compressor. The tin coating aids initial running-in by covering surface irregularities and acts as a temporary lubricant [54]. Molybdenum is known to be one of the best coating materials in terms of scuffing resistance [55]. Prasse et al. [56] attribute this to delayed welding due to its high melting point (2600 °C).

1.3 Scope of Research

The present work is part of a larger research project which addresses various tribological problems arising from the replacement of ozone-depleting refrigerants by ozone-safe refrigerants. The successful operation of compressors used in air-conditioning and refrigeration systems is mainly governed by the tribological behavior at the critical contacts within the compressors. Among the critical contacts are a wrist pin/bearing contact in a reciprocating compressor, a vane/piston contact in a rotary compressor, and shoes/plate contacts in a swashplate compressor. Increased scuffing problems associated with the latter contact are the focus of this study. These problems have arisen as the result of the phaseout of R12 (dichlorodifluoromethane). Presently, R134a (tetrafluoroethane) is the refrigerant of choice for swashplate compressors. Mineral oils which were used with R12 are not miscible with R134a. A family of miscible lubricants used with R134a, and presently used in swashplate compressors, are polyalkylene glycols (PAG). This new lubricant/refrigerant mixture poses new problems, both for its thermodynamic properties as well as its tribological properties. R134a lacks the lubricative properties of R12. It is known that R12 reacts with metal surfaces to form metal chlorides which are good solid lubricants. R134a possess limited, if any, lubricative properties. This lack of lubricative properties is thought to be one of the major reasons for the observed increased scuffing failures in some automotive swashplate compressors using the PAG/R134a mixture. The interest in the air conditioning

and refrigeration industry for a better understanding of these failures was one of the reasons which led to the present study.

The swashplate drive mechanism features an inclined plate which is rigidly attached to the rotating shaft. The unidirectional rotation of the shaft is transformed to simple reciprocal motion of the piston through the swashplate/shoe contact mechanism. A schematic of a typical automotive air conditioning swashplate compressor is given in Fig. 1.3. The shoes/plate contacts in a swashplate refrigerant compressor are lubricated by a lubricant/refrigerant mist. It is not uncommon for these contacts to experience starved lubrication conditions. In the present study, therefore, the scuffing characteristics of various contacts pairs are examined under starved lubrication. Starved lubrication is a condition where a lubricant is supplied but increasing its amount would improve the lubrication process. Under boundary lubrication conditions, this means that, for given load and sliding speed, asperity interaction increases as the degree of starvation increases. This leads to higher local temperatures and pressures, resulting in earlier failure of the sliding system.

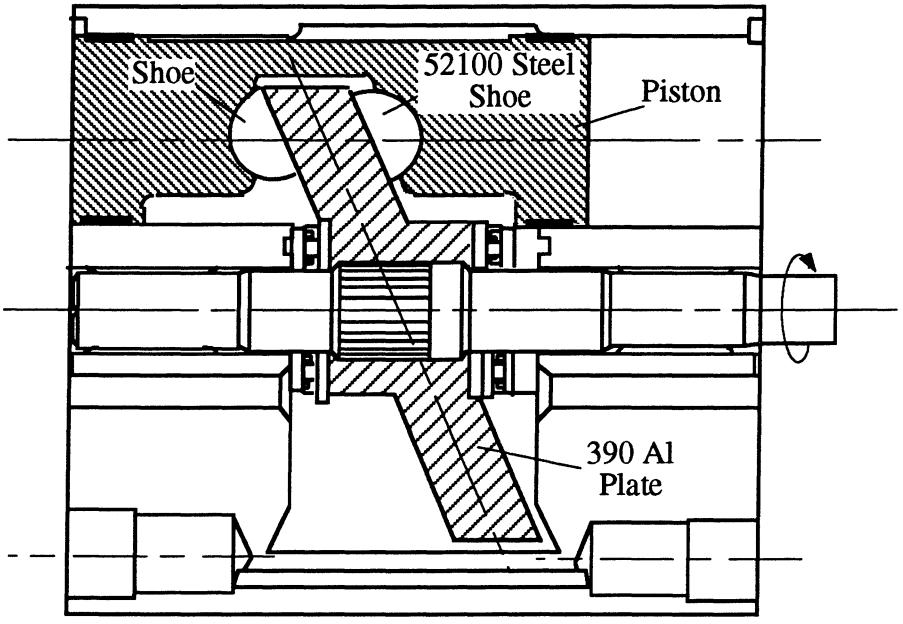

Fig. 1.3 - Schematic of a typical swashplate compressor

Ideally, the scuffing behavior of shoes/plate contacts can be examined by testing compressors under conditions that they experience in service. Such a testing program may ensure that all contacts closely reproduce expected operating and environmental conditions. The main drawback to component testing is the time and cost requirements, especially when it is desirable to examine a large number of variables; for example, a number of contact geometries, lubricants or materials contact pairs. To reduce cost and time, specimen testing can be considered. With specimen testing, it is also likely that a more fundamental understanding of contact behavior can be obtained since there is more control of the numerous variables which the contact experiences in practice.

In the present work, a specimen testing program is used to study scuffing under starved lubrication conditions. In the first part, the scuffing characteristics of the shoes/plate contacts are examined. The material pairs generally used in the refrigerant swashplate compressors are 52100 steel shoes sliding against a 390-T6 Al plate or Si-Pb brass shoes sliding against a hardened ductile cast iron plate. Scuffing problems, however, seem to be more prevalent with the aluminum/steel contact. Therefore, the major emphasis of this study is on this contact. The information obtained in this study will help to identify conditions under which the scuffing resistance of swashplate compressors may be improved.

The scope of this research is not limited to the practical problem of scuffing in swashplate compressors. The second part of the study is geared towards obtaining a better understanding of the fundamental mechanisms of scuffing failure under starved lubrication conditions. The contact geometry used in swashplate compressors is not suitable for a fundamental study because it is difficult to section and instrument. For these reasons, a pin-on-disc geometry is also used to examine the effect of materials, lubricant/refrigerant mixtures and loading history on scuffing. In order to better understand the processes and the failure mechanisms of scuffing, the surfaces of the test specimens are studied with an optical microscope, a surface profilometer, SEM (Scanning Electron Microscope) and AES (Auger

Electron Spectroscopy). The subsurfaces are studied by sectioning the pin specimens tested under scuffing and non-scuffing conditions and examining the sections with SEM and AES.

1.4 Objectives of Research

The main purpose of the present study is to better understand the scuffing process under starved lubrication conditions. The research focuses on two major goals. The first is to obtain a set of experimental data for the scuffing behavior of 52100 steel shoes/390-T6 Al plate contacts which approximately simulate the shoes/plate contacts in a swashplate compressor. The primary purpose of this part of the study is to see how scuffing of an actual critical contact can be affected by contact geometry, surface topography, coating, and the socket geometry supporting the shoe. As previously stated, these data provide valuable information on the conditions under which scuffing problems may be reduced in swashplate compressors. The second goal is to examine the fundamental failure mechanisms of the scuffing process and evaluate the existing hypotheses for scuffing based on the experimental data obtained. A more detailed description of these objectives is given below:

(1) Develop an experimental technique and instrumentation, which will result in reliable scuffing study under starved lubrication conditions.

(2) Obtain experimental data for scuffing with both shoe/disc and pin/disc geometries under starved lubrication conditions.

(3) With a shoe/disc geometry, study the effects of degree of starvation, sliding velocity, contact geometry, surface topography, tin coating, and socket geometry supporting the shoe. With a pin/disc geometry, study the effects of materials, lubricant/refrigerant mixtures, and loading history on scuffing.

(4) Examine the failure mechanisms of the scuffing process under starved lubrication conditions.

(5) Evaluate various existing hypotheses for scuffing based on the experimental data obtained.

(6) Based on the experimental observations, obtain a better understanding of the transition behavior of the scuffing process from dry to lubricated conditions.

CHAPTER 2

EXPERIMENTAL SETUP

2.1 High Pressure Tribometer

The research to be presented in this thesis focuses on scuffing of contacts in refrigerant environments. Since the contacts are lubricated, the amount of refrigerant dissolved in the lubricant is affected by the environmental pressure and temperature. If the lubricant and refrigerant are miscible, increasing the pressure and decreasing the temperature will increase the amount of refrigerant which will saturate into the lubricant. Therefore, in this study, a specially designed high pressure tribometer (HPT) was used to provide accurate control of the environmental pressure and temperature, and thus approximately simulate the environmental conditions found in refrigerant compressors. The high pressure tribometer and a schematic of the pressure chamber are shown in Figs. 2.1 and 2.2, respectively. In the HPT, the environmental pressure and temperature can be controlled up to 1.72 MPa and 120 °C, respectively. The desired temperature of the contact is obtained by an external recirculating unit which is capable of controlling the temperature from -10 °C to 130 °C. The lower specimen is secured in place by a specimen holder and the upper specimen is attached to the rotating spindle. The force transducer, which is outfitted with an intricate array of strain gages, is used to measure the applied normal load and the frictional torque during a test. A contact load of up to 4.45 kN can be applied to the specimens. The spindle is driven by a dc servo motor, giving a maximum unidirectional rotation of 2000 rpm.

For the purpose of this study, the HPT is equipped with a computer control of the axial load and the angular velocity of the spindle. The computer control is achieved through control boards and a set of solid-state relays. The corresponding software, which was also developed, allows for complicated loading and sliding velocity histories.

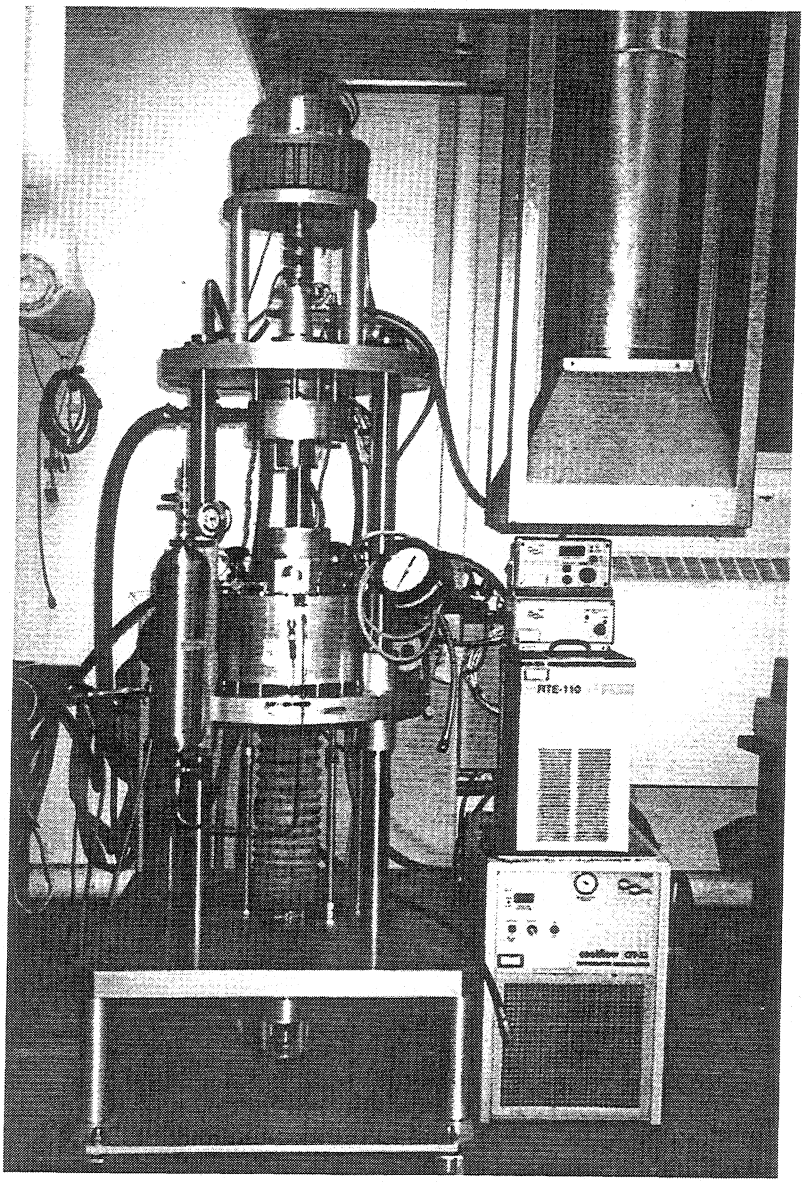

Fig. 2.1 - The high pressure tribometer

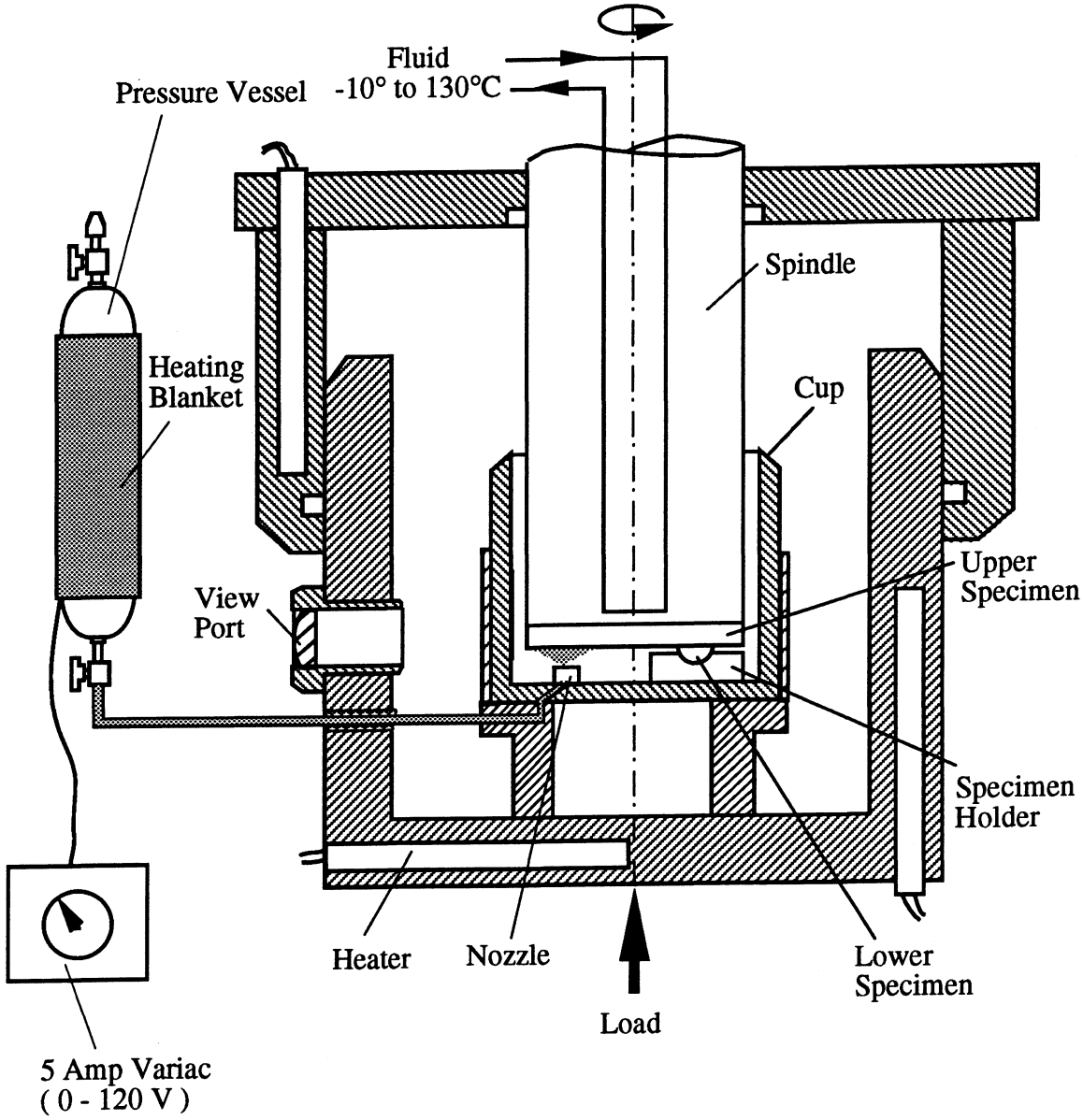

Fig. 2.2 - Schematic of the HPT pressure chamber and a lubricant/refrigerant delivery system

2.2 Geometries of Contact

In this study, both a shoe-on-disc and a pin-on-disc geometries (Fig. 2.3) were used to study the scuffing process under starved lubrication conditions. The shoe-on-disc tests simulate the shoes/plate contacts in a swashplate compressor (Fig. 1.3). During a test, a shoe is supported in a socket, giving the shoe freedom to align with the disc. Four different shoe geometries (flat shoe, crowned shoe, crowned shoe with a dimple at the center and crowned shoe with a groove) were tested. The crowned shoes are the actual shoes presently used in swashplate compressors. The crown height of these shoes varies between 2-10 μm. A picture showing the faces of the shoes tested is given in Fig. 2.4. Typical surface profiles across the diameter of these shoes are also given in Fig. 2.5. Shoes which have a crown height between 4 and 7 μm were tested in this study. The purpose of crowning is to help the plate/shoe contacts generate hydrodynamic films during operation. A perfectly smooth and flat shoe, which is supported at its geometric center, theoretically cannot generate these films. The custom-made flat shoes were tested to examine the effects of the crown height on scuffing under starved lubrication conditions. The size and apparent areas of contacts for these shoes are given in Table 2.1.

The geometry of contact used in the swashplate compressors is not well suited for a fundamental study because it is difficult to section and instrument. Pin specimens are also less costly to machine than discs. Therefore, a pin-on-disc geometry was also used to study scuffing under starved lubrication conditions. In this geometry, 6.35 mm diameter pins were tested. The pins are inserted into a hole in the shoe, which, in turn, is supported in a socket as shown in Fig. 2.3(b). This design helps align the pins with the counterface when a load is applied. After a test, the pin materials can be easily sectioned and examined to better understand the failure mechanisms associated with scuffing. The bulk temperature of the pin was also measured during the test by a miniature thermocouple inserted up to 2 mm below the sliding surfaces as shown in Fig. 2.3(b). The pin-on-disc was also used in a previous study [57] for tests conducted under dry sliding conditions. The same geometry is

used in this study so that the results obtained under dry sliding conditions can be compared to those obtained under starved lubrication conditions.

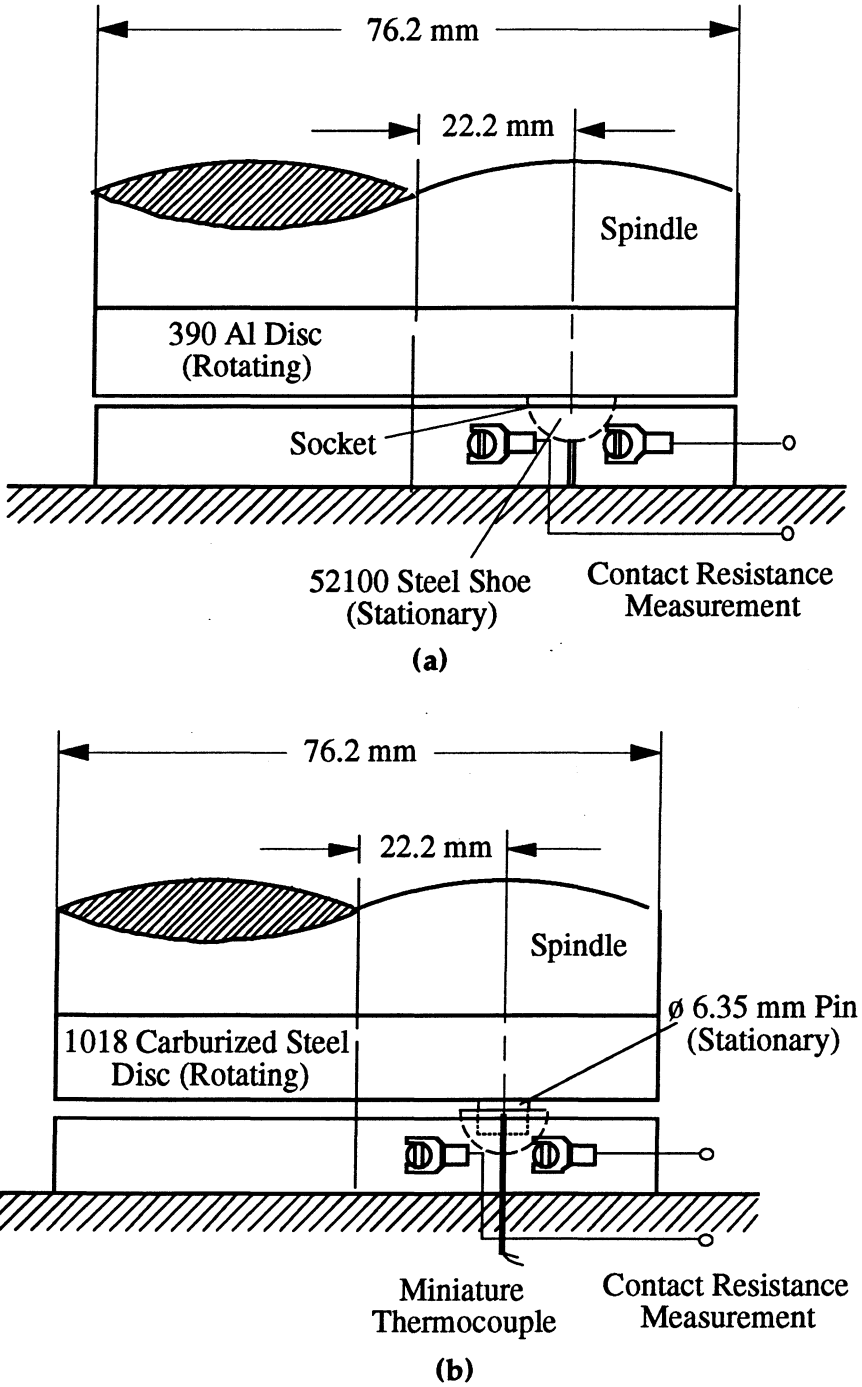

Fig. 2.3 - Geometries of contact (a) Shoe-on-disc, (b) Pin-on-disc

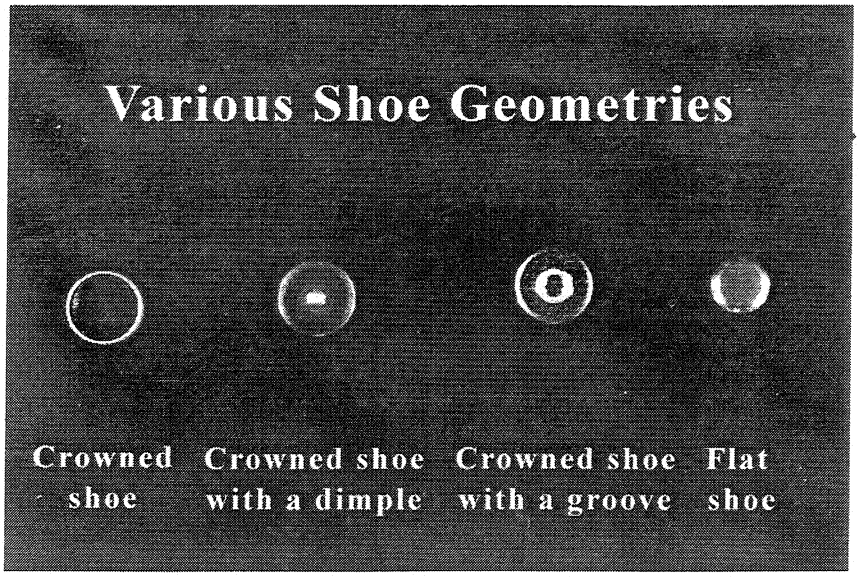

Fig. 2.4 - The top views of the various shoe geometries tested

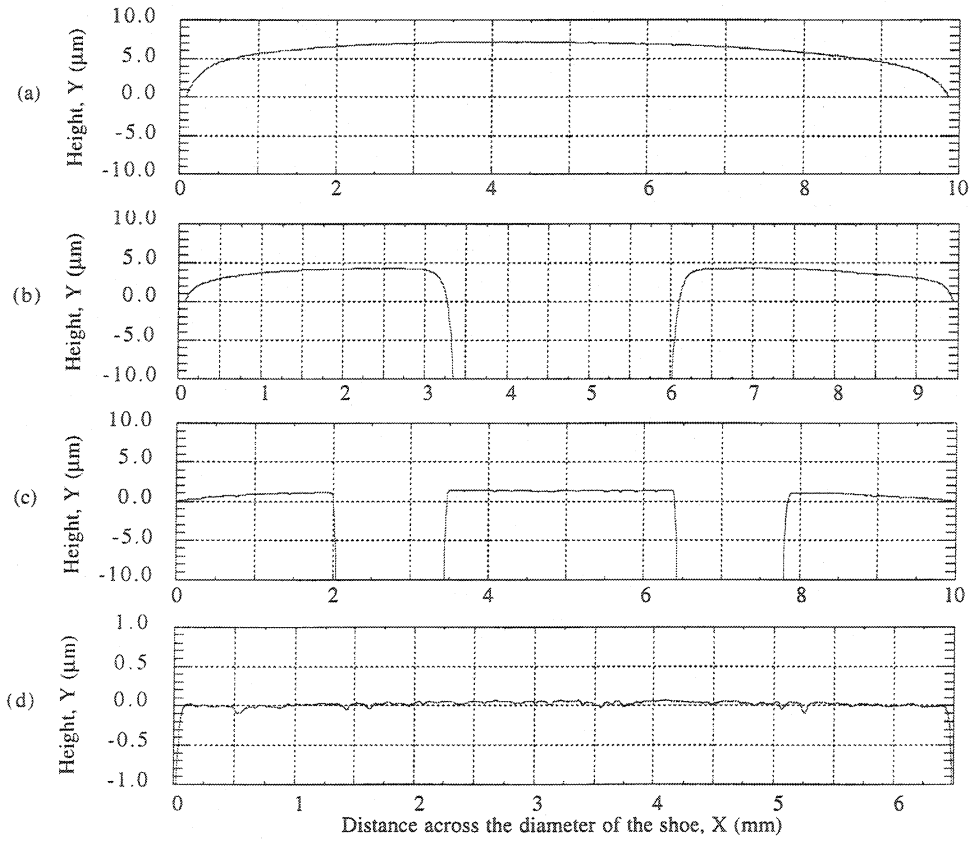

Fig. 2.5 - Typical surface profiles of various shoe geometries

(a) Crowned shoe, (b) Crowned shoe with a dimple

(c) Crowned shoe with a groove, (d) Flat shoe

Table 2.1 - Geometric dimensions of various shoes

Shoe Geometries	Diameter (mm)	Area of Dimple or Groove (mm^2)	Apparent Area of Contact (mm^2)
Crowned shoe	10.0	-	78.5
Crowned shoe with a dimple	9.6	5.5	66.9
Crowned shoe with a groove	10.0	18.1	60.4
Flat shoe	6.35	-	31.7

2.3 Materials Tested

For shoe-on-disc tests, all shoes tested were made of 52100 steel with an average hardness of 62 HRC and average surface roughness of 0.03 μm Ra. All tests were conducted with 390-T6 aluminum discs with an average hardness of 72 HRB. Unless otherwise noted, the average surface roughness of the discs was 0.04 μm Ra. The 390-T6 Al/52100 steel contact pair is the actual material combination used in the plate/shoe contact of many swashplate compressors.

For pin-on-disc tests, four materials were used for the pin specimens. They are 390-T6 aluminum alloy, DHT3 (a bismuth-containing aluminum alloy (46 HRB)), Si-Pb brass (80 HRB) and an ASTM number 40 gray cast iron (HRB 98). Most of the tests were conducted with the 390-T6 aluminum. These materials were tested against 1018 carburized steel discs with an average hardness of 62 HRC and average surface roughness of 0.1 μm Ra. Data for the chemical composition of the aluminum alloys and Si-Pb brass are given in Table 2.2. The gray cast iron contains 3.0-3.3 % C and 1.8-2.1 % Si.

Table 2.2 - Chemical composition of various materials

Material	Alloying elements, % by weight									
	Al	Si	Fe	Cu	Mn	Mg	Zn	Pb	Ti	Bi
390	Bal.	16-18.5	1.0	3.0-4.0	0.5	0.4-1.0	1.0	-	0.25	-
DHT3	Bal.	6.5-12.0	0.20	2.0-5.0	0.15	-	0.15	-	-	1.0-5.0
Brass	0.5	0.5-1.5	0.4	61.5-63.0	1.5-3.5	-	35.0-30.0	0.4-0.8	-	-

2.4 Test Conditions and Lubricants

Starved lubrication conditions are obtained by applying various amounts of lubricant on the surface of the upper specimen (disc) through the lubricant delivery system shown in Fig. 2.2. A pre-determined weight proportion of a miscible lubricant is added to the liquid refrigerant in the pressure vessel. The desired amount of lubricant/refrigerant mixture is fed to the contact regions through a nozzle by heating the pressure vessel. The setup for a spraying nozzle and a shoe specimen holder is given in Fig. 2.6. The average lubricant supply rate is determined by dividing the weight of the lubricant used by the test duration. The carrier gas used for the lubricant is the refrigerant under study. The shoes/plate contacts in a swashplate compressor are presently lubricated by a PAG/R134a mixture, therefore, most of the tests were conducted under R134a (tetrafluoroethane) environment with a base PAG (polyalkylene glycol) lubricant. Limited number of tests were also conducted with a base POE (polyolester)/R134a and a formulated PAG/R134a to examine the effects of lubricant and additives on scuffing. It should be noted that the POE's are the most widely used lubricants in air-conditioning and refrigeration systems. The data for the lubricants tested are given in Table 2.3.

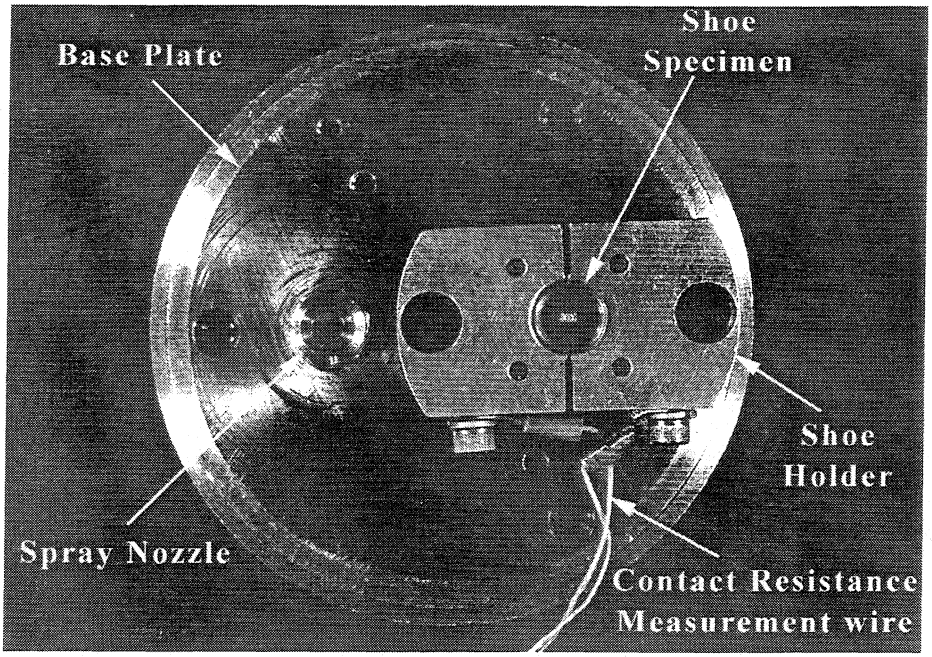

Fig. 2.6 - The setup for a spraying nozzle and a shoe specimen holder

Table 2.3 - Data for the lubricants

Designation	Lubricant Type	Family	Additives	Density	Viscosity, cS	
				g/ml	at 40 °C	at 100 °C
POE	Polyolester	Pentaerythritol	No	0.990	23.9	4.9
PAG	Polyalkylene glycol	Uncapped	No	0.990	49.5	9.8
Formulated PAG	Polyalkylene glycol	Uncapped	Yes	0.990	49.5	9.8

As previously indicated, the environmental pressure and temperature affect the amount of refrigerant dissolved in the lubricant. They also affect the surface properties of contacts by chemical reactions of active species with the metal surfaces. In order to approximately simulate the environmental conditions existing in swashplate compressors, the test chamber is initially purged to a vacuum of 0.2 torr to remove as much oxygen or water vapor as possible from the chamber. This vacuum is more than adequate for air-conditioning

and refrigeration systems. After purging, the test is initiated with continuous spraying of a lubricant/refrigerant mixture. The chamber pressure was kept constant during the test by means of a pressure release valve. All tests were conducted at an environmental pressure of 0.17 MPa and temperature of 121 °C. These conditions are close to the nominal conditions found at the plate/shoe contact of a swashplate compressor.

In general, there are two ways that scuffing tests can be conducted. One way is an endurance test, from which the time to failure is obtained for given constant load and velocity conditions. The more widely used procedure is the step-loading test because it requires a considerably shorter time. In this test, for a given constant sliding velocity, a load is progressively increased stepwise with a specified step duration until failure occurs. It has been shown [58] that a good correlation exists between the two testing procedures. In the present study, the step-loading test procedure is used for all tests conducted. With the exception of the tests conducted to determine loading-history effects, a 222.5 N load step and a step duration of 15 seconds were used. The 15 second step duration was chosen since, under starved lubrication conditions, a steady state temperature is reached after approximately 10 seconds. In this study, scuffing was based on the sharp transitions of the contact resistance (indicating the destruction of surface films), friction coefficient and, for the pin-on-disc geometry, subsurface temperature (2 mm below the surface) of the pin specimens. A typical record of a scuffing test is shown in Fig. 2.7 for the pin-on-disc geometry. The process of stepwise increasing the load eventually leads to scuffing failure, which causes sharp transitions of the contact resistance, friction coefficient and subsurface temperature of the pin specimens. At this stage, the load is quickly released and the test stopped.

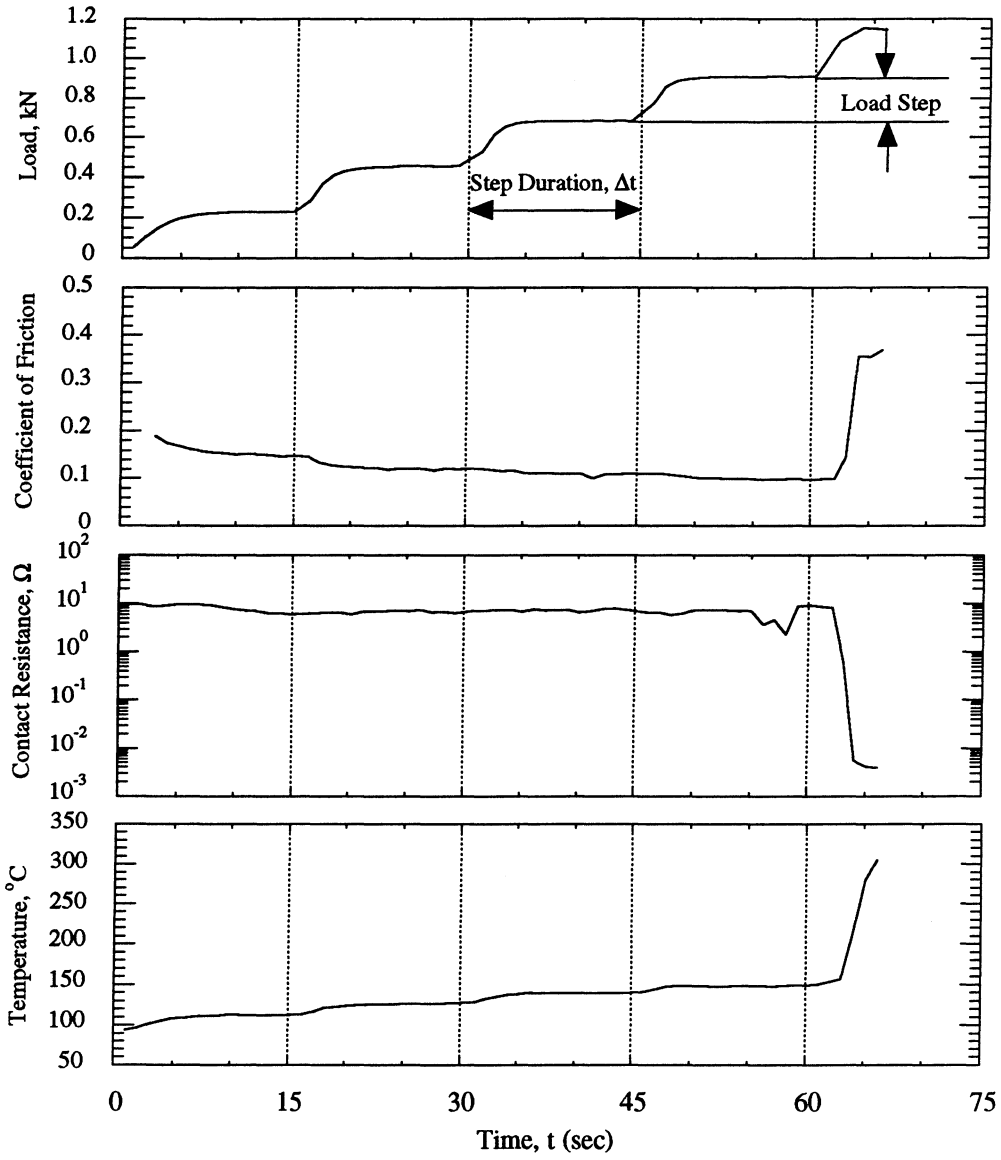

Fig. 2.7 - Typical scuffing test data for the pin-on-disc geometry

2.5 Instrumentation

Scuffing can have various manifestations. In practice, the first obvious signs of scuffing are the increased noise and vibrations, followed by a progressive increase in the operating temperature. In a laboratory environment, scuffing can be detected by sharp transitions in various parameters. As indicated previously, the scuffing condition is identified by transitions in friction, contact resistance, and subsurface temperature.

The electric contact resistance between the test specimens provides indirect information about the regime of lubrication, the formation of protective surface films and the extent of metal-to-metal contact. A schematic of the contact resistance measuring setup is given in Fig. 2.8. The measurement range of the circuit used is 10^{-6} - 10^{+4} Ω. This sensitivity was achieved by the development of a special four-terminal measurement circuit, methods for noise suppression and data processing software [57]. A large drop in the contact resistance is often a more sensitive indicator for scuffing than the coefficient of friction.

The surface temperature at the contact is one of the most important tribological parameters. The surface temperature is often measured by utilizing an infrared sensor, positioned directly under the transparent specimen [59]. This method has obviously limited application. Due to the experimental difficulties, the temperature in the vicinity of the sliding interface is often estimated with the aid of thermal models and subsurface temperature measurements. In this study, the subsurface temperature for the pin-on-disc geometry was measured by a miniature thermocouple implanted 2 mm below the sliding surface of the pin.

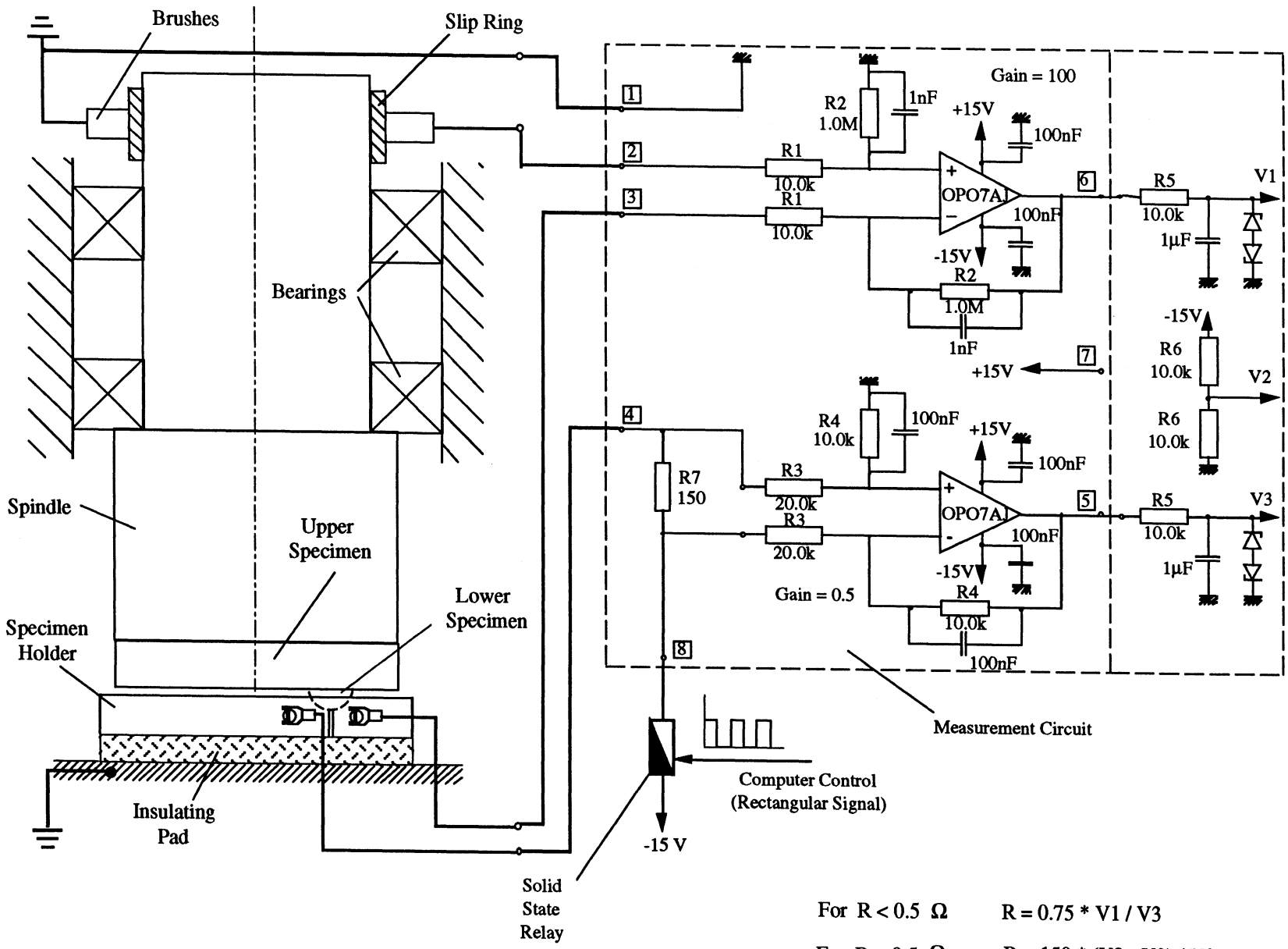

Fig. 2.8 - Schematic of the electric contact resistance measuring circuit

CHAPTER 3

EXPERIMENTAL RESULTS - PART I (SHOE/DISC GEOMETRY)

In this chapter, the scuffing characteristics of 390-T6 aluminum-silicon alloy sliding against 52100 steel shoes are examined under starved lubrication conditions. The evaluation is based on a shoe-on-disc geometry which simulate the plate/shoe contacts in an automotive air conditioning swashplate compressor. The main goal of this chapter is to obtain design data for these compressors by varying a number of parameters which may affect scuffing. Even though, where necessary, an explanation is given for the trends observed, it is not the purpose of this chapter to do an in-depth study of these parameters. Four shoe geometries (flat shoe, crowned shoe, crowned shoe with a dimple at the center and crowned shoe with a groove) are tested against 390-T6 aluminum discs. All tests are conducted in a high pressure tribometer (HPT) under R134a (tetrafluoroethane) environment with a base polyalkylene glycol (PAG) lubricant. The effects of degree of lubricant starvation, sliding velocity, shoe geometry, surface topography, a tin coating, and socket geometry supporting the shoe are evaluated. For shoe-on-disc tests, scuffing data were based on the sharp transitions of the contact resistance and friction coefficient measurements. Typical scuffing failure of a shoe-on-disc contact is shown in Fig. 3.1. Scuffed surface shows the plastic deformation and macroscopic material removal. Some of the aluminum material is transferred to the counterface steel shoe as the result of formation of cold welds. It should be noted that scuffed surface on the aluminum disc is very similar to the scuffing failure of a actual swashplate/shoe contact as shown in Fig. 1.1.

3.1 Effect of Degree of Starvation and Sliding Velocity

The contact pressure at which scuffing occurs is a function of the degree of lubricant starvation and sliding velocity. Figure 3.2 shows scuffing data for crowned shoes with a dimple. The contact pressures given are calculated based on an area which excludes the area

of the dimple. As expected, for every sliding velocities used, the scuffing pressure increases as the lubricant supply rate (LSR) increases. For a given LSR, the scuffing pressure decreases as the sliding velocity increases. This phenomenon can be attributed to thermal effects. More heat is generated at the interface with higher sliding velocities, causing a breakdown of the protective surface films and subsequent scuffing failure. The results given in Fig. 3.2 are plotted in Fig. 3.3 as pressure (P) vs. velocity (V), for various lubricant supply rates. Three lubricant supply rates (20, 30, 40 mg/min), from which three pressure data points can be obtained in the curve fits given in Fig. 3.2, are chosen for this plot. This curve is commonly referred to as PV curve for evaluating the scuffing resistance for a particular lubricant-bearing material system. It should be noted that the data points shown in Fig. 3.3 fall closely on lines given by $PV = constant$. The value of this constant increases as the degree of lubricant starvation decreases.

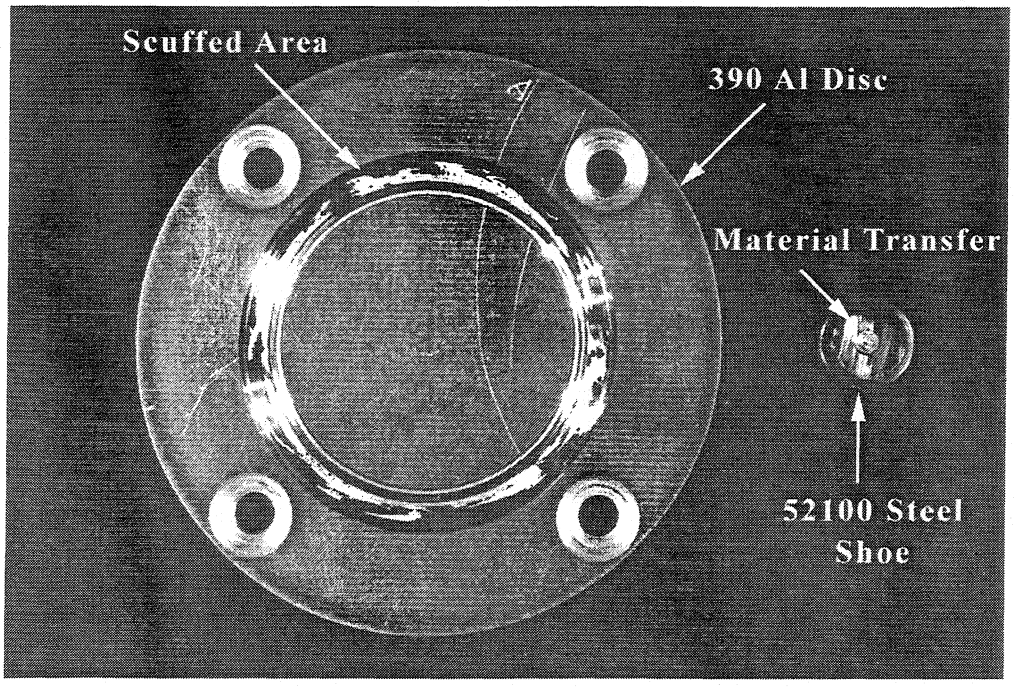

Fig. 3.1 - Typical scuffing failure of a shoe-on-disc contact

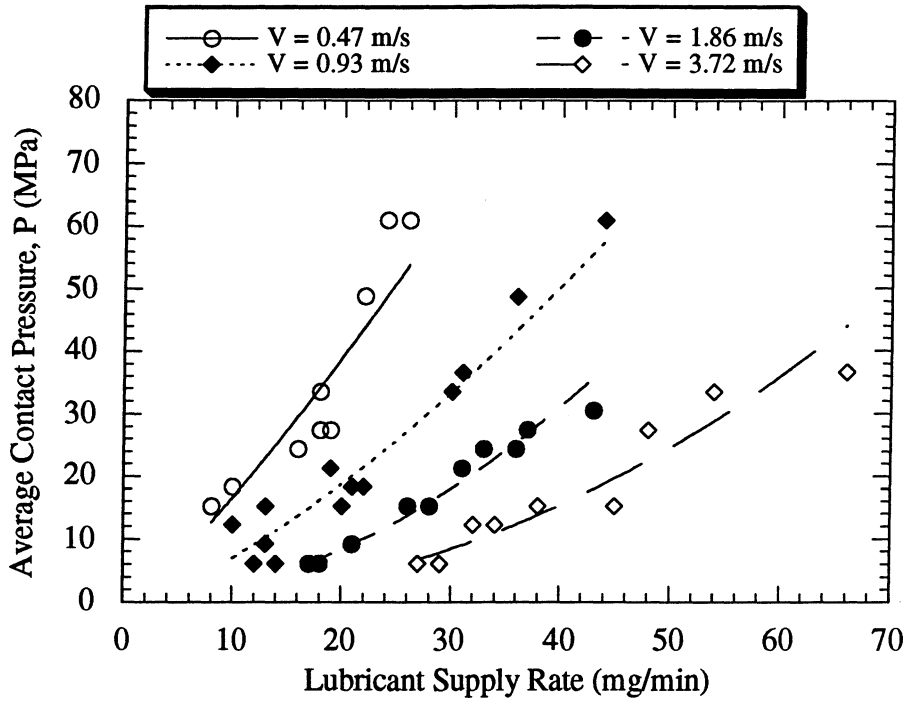

Fig. 3.2 - Scuffing results for 390-T6 Al for various lubricant supply rates and velocities

Shoe geometry: Crowned shoes with a dimple

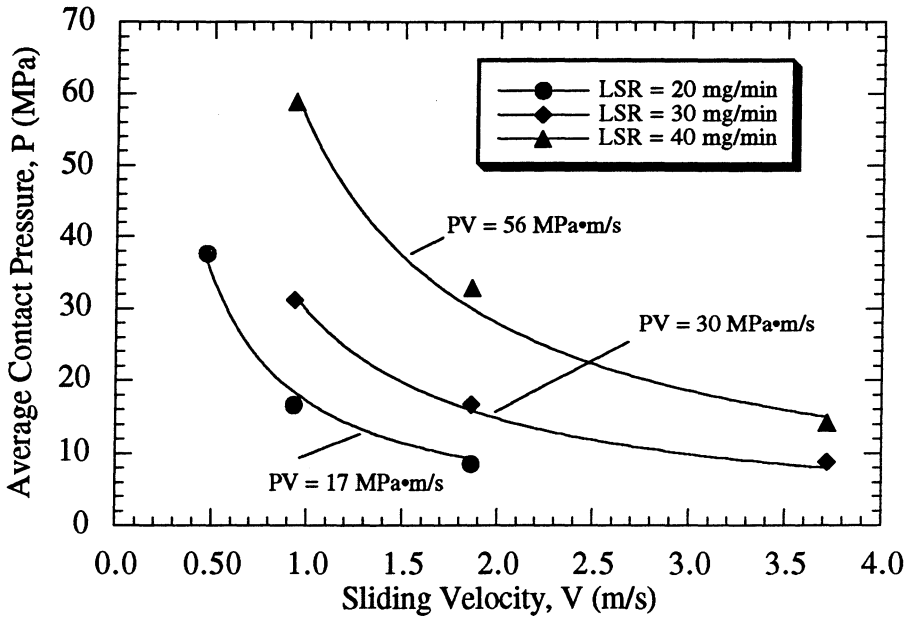

Fig. 3.3 - Scuffing *PV* curves for various lubricant supply rates

Solid lines indicate *PV* = constant

Shoe geometry: Crowned shoes with a dimple

3.2 Effect of the Contact Geometry

As previously indicated, a perfectly smooth and flat shoe, which is supported at its geometric center, theoretically cannot generate hydrodynamic films and thus can only operate in the boundary lubrication regime [60]. The steel shoes presently used in swashplate compressors have a small crown. Some shoes also has a dimple or groove. However, the effects of shoe geometry on scuffing are not well known. Scuffing data for 390-T6 Al have been obtained with flat shoes, crowned shoes, crowned shoes with a dimple and crowned shoes with a groove. Scuffing results obtained with flat shoes are compared with those obtained with crowned shoes in Fig. 3.4. The data show that, for severely starved conditions (LSR < 30 mg/min), the scuffing pressure obtained with flat shoes is higher than that obtained with crowned shoes. However, as the lubricant supply rate increases, the scuffing pressure obtained with crowned shoes is much higher than that obtained with flat shoes. This indicates that scuffing is a function of crown height and the degree of starvation. When the contact is severely starved, the crowning is detrimental because, for a given average pressure, the peak contact pressure and temperature for the crowned shoe are higher than those for a flat shoe.

Scuffing results for 390-T6 Al obtained with various crowned shoes are shown in Fig. 3.5. The major role of a dimple or groove in a shoe is to trap debris and lubricant during operation. However, when the contact is starved, a dimple or groove seems to be detrimental. Again, this might be due to higher local pressures and temperatures on shoes with a dimple or groove for a given average pressure distribution. Also, for the lubricant supply rates used, the amount of lubricant supplied at the contact is not enough for a dimple or groove to be effective as a lubricant reservoir. Due to the limiting load capacity (4.45 kN) of the HPT, scuffing data at higher lubricant supply rates could not be obtained. It should also be noted that, in swashplate compressors, the shoes/plate contacts experience a squeezing action. What effects, if any, the dimple or groove has on scuffing with the addition of this squeezing is not known.

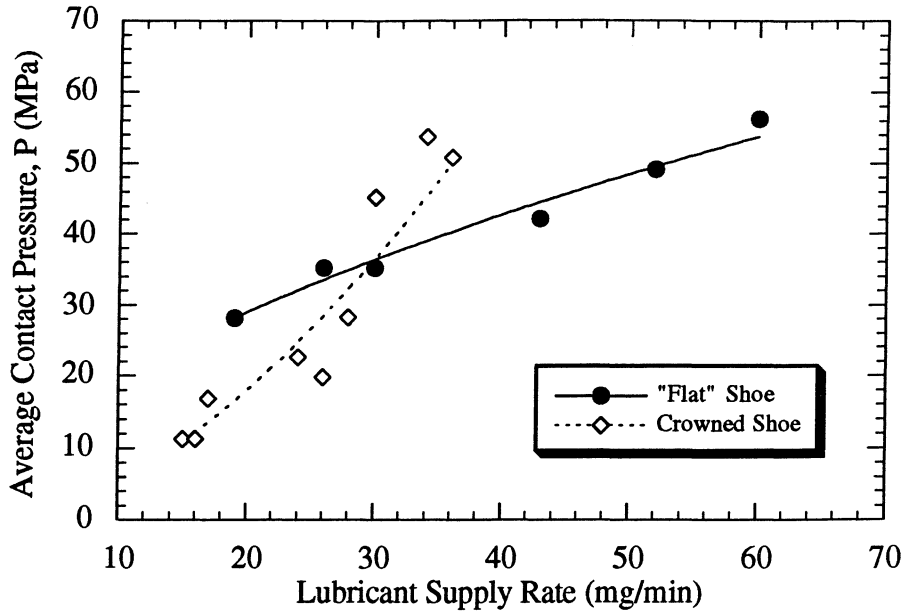

Fig. 3.4 - Scuffing results for 390-T6 Al obtained with flat and crowned shoes

V = 1.86 m/s

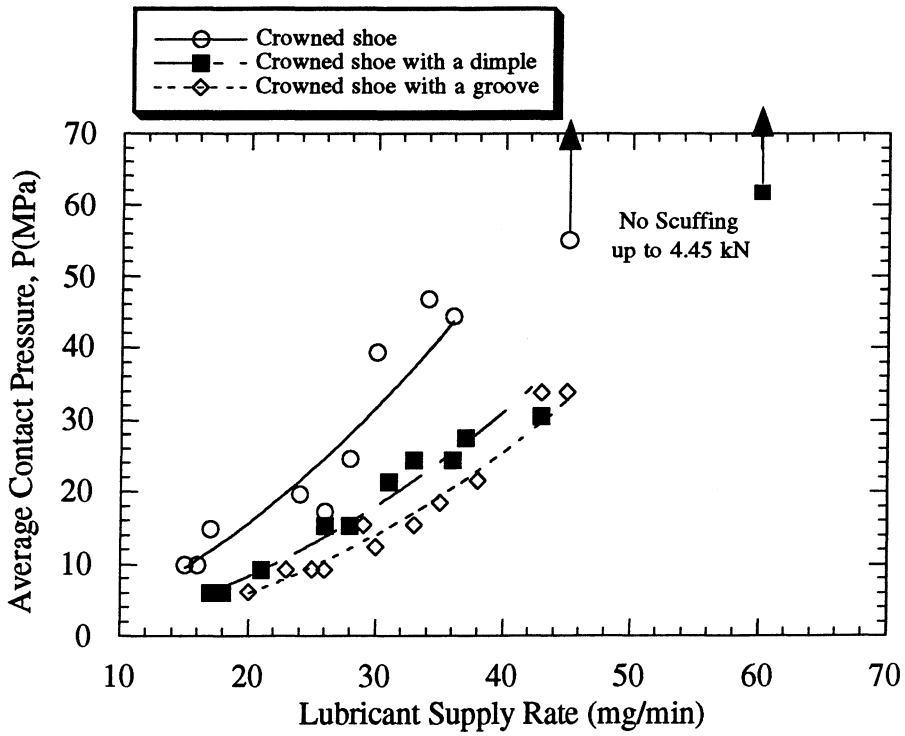

Fig. 3.5 - Scuffing results for 390-T6 Al obtained with various crowned shoes

V = 1.86 m/s

3.3 Effect of Surface Topography

Surface topography is known to play an important role in friction, wear and scuffing behavior of lubricated contacts. Surface roughness affects the magnitudes of the real area of contact, and the local contact pressures and temperatures. It also plays a major role in the establishment of hydrodynamic or elastohydrodynamic films. To examine the effects of surface roughness on scuffing, tests were conducted using 390-T6 aluminum discs with three different surface roughness values. The average surface roughnesses tested were 0.03 μm, 0.49 μm and 1.50 μm Ra. The 0.03 μm Ra surfaces were obtained by superfinishing, while the 0.49 μm and 1.5 μm Ra surfaces were produced by conventional grinding and abrasion with 60 grit Al_2O_3 abrasive paper, respectively. These discs were tested against crowned shoes with a dimple. The scuffing pressures as a function of sliding velocity for these specimens are given in Fig. 3.6. For the given LSR, the results show that the scuffing resistance increases as surface finish improves.

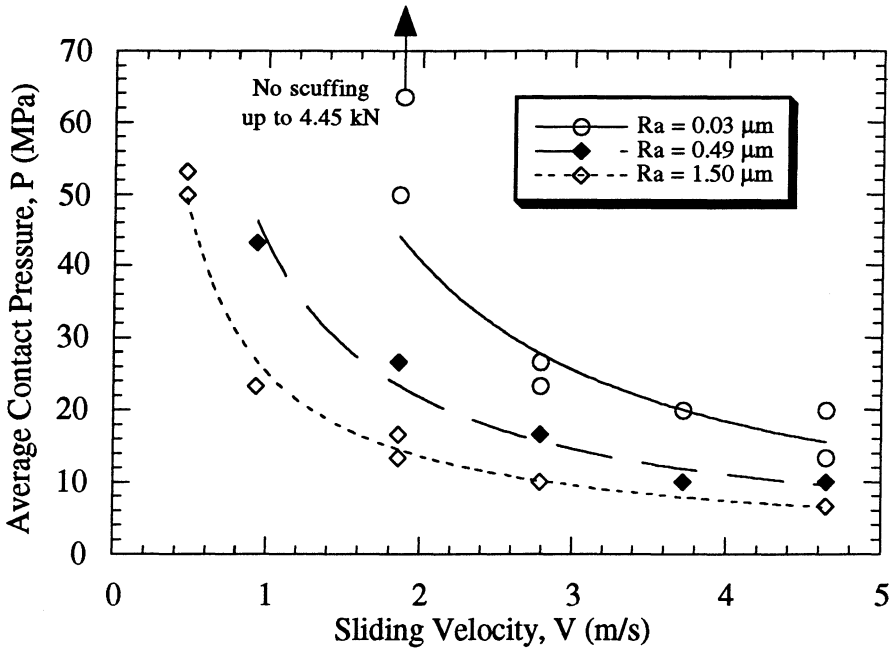

Fig. 3.6 - Effect of surface roughness on scuffing pressure as a function of sliding velocity

LSR = 40 mg/min, Shoe geometry: Crowned shoes with a dimple

As illustrated in Fig. 3.7(a), the 0.03 μm R_a surface gives a much lower coefficient of friction preceding scuffing failure than the other surfaces. It is also shown in Fig. 3.7(b) that the friction force obtained with 0.03 μm Ra surface is significantly lower than those of the other surfaces. Thus, much less heat is generated at the interface with the 0.03 μm Ra surface, resulting in improved scuffing performance. Surface roughnesses of both steel shoe and aluminum disc specimens just before scuffing are obtained to see the change of roughness during the tests. These data are obtained at a lubricant supply rate of 40 mg/min and a sliding velocity of 1.86 m/s. Surface roughnesses just before scuffing are compared to those of the virgin specimens in Table 3.1. Data show that, even though the shoe specimens are harder than 390-T6 Al, they are roughened during the tests, and the roughening increases as the roughness of the discs increases. The roughening of steel shoes is attributed to the hard silicon particles in the 390-T6 Al disc. For Al disc specimens, except for the superfinished disc (0.03 μm Ra), surfaces are smoothened during the tests.

The effects of surface roughness on scuffing were also examined as a function of lubricant supply rates with 0.03 μm and 1.50 μm Ra specimens. As shown in Fig. 3.8, for the sliding velocity used, surface roughness effects are more significant as the lubricant supply rate increases, i.e., scuffing of the smoother specimen is affected to a greater degree than that of the rougher specimen as the lubricant supply rate increases. However, it should be noted that, if the contact is severely starved (LSR = 25 mg/min), the scuffing pressures are about the same for both roughnesses. For a given nominal contact pressure, the local asperity contact pressures are higher for the rougher specimens since their real area of contact is smaller. It is believed that, when the contact is severely starved, more protective surface films are formed with the rougher specimens due to more asperity interactions, resulting in approximately the same scuffing resistance for both surfaces.

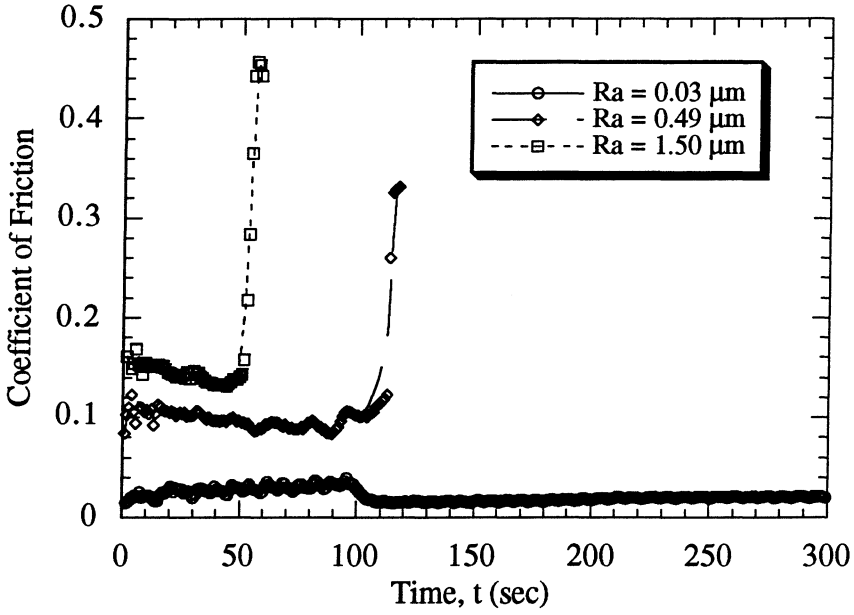

(a)

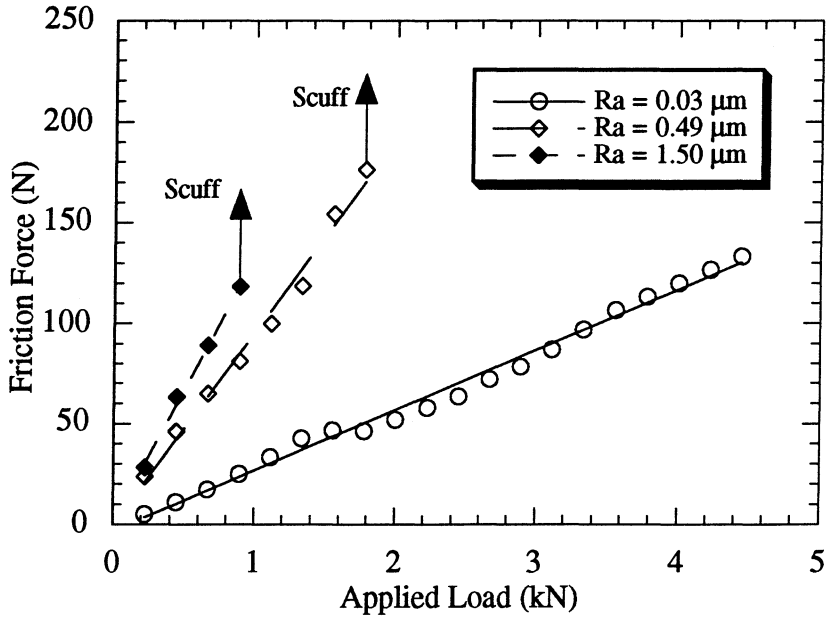

(b)

Fig. 3.7 - Variation of coefficient of friction and friction force for different surface roughnesses

LSR = 40 mg/min, V = 1.86 m/s

(a) Coefficient of friction, (b) Friction force

Table 3.1 - Representative roughnesses for steel shoe and aluminum disc specimens

Specimen	Virgin	Just before scuffing
Shoes	0.02-0.03 μm Ra	0.11 μm Ra with 0.03 μm Ra Discs
		0.17 μm Ra with 0.49 μm Ra Discs
		0.40 μm Ra with 1.50 μm Ra Discs
Aluminum Discs	0.03 μm Ra	0.03 μm Ra
	0.49 μm Ra	0.15 μm Ra
	1.50 μm Ra	1.28 μm Ra

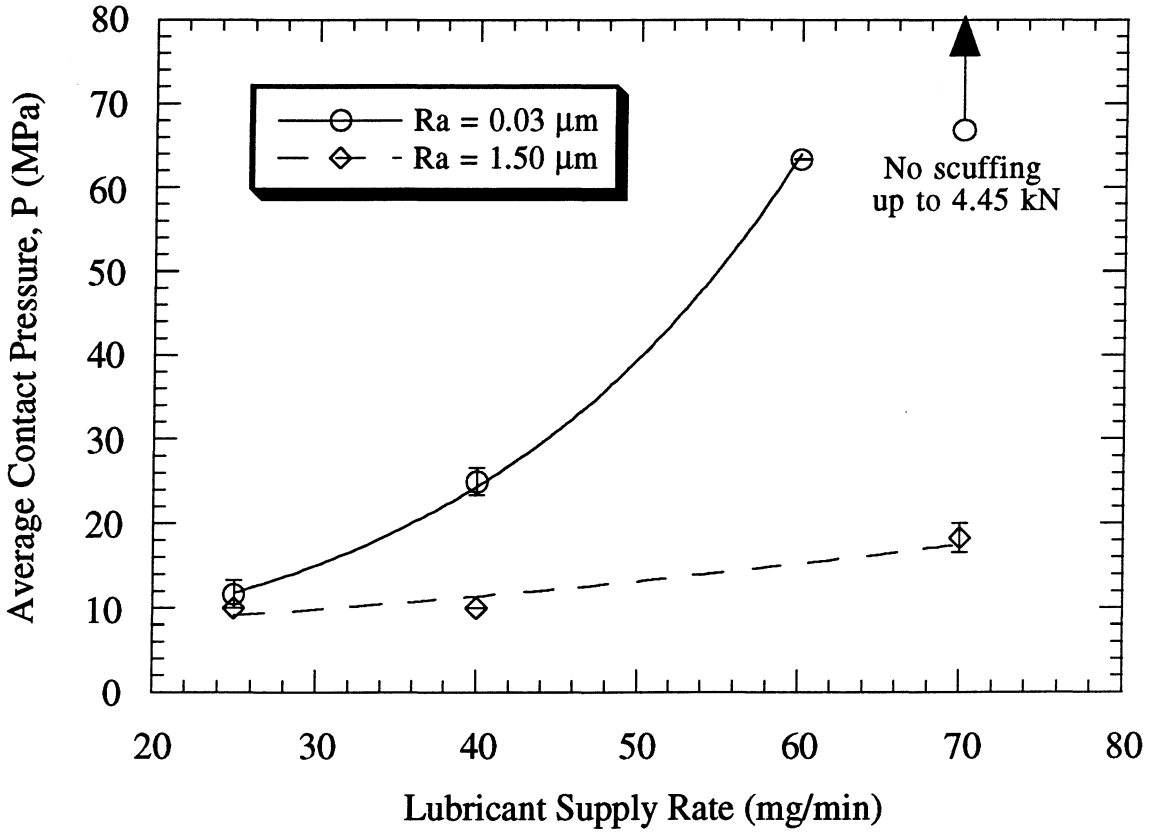

Fig. 3.8 - Effect of surface roughness on scuffing as a function of lubricant supply rate

V = 2.79 m/s, Shoe geometry: Crowned shoes with a dimple

Skewness is another important parameter characterizing the behavior of sliding surface. This parameter gives some measure of the degree of asymmetry of the asperity height distribution. If the surfaces have deeper valleys than peaks, the skewness will be some negative value. Typical surface profiles which show two different skewnesses with approximately the same surface roughness are shown in Fig. 3.9.

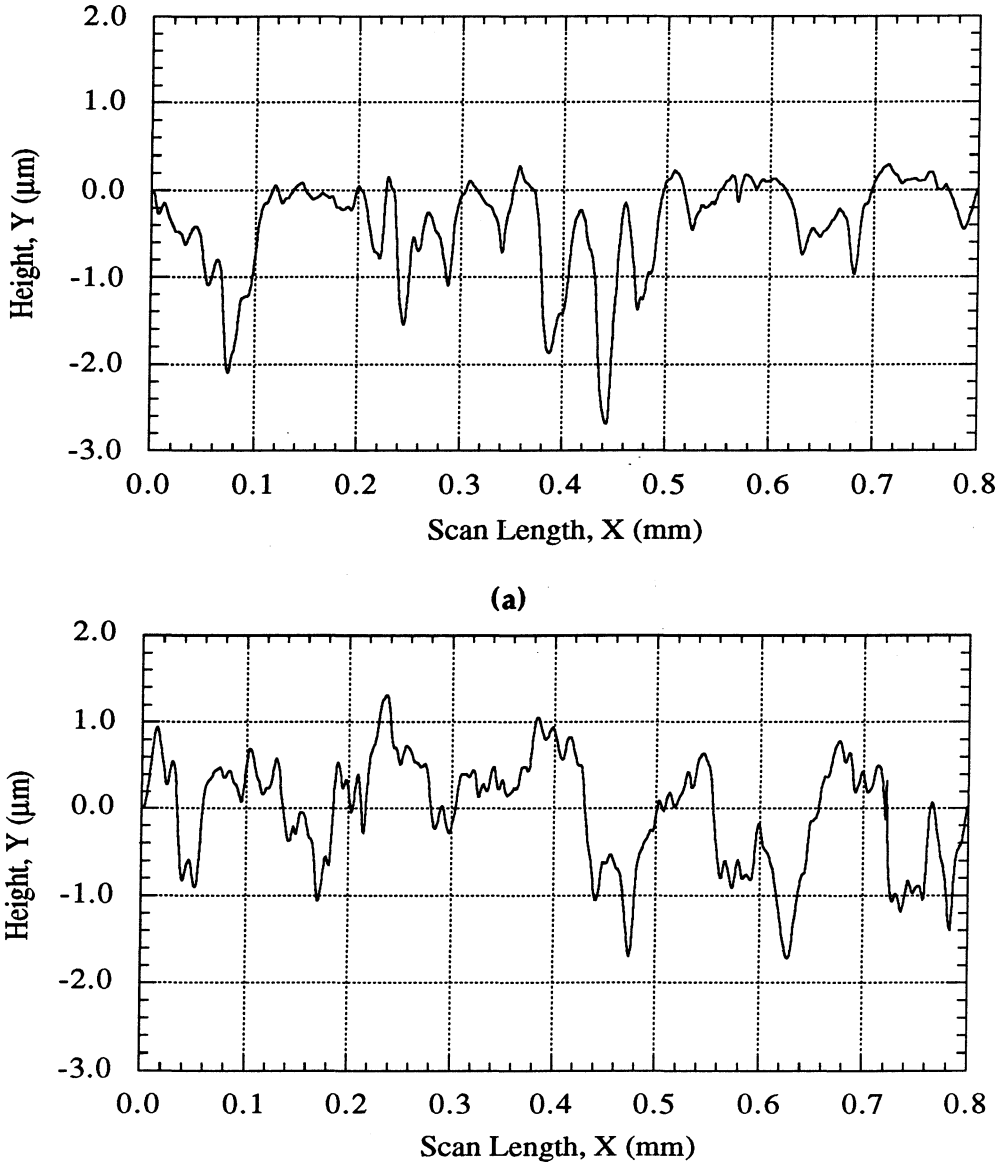

Fig. 3.9 - Typical surface profiles of two different skewnesses

(a) Skewness = -1.59 and 0.41 μm Ra, (b) Skewness = - 0.31 and 0.44 μm Ra

It is known that, in some tribological applications, surfaces with higher negative skewness are beneficial under mixed or boundary lubrication conditions. Surfaces with higher negative skewness have higher real contact area, resulting in lower local contact pressure and temperature for a given nominal pressure. In order to evaluate the effect of skewness on scuffing, discs having two different skewnesses (-0.34 and -1.26) but the same surface roughness value (0.49 μm Ra) were tested. Scuffing data were obtained at various sliding velocities as shown in Fig. 3.10. The results show that, for the given test conditions, these different skewnesses do not seem to improve the scuffing resistance. It is believed that the effect of skewness difference would be more apparent if a significant skewness difference was present on the harder counterface material.

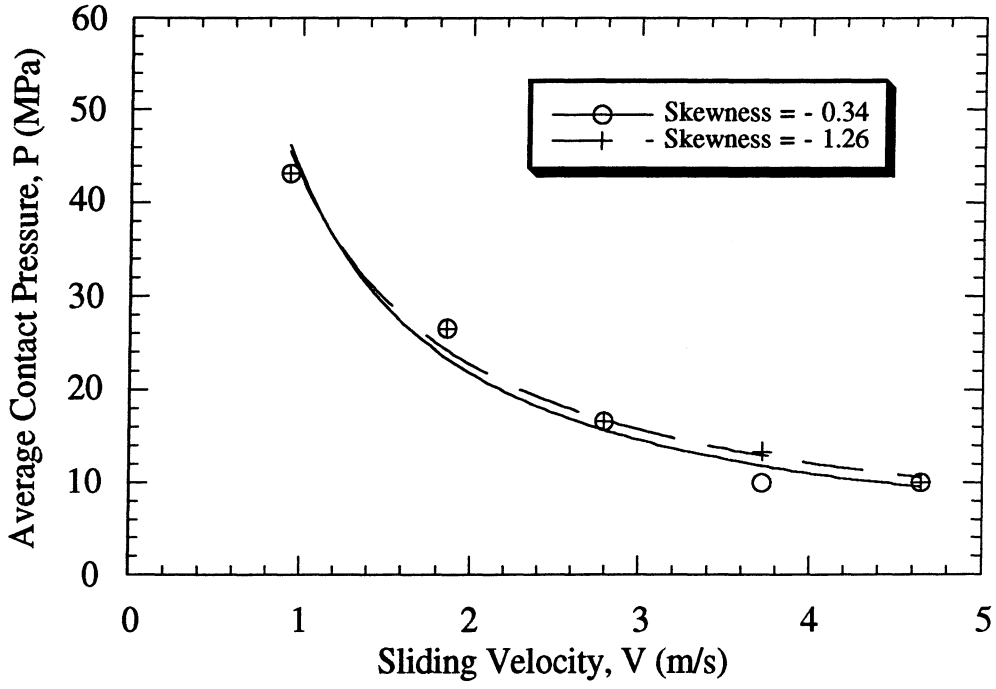

Fig. 3.10 - Effect of skewness on scuffing pressure as a function of sliding velocity

LSR = 40 mg/min, Average surface roughness: 0.49 μm Ra

Shoe geometry: Crowned shoes with a dimple

3.4 Effect of a Tin Coating

Scuffing failure can be prevented or minimized by using some form of surface coatings or surface treatments on the sliding contacts. Tin coatings have been widely used in many automotive sliding components such as piston rings and swashplates in air conditioning compressors. Together with surface roughness, coatings can affect local pressures and temperatures which, in turn, affect scuffing. In order to examine the effect of a tin coating on scuffing under starved lubrication conditions, scuffing data were obtained with tin-coated 390 aluminum discs (1.22 μm Ra) and are compared to the uncoated discs (0.49 μm Ra) in Fig. 3.11.

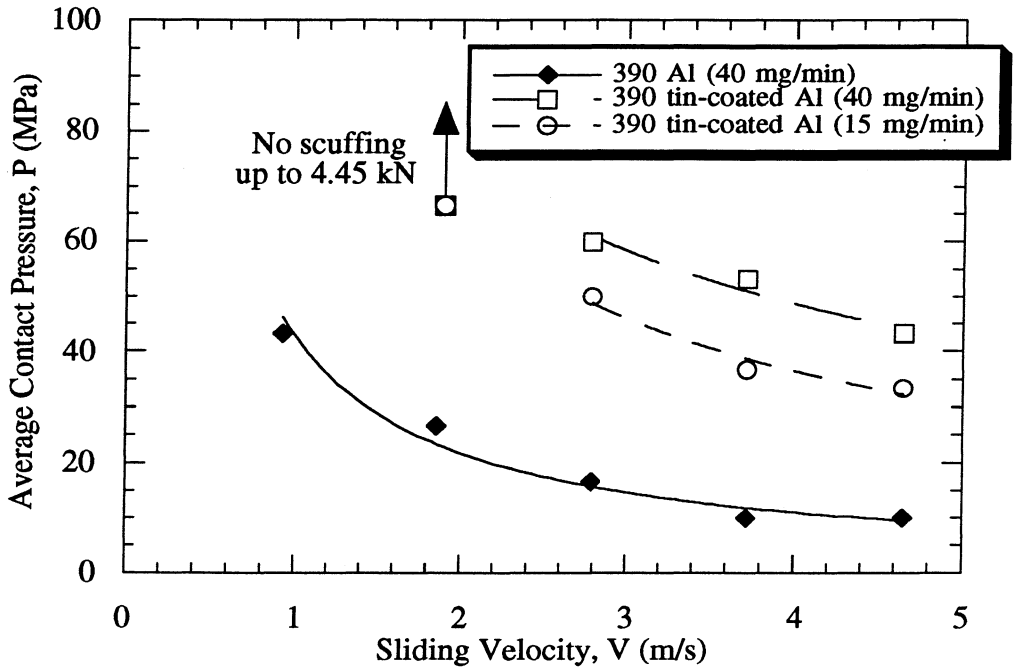

Fig. 3.11 - Effect of a tin coating on scuffing pressure as a function of sliding velocity

Shoe geometry: Crowned shoes with a dimple

Even though the initial surface roughness of the tin-coated discs is much higher than that of the uncoated discs, for the 40 mg/min lubricant supply rate, the scuffing pressure of the tin-coated discs is about three times higher than that of the uncoated discs. Scuffing data for the coated discs, at a much more severe starved lubrication condition (15 mg/min),

are also given in Fig. 3.11. These data show that, even at this severely-starved lubrication condition, the coated discs provide better scuffing resistance than the uncoated discs. This behavior is attributed to the low-shear strength characteristics of the tin material. Tin tends to deform quickly and increases the conformity of the sliding surfaces, resulting in lower local pressures and temperatures. It is also noted that the tin coating aids initial running-in by covering surface irregularities and acts as a temporary lubricant [54]. Typical surface roughness data, given in Table 3.2, also show that the coated discs are smoothened much more than the uncoated discs during the test.

Table 3.2 - Representative roughnesses for tin-coated and uncoated Al disc specimens
Lubricant supply rate: 40 mg/min, Sliding velocity: 1.86 m/s

Specimen	Virgin	Just before scuffing
Tin-coated discs	1.22 μm Ra	0.05 μm Ra
Uncoated discs	0.49 μm Ra	0.15 μm Ra

For scuffed tin-coated aluminum discs, some of the aluminum substrate is exposed due to the wear of the coating. As indirectly illustrated in Fig. 3.12, the coated disc experiences a severe wear regime before scuffing occurs, as indicated by the increased friction coefficient. Increased noise and vibrations are also typical in this regime. Typical scuffed tin-coated disc and its corresponding surface profile are given in Fig. 3.13. Fig. 3.13(a) shows the smeared tin-coating and local scuffed areas accompanied by deep grooves as shown in Fig 3.13(b). It should also be noted that the contact resistance for the coated discs is relatively low from the beginning of the test when compared to that of the uncoated discs. This indicates that the coated discs have more surface interactions due to their high initial surface roughness and low hardness. However, their average friction coefficient is lower than that of the uncoated specimens, which is again due to their low-shear strength characteristics. From visual observations, scuffing of the tin-coated

specimens seems to be caused by the removal of the coating, which leads to the formation of macroscopic adhesion between the exposed aluminum substrate and the steel counterface. Ni and Cheng [50] also indicated that the aluminum-tin bearings fail because of the rapid depletion of tin at the contact area due to high temperature. They considered the melting temperature of tin as a scuffing criterion for aluminum-tin bearings.

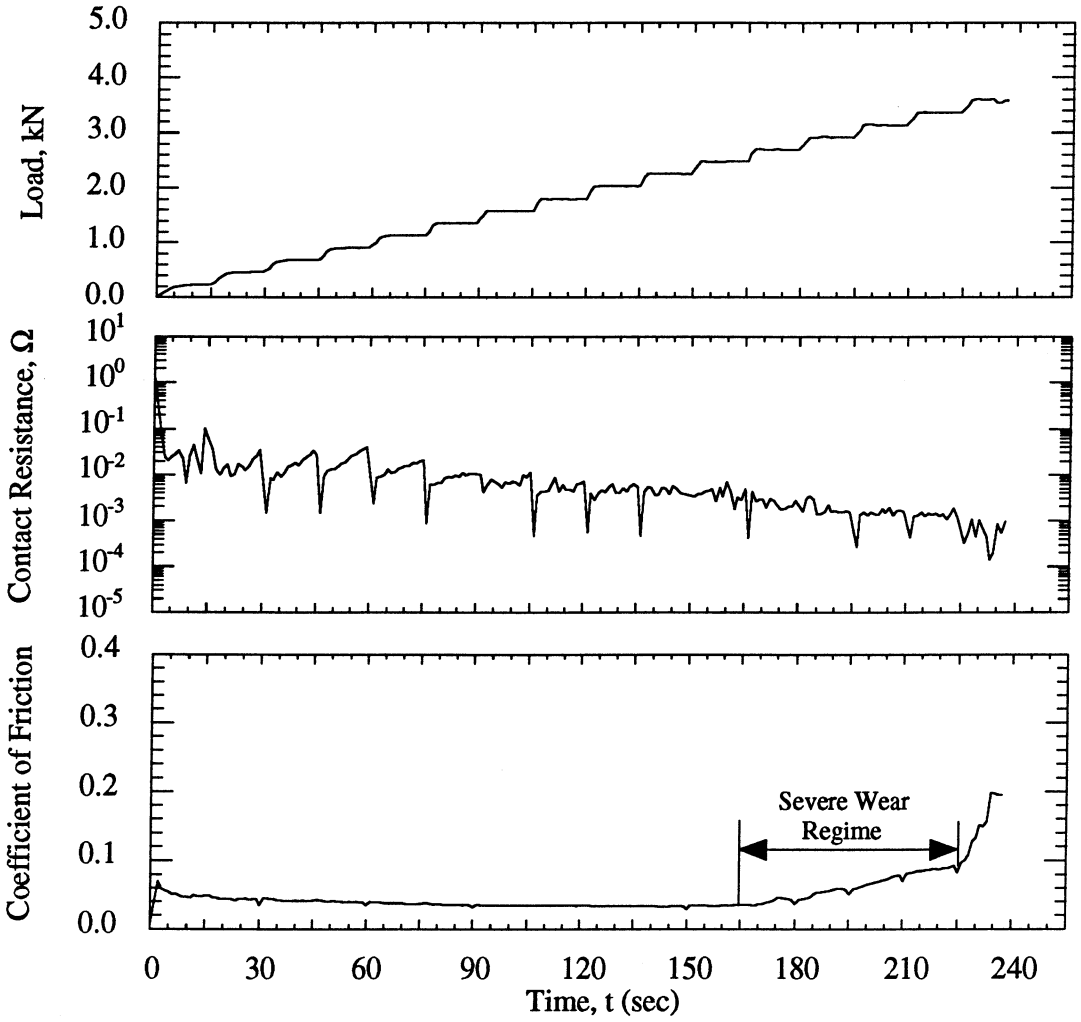

Fig. 3.12 - Typical scuffing test data for a 390 tin-coated aluminum disc

LSR = 40 mg/min, V = 3.72 m/s

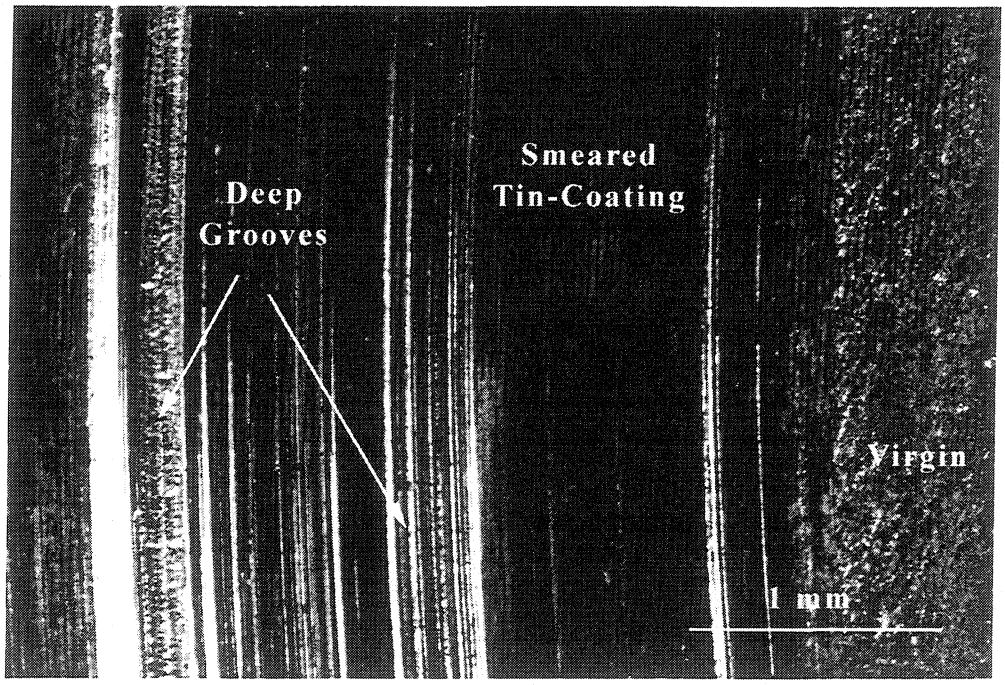

(a)

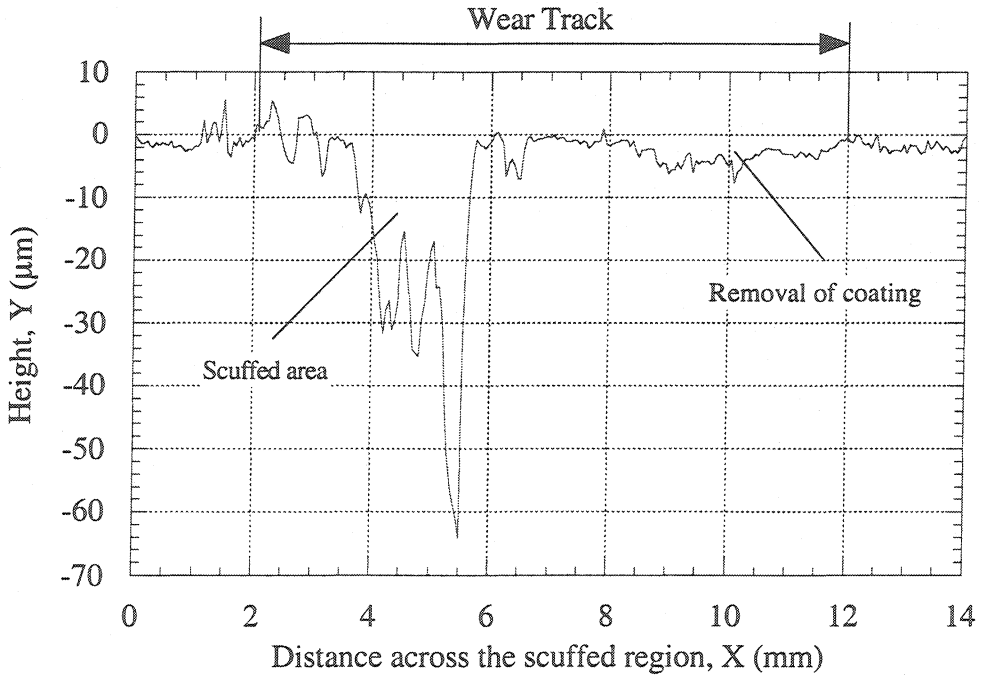

(b)

Fig. 3.13 - (a) Typical scuffed tin-coated Al disc and (b) its corresponding surface profile

3.5 Effect of Socket Geometry Supporting the Shoe

The lubrication condition at shoes/plate contacts might be affected by the geometry of the socket supporting the shoe. Ideally, the shoe/socket contact should be frictionless so that there is no significant resisting moment to affect the orientation of the shoe. This is especially critical under hydrodynamic lubrication condition. In order to examine the effects of the resisting moment, due to the friction at the shoe/socket interface, on scuffing, two socket geometries were examined. A schematic of the socket geometries is given in Fig. 3.14. For the existing socket geometry, the contact is near the bottom of the shoe, resulting in a relatively small resisting moment. For the other socket geometry, the contact is near the top of the shoe. This contact will give a larger resisting moment than that in the existing socket. Scuffing data for these geometries, at a function of sliding velocities, are given in Fig. 3.15. Except for one data point for the existing socket geometry at 60 mg/min, scuffing pressures are about the same for both socket geometries. Since the hydrodynamic effect is more dominant at higher velocities and lubricant supply rates, it is possible that the effects of socket geometry supporting the shoe, if any, is more apparent at those conditions. Due to the limiting sliding velocity and load capacities of the HPT, scuffing data at higher velocities and lubricant supply rates could not be obtained.

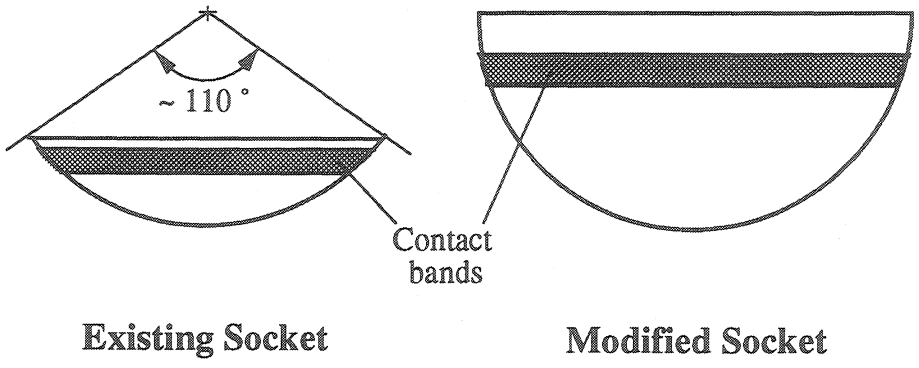

Fig. 3.14 - Schematic of the socket geometries

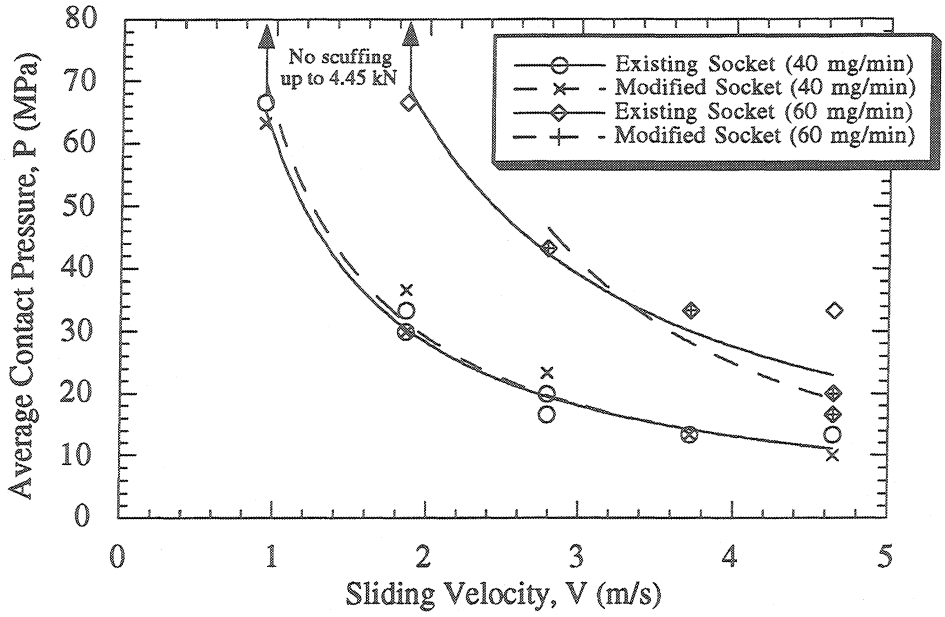

Fig. 3.15 - Effect of socket geometry supporting the shoe on scuffing pressure as a function of sliding velocity

3.6 Examination of Scuffed Surfaces with SEM and AES

The scuffed surfaces of the uncoated discs were examined using SEM and AES. A typical scuffed surface of the disc and aluminum transfer on the counterface steel shoe are shown in Fig. 3.16. Figure 3.16(a) shows small grooves caused by plastic shearing in the scuffed region. When scuffing occurs, due to the macroscopic adhesions formed at the sliding interface, some aluminum material is smeared to the counterface steel shoe, resulting in macroscopic cold welds as shown in Fig. 3.16(b). Figure 3.17 shows an AES depth profile obtained by sputtering the top of the smeared aluminum on the steel shoe. The purpose of the profile is to examine the chemical compositions of the smeared material. It is seen that the concentration of aluminum is almost constant until a depth of 0.43 μm, a typical thickness of the smeared aluminum. Oxygen decreases rapidly up to a depth of 0.06 μm, after which it remains at a concentration level which is considered to be in the noise range. However, there is a small increase in the amount of oxygen at the aluminum/steel

interface (0.5 - 0.6 μm depth). This suggests that there may be a thin oxide film between the transferred aluminum and steel shoe.

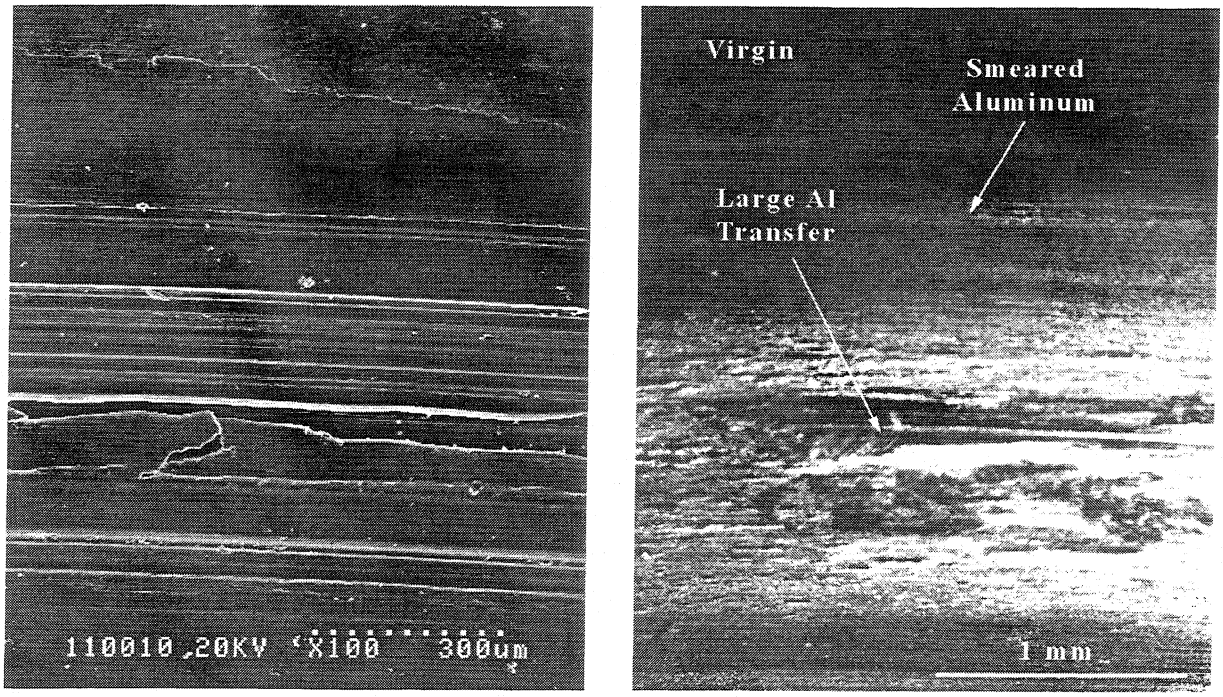

(a) (b)

Fig. 3.16 - (a) Typical scuffed 390-T6 Al surface and (b) material transfer on the steel shoe

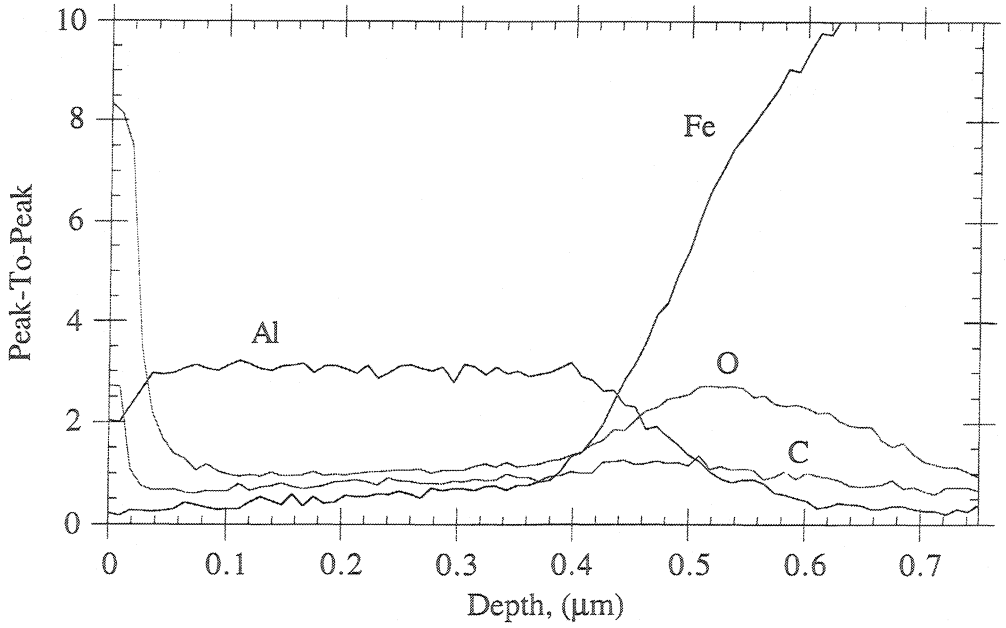

Fig. 3.17 - An AES depth profile of the smeared aluminum on the steel shoe

It is also typical that, due to gross plastic deformation during the scuffing process, the subsurface is damaged. The scuffed area of the specimen shown in Fig. 3.16(a) is sectioned along the direction of sliding and the subsurface is examined. Figure 3.18 shows that both cracks and voids are formed in the subsurface. Also, it is seen that all the features are oriented in the direction of sliding, and silicon particles are fractured due to the large plastic strain at the sliding surface. Scuffed surfaces and subsurfaces of the test specimens will be examined in more details in Chapter 5, where the pin-on-disc data are presented.

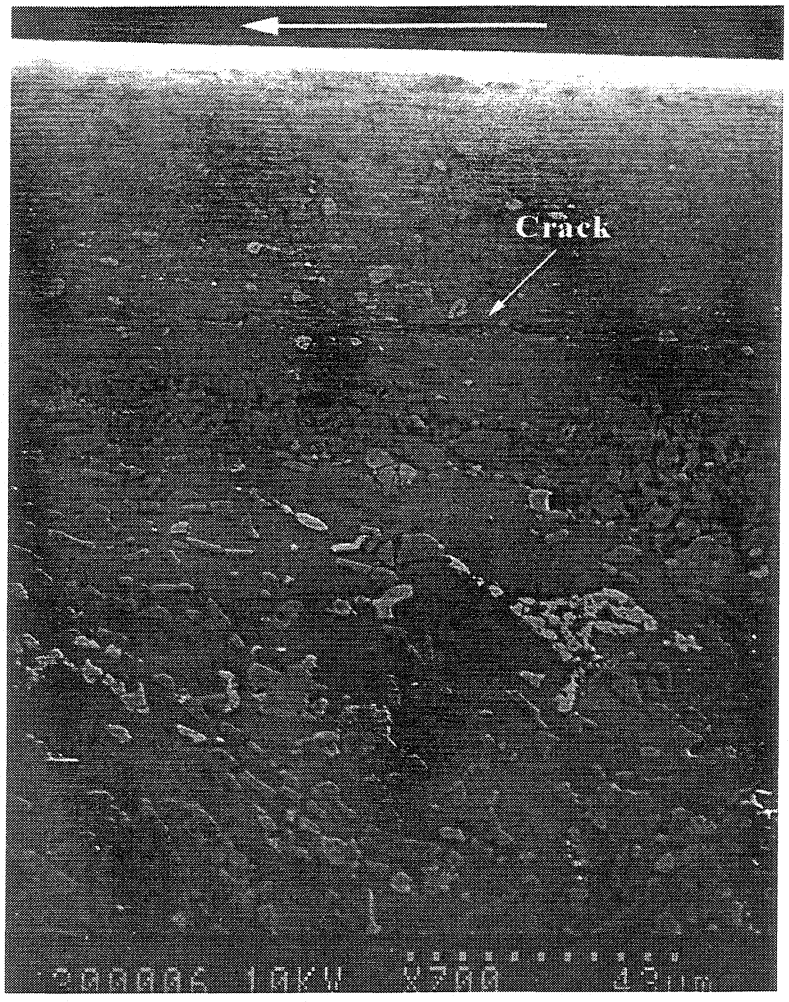

Fig. 3.18 - Subsurface damage of 390-T6 Al disc after scuffing

CHAPTER 4

EXPERIMENTAL RESULTS - PART II (PIN/DISC GEOMETRY)

In this chapter, a pin-on-disc geometry is used to facilitate a more fundamental study of the scuffing process. The data obtained will be used in Chapters 5 and 7 to more fully characterize scuffing failures and to propose a scuffing hypothesis. Scuffing data for 390-T6 and DHT3 aluminum alloys, Si-Pb brass and gray cast iron, sliding against 1018 carburized steel, are obtained under starved lubrication conditions. All these materials are used in critical contacts of various refrigerant compressors. Most of the tests were conducted with 390-T6 aluminum. The choice of 1018 carburized steel for the counterface was somewhat arbitrary. Since the focus of this chapter is on the fundamental study of the scuffing process, it is believed that the type of steel used for the counterface will not significantly affect the general behavior of the contact. Also, the same material was used in a previous study [57] for tests conducted under dry sliding conditions. Therefore, the results obtained in this study can be compared to those obtained under dry sliding conditions. As indicated previously, a pin specimen was used because it is more suitable for a fundamental study. The effects of material, lubricant/refrigerant (L/R) mixture, and loading history on scuffing were examined. Scuffing data were based on initial sharp transitions of the friction coefficient, the contact resistance, and subsurface temperature measured 2 mm below the surface. However, it was observed that, for a certain range of lubricant starvation, a second transition occurs if the load is further increased. Therefore, the transition behavior of a 390-T6 aluminum pin as a function of lubricant supply rate was also examined. Typical scuffing failure of a pin-on-disc contact is shown in Fig. 4.1. As with scuffed surface of a shoe-on-disc contact presented in Fig. 3.1 (Chapter 3), when scuffing occurs, part of the surface of the softer material is often destroyed, and some material transfer occurs from the pin to the counterface steel disc. In some cases, increased noises and vibrations occur in the process of scuffing.

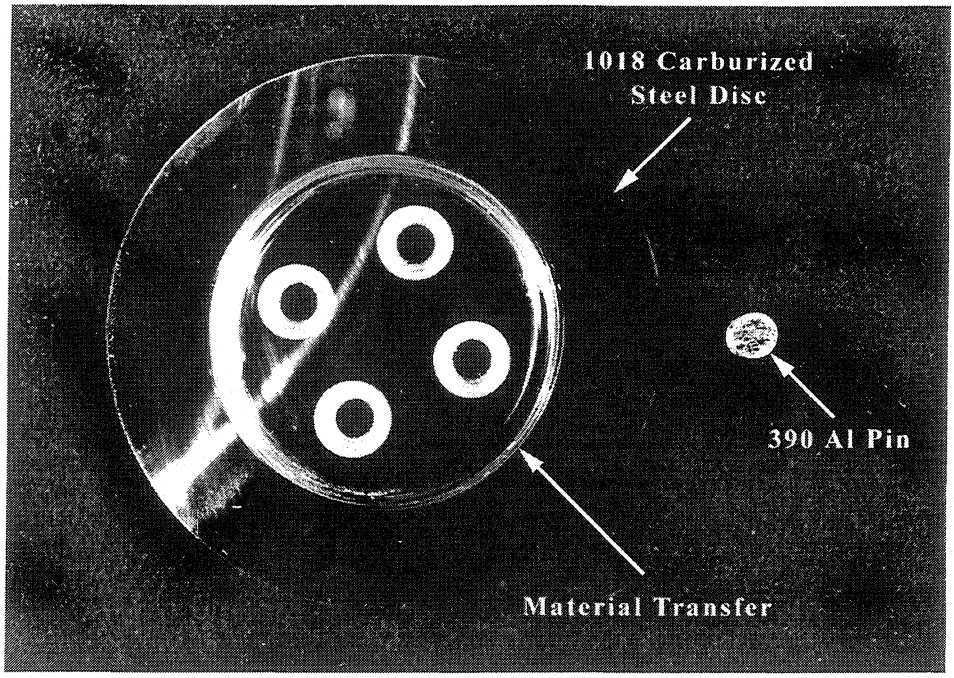

Fig. 4.1 - Typical scuffing failure of a pin-on-disc contact

4.1 Effect of the Material

The scuffing behavior of pins made from aluminum, brass and gray cast iron sliding against 1018 carburized steel is examined using a base PAG/R134a mixture. The scuffing resistance of 390-T6 and DHT3 aluminum alloys tested with various lubricant supply rates is given in Fig. 4.2. As with the results presented in Fig. 3.2 (Chapter 3), the contact pressure at scuffing increases as the lubricant supply rate increases. From the figure, it is evident that, for all lubricant supply rates used, the scuffing resistance of 390-T6 aluminum alloy is better than that of the DHT3 alloy. This can probably be attributed to its higher strength and silicon content. The subsurface temperatures at scuffing are also given in the figure. The data show that the subsurface temperature at which scuffing occurs changes with the materials and the amount of lubricant supplied to the contact region. The subsurface temperatures at scuffing tend to increase as the contact pressure increases. This indicates that, for the given conditions, the frictional heat generated due to the higher contact pressure dominates that which is dissipated due to the higher lubricant supply rate.

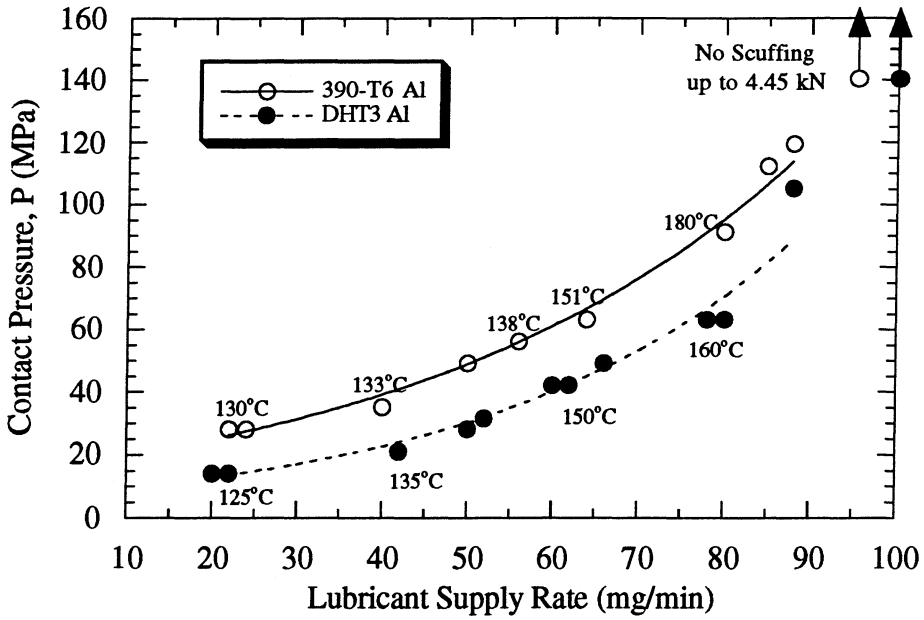

Fig. 4.2 - Scuffing results for aluminum alloys under various lubricant supply rates

Lubricant/Refrigerant mixture: PAG/R134a; V = 1.86 m/s

Temperature given are obtained just before scuffing

The friction coefficient data at scuffing are plotted as a function of the lubricant supply rate in Fig. 4.3. For both aluminum alloys tested, the coefficient of friction at scuffing decreases as the lubricant supply rate increases. Due to the limiting load capacity of the HPT (4.45 kN), for the given conditions, scuffing data could not be obtained if the lubricant supply rates are higher than 90 mg/min, as shown in Fig. 4.2. It should also be noted that, for the area contact geometry tested, scuffing does not seem to occur if the contact is well lubricated. For example, tests conducted with a 390-T6 Al pin, under fully lubricated conditions, showed that scuffing does not occur before the compressive yield strength of the bulk material is reached. It is believed that macroscopic adhesions at the sliding interface, which leads to scuffing, do not form with well lubricated area contacts.

The scuffing PV curves for the four materials tested are shown in Fig. 4.4. For these tests, 0.07 % by weight of a base PAG lubricant in R134a was used with a lubricant supply rate of 45 mg/min. For all materials tested, the scuffing pressure decreases as the sliding

velocity increases. Due to the limiting speed capacity of the HPT, scuffing data at velocities higher than 4.65 m/s could not be obtained. At any given sliding velocity, the scuffing resistance of the 390-T6 is again better than that of the DHT3 alloy. The scuffing pressure of Si-Pb brass and gray cast iron is about the same and the scuffing resistance of these materials is better than that of the aluminum alloys tested. With the exception of the 390-T6 aluminum alloy, the curve fits of the data points are close to the PV = *constant* relationship, where P is the contact pressure based on the apparent area and V is the sliding velocity. The data points for 390-T6 Al slightly deviate from the PV = *constant* relationship. It should be noted that, for a given material, the subsurface temperatures just before scuffing are approximately constant. Note that the heat flux (q) generated at the sliding surface is given by $q = \mu PV$, where μ is the coefficient of friction. Since the data follow the $PV = C$ curve and the coefficient of friction is approximately constant until scuffing occurs, then the heat generated is approximately constant at scuffing for a given material as shown in Table 4.1. Since the same machine and specimen holder were used for all tests, for a given material, these conditions result in a constant subsurface temperature at scuffing. The subsurface temperatures just before scuffing for Si-Pb brass and gray cast iron are typically in the range of 140-150°C and 160-170°C, respectively. It should be noted that the subsurface temperatures of the gray cast iron are generally higher compared to those of the Si-Pb brass even though their scuffing PV's are about the same. This is attributed to higher friction coefficients of gray cast iron compared to those of Si-Pb brass as shown in Table 4.1. The sliding surface of Si-Pb brass tends to smoothen very quickly during the rubbing process. This is due to the soft lead in the material. Even though the initial surface roughness of gray cast iron is slightly higher than that of Si-Pb brass as given in Table 4.2, the surface of Si-Pb brass at one load step before scuffing is much smoother than that of gray cast iron, as shown in Fig. 4.5. Tiwari et al. [48] also found that the addition of lead to aluminum alloys reduce interface friction and improve their ability to resist seizure. It is

believed that the lead contained in Si-Pb brass similarly affects the tribological behavior of Si-Pb brass material.

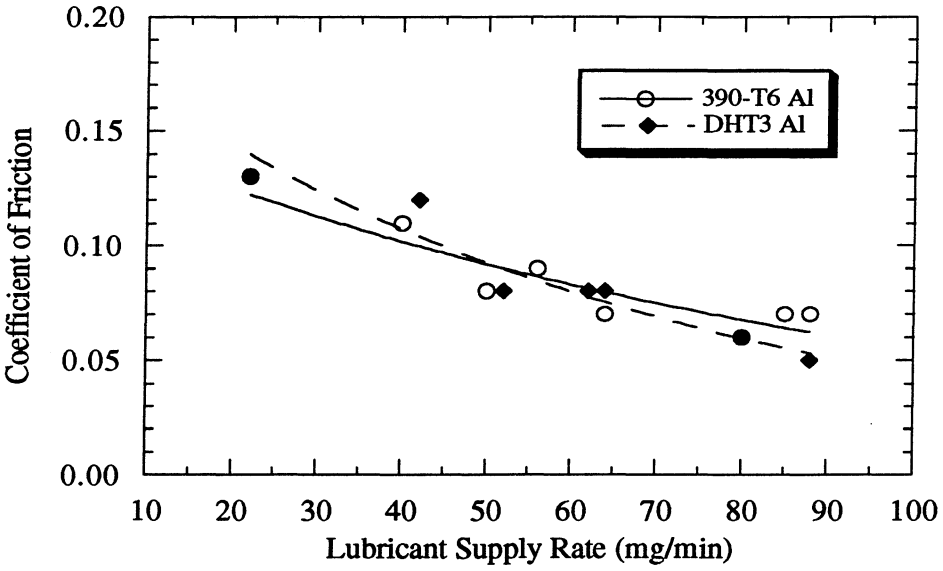

Fig. 4.3 - The friction coefficient data as a function of the lubricant supply rate

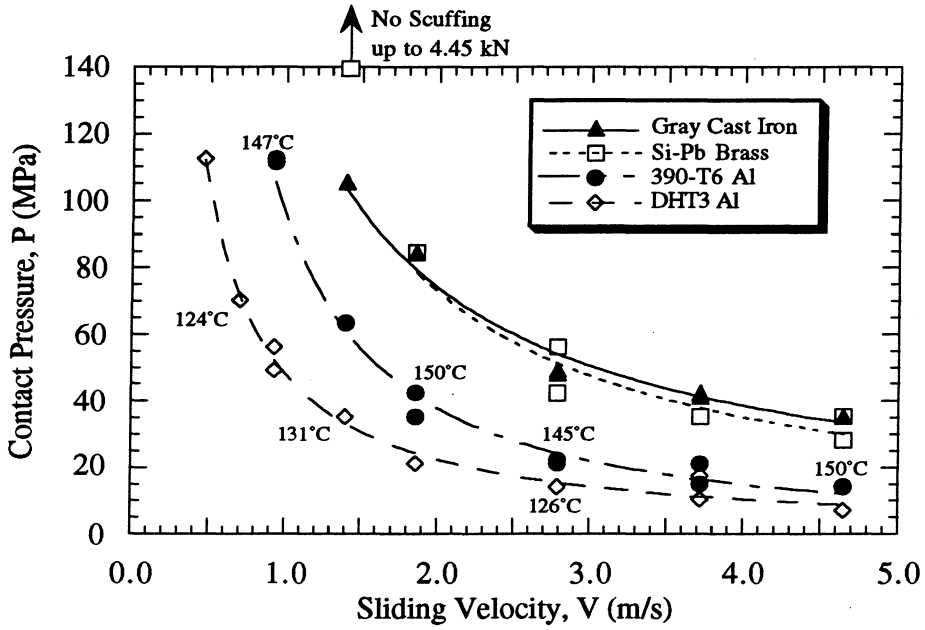

Fig. 4.4 - Scuffing *PV* for various materials tested

Lubricant/Refrigerant mixture: PAG/R134a

Lubricant % in L/R mixture: 0.07 weight %; LSR = 45 mg/min.

Temperatures given are obtained just before scuffing.

Table 4.1 - Scuffing *PV* and friction coefficient data for the materials tested

Material	*V* (m/s)	*P* (MPa)	μ	μ*PV* (W/mm^2)
Gray Cast Iron	1.40	105.5	0.10	14.8
	1.86	84.4	0.11	17.3
	2.79	49.2	0.12	16.5
	3.72	41.2	0.11	16.9
	4.65	35.2	0.10	16.4
Si-Pb Brass	1.86	84.4	0.07	10.9
	2.79	42.2	0.07	8.24
	3.72	35.2	0.06	7.86
	4.65	28.1	0.07	9.15
390-T6 Al	0.93	112.5	0.09	9.42
	1.40	63.3	0.09	7.99
	1.86	42.2	0.12	9.42
	2.79	21.1	0.13	7.65
	3.72	21.1	0.11	8.63
	4.65	14.1	0.17	11.1
DHT3 Al	0.47	112.5	0.07	3.70
	0.70	70.3	0.07	3.44
	0.93	56.2	0.09	4.70
	1.86	21.1	0.09	3.53
	2.79	14.1	0.14	5.51
	3.72	10.5	0.12	4.69
	4.65	7.03	0.15	4.90

Table 4.2 - Initial surface roughnesses of pin specimens tested

390-T6 Al	DHT3 Al	Si-Pb Brass	Gray Cast Iron
0.62-0.70 μm Ra	0.67-0.75 μm Ra	0.69-0.78 μm Ra	0.83- 0.92 μm Ra

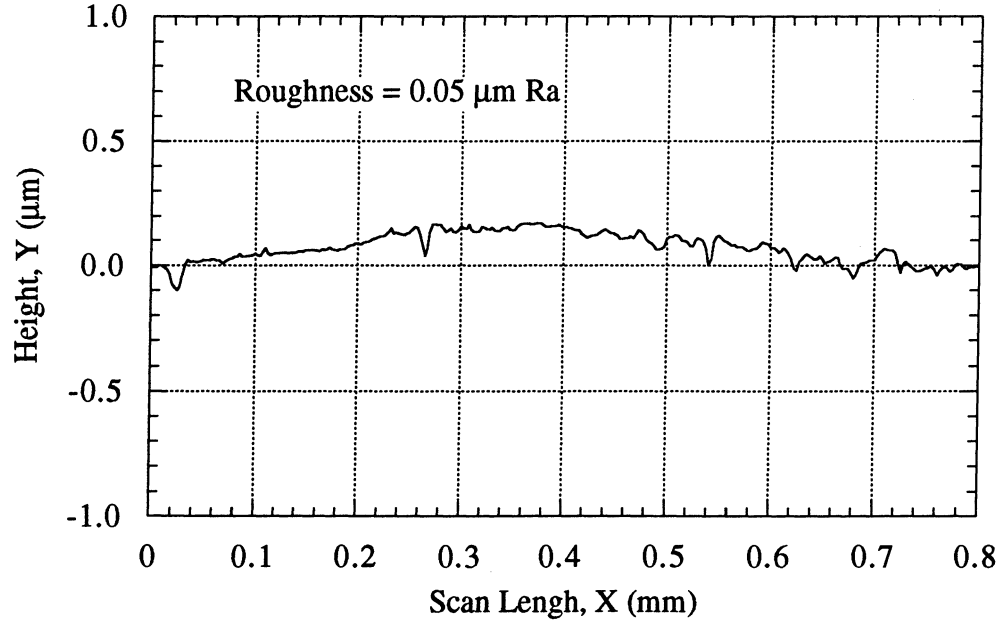

(a)

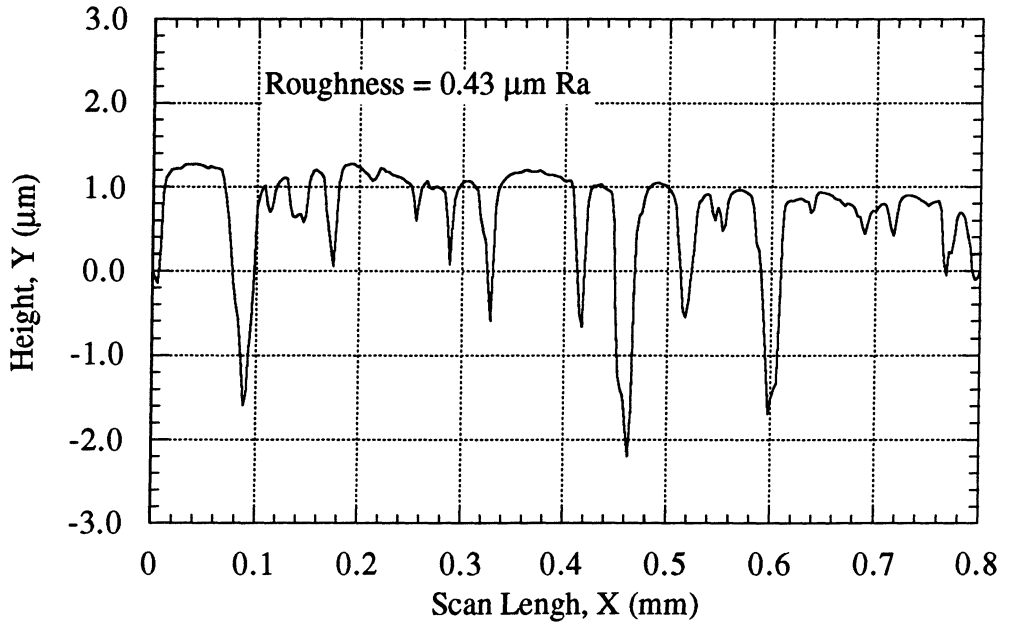

(b)

Fig. 4.5 - Typical surface profiles of (a) Si-Pb Brass and (b) gray cast iron before scuffing

P = 35.2 MPa, V = 3.72 m/s

4.2 Effect of the L/R Mixture

All the data presented so far have been obtained using a base PAG lubricant. Another widely used family of lubricants in compressors of air conditioning and refrigeration systems are the POE's. From the previous study [61], it was found that the lubricity of a base POE was consistently better than that of a base PAG for all the aluminum alloys tested. This was attributed to the tendency of a POE forming bidentate bonds on the aluminum surfaces. The bidentate bond is known as a cyclic bonding of the lubricant molecules with the aluminum atoms at the metal surface [62]. The bidentate structure forms two bonds instead of one to each aluminum atom. Hotten [62] and Laemmle et al. [63] have proven that aluminum is able to form strong bidentate bonds with some polar organic compounds such as pentaerythriol partial esters. The molecules orient themselves vertically, thus forming a layer which protects the surface. In fact, esters have proved to be very effective lubricants for aluminum surfaces [64-66]. In general, lubricant additives also improve the friction and wear characteristics by forming a stable and durable adsorbed film through chemical interaction with the metal surface. The extreme pressure (EP) additives, for example, are designed to react with metal surfaces under extreme conditions of load and velocity creating protective, low shear strength surface films, which reduce friction and wear. Carefully chosen additives are extremely effective in improving the performance of an oil.

In order to examine the effects of lubricants and additives on scuffing, 390-T6 aluminum alloy sliding against 1018 carburized steel is tested with a base POE/R134a, a base PAG/R134a and a formulated PAG/R134a mixtures. The lubricant supply rate for all tests conducted was again 45 mg/min. The results obtained from these tests are shown in Figs. 4.6 and 4.7. The scuffing pressures of 390-T6 aluminum alloy tested with both a base POE/R134a and a formulated PAG/R134a mixtures are higher than those of the aluminum alloy tested with a base PAG/R134a mixture. Probably the bidentate bonds formed on the aluminum surface with a base POE improved the scuffing resistance of the aluminum alloy. The formulated PAG contains a phosphorus compound and other additives. Phosphorus is

one of the widely used extreme pressure (EP) additives. It was found [67] that, if phosphorus is combined with other additives such as sulfur, scuffing load obtained with steel surfaces increases significantly. Therefore, it is possible that the films formed by these additives can also improve the scuffing characteristics of the aluminum surface.

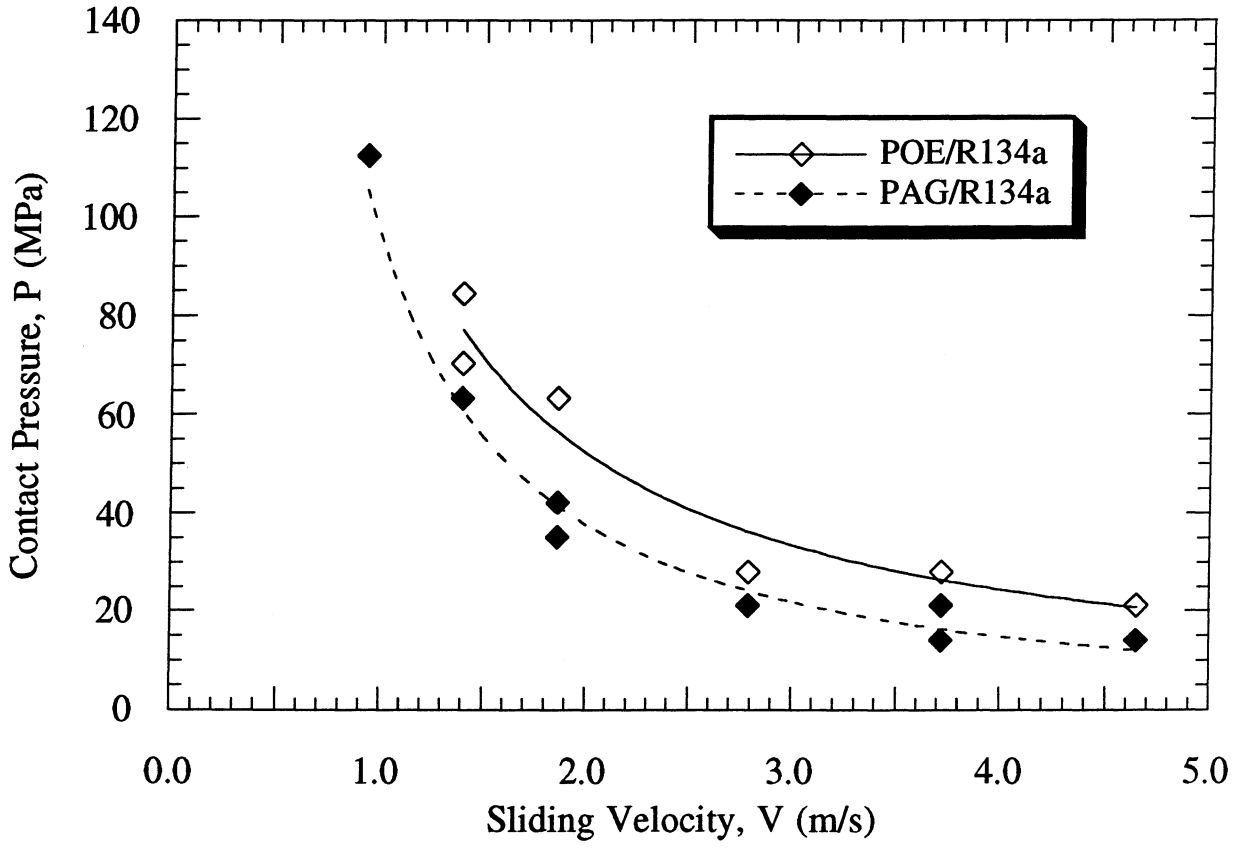

Fig. 4.6 - Scuffing results for 390-T6 Al tested with a base POE/R134a and a base PAG/R134a

Lubricant % in L/R mixture: 0.07 weight %; LSR = 45 mg/min.

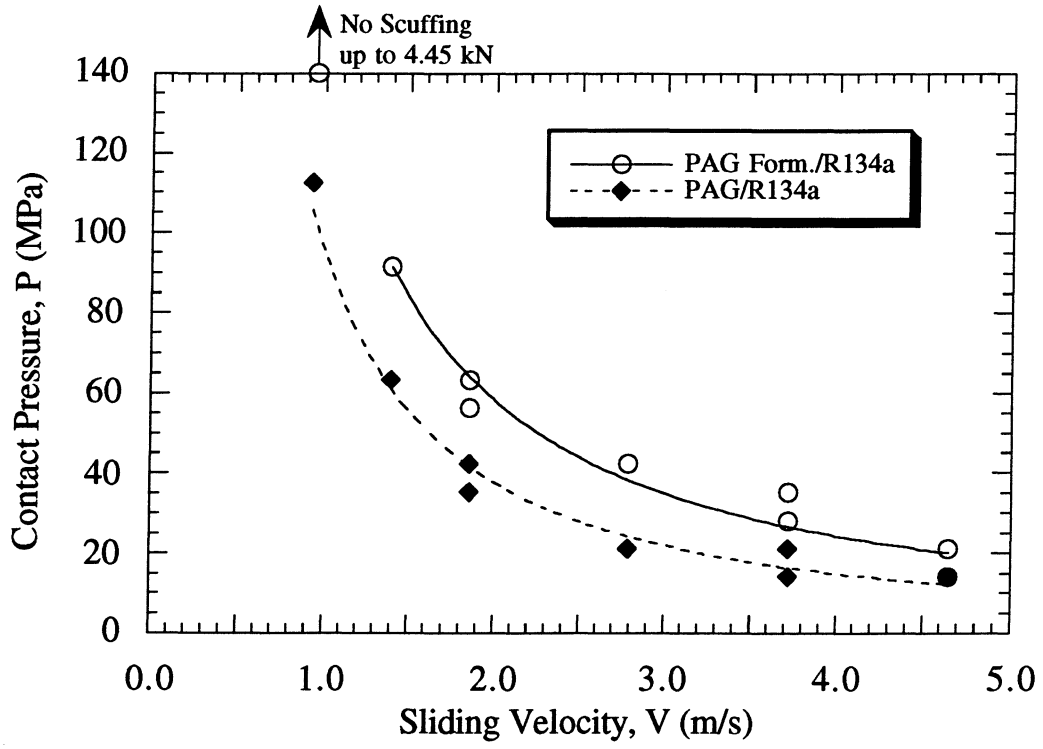

Fig. 4.7 - Scuffing results for 390-T6 Al tested with a base PAG/R134a and a formulated PAG/R134a mixtures

Lubricant % in L/R mixture: 0.07 weight %; LSR = 45 mg/min.

4.3 Loading History Effects on Scuffing of 390-T6 Aluminum Alloys

For step-loading tests, it is likely that scuffing results vary depending on the magnitude of load step and step duration. For example, in a previous study [57] for tests conducted under dry sliding conditions, it was found that the time to scuffing at a given load step was a function of load level, as shown in Fig. 4.8. As the load level increased, the time to scuffing was reduced. A longer step duration, at a given load, also seems to be slightly detrimental. It was hypothesized that scuffing under dry sliding conditions is due to a subsurface failure by fatigue. Therefore, this phenomenon was explained by damage accumulation in the subsurface.

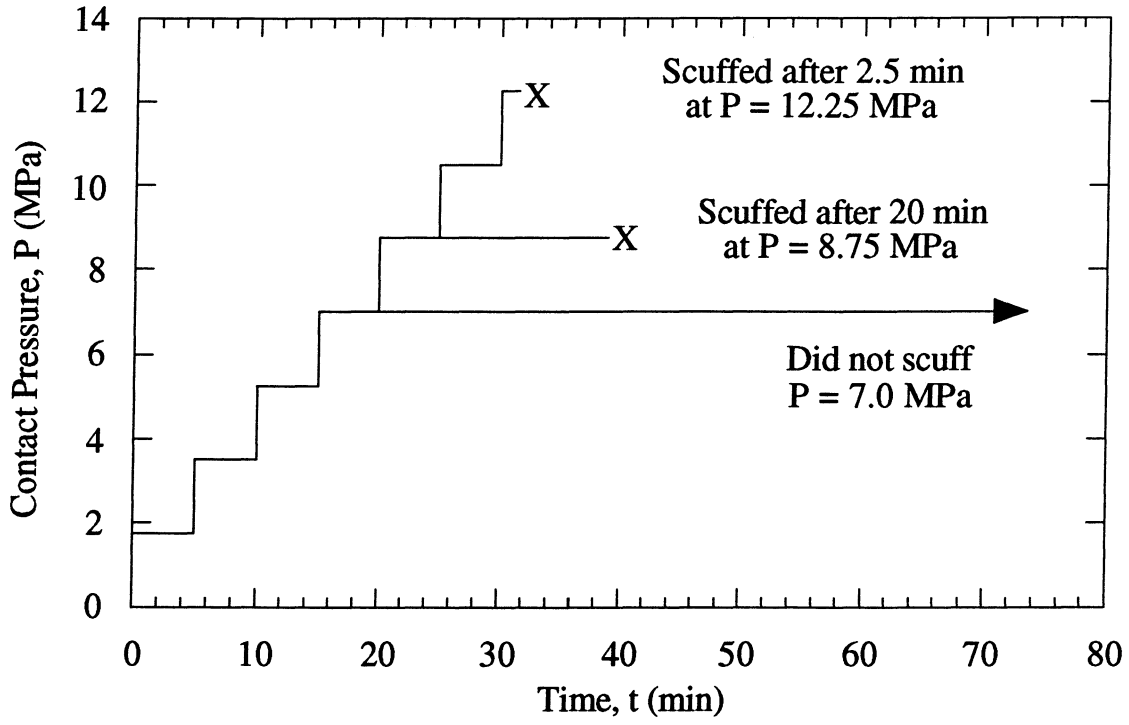

Fig. 4.8 - Loading history effects on scuffing of 390-T6 Al alloy under dry sliding conditions

V = 0.66 m/s, Environmental temperature: 30 °C, Environment: Air, Ref. [57]

In order to examine the effects of loading history under starved lubrication conditions, three series of tests were conducted using 390-T6 Al alloy. For all three series, the load was increased in steps of 222.5 N. In the first series, as with the tests conducted under dry sliding condition shown in Fig. 4.8, tests were conducted by increasing the load stepwise up to one load step below the pre-determined scuffing load, using 15 seconds step duration, and then maintaining the load constant for a reasonably long test duration. A typical result is shown in Fig. 4.9. The figure shows that, for the given lubricant supply rate, scuffing did not occur after 20 minutes at this load level. As shown in Fig. 4.10, the contact resistance, friction coefficient and subsurface temperature are approximately constant during the 20 minutes. The surface of the pin after the test, given in Fig. 4.11, shows many black patches which indicate surface

films formed on top of the asperities. As a result of local plastic deformation of these asperities, some surface smoothening is also obtained. Due to the volume limitation of the pressure vessel used and a large consumption of refrigerant, longer tests were not conducted.

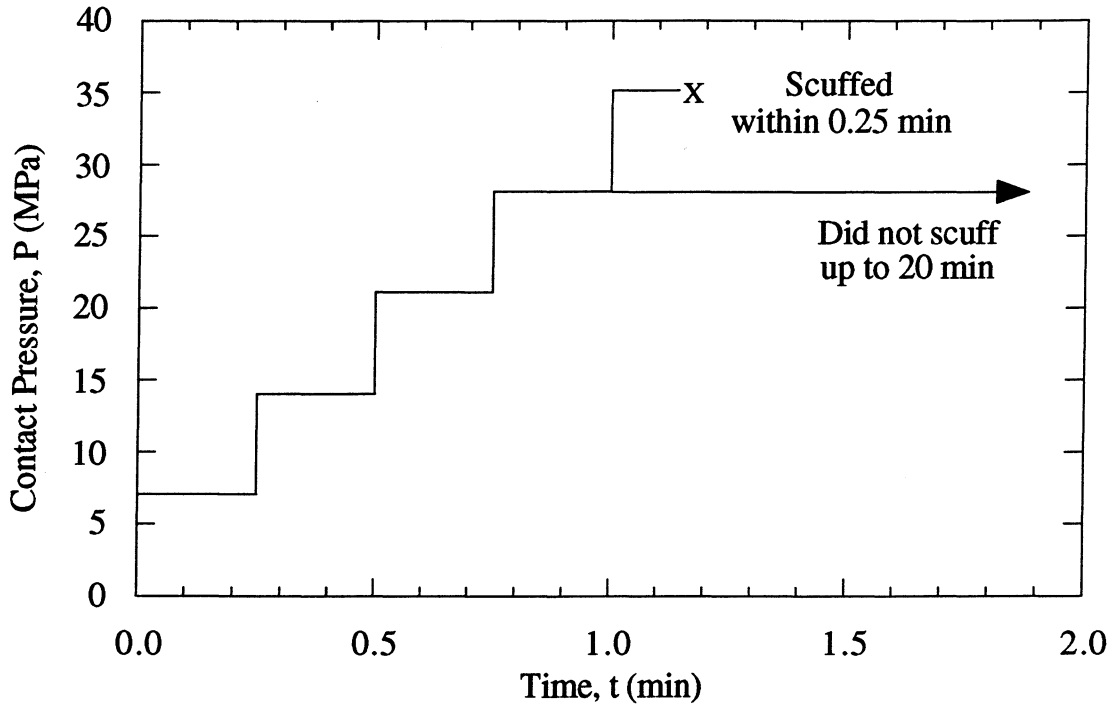

Fig. 4.9 - Loading history effects on scuffing of 390-T6 Al alloy

under starved lubrication conditions

LSR = 45 mg/min, V = 1.86 m/s, L/R mixture: PAG/R134a

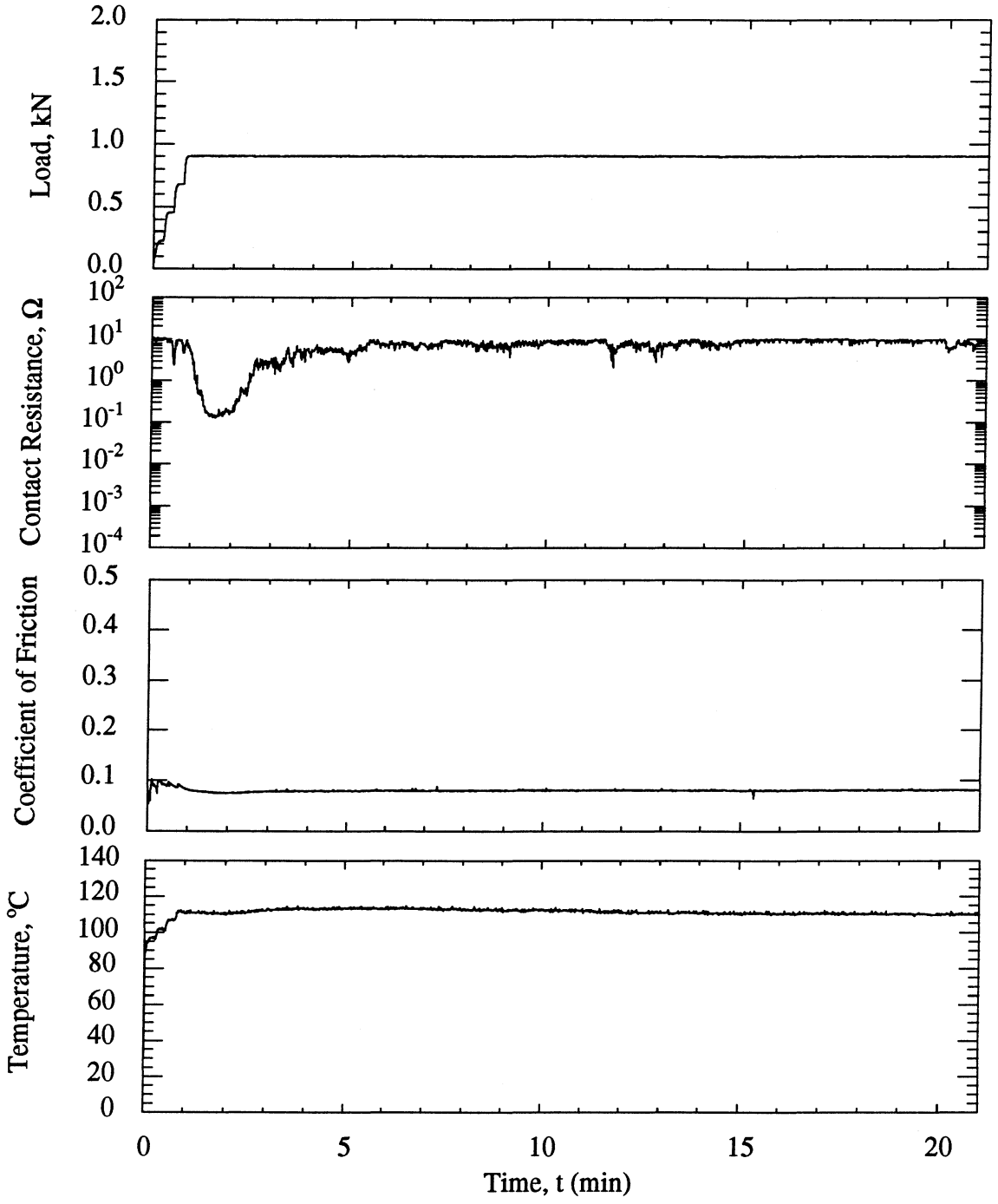

Fig. 4.10 - Typical test data for loading history effects on scuffing of 390-T6 Al

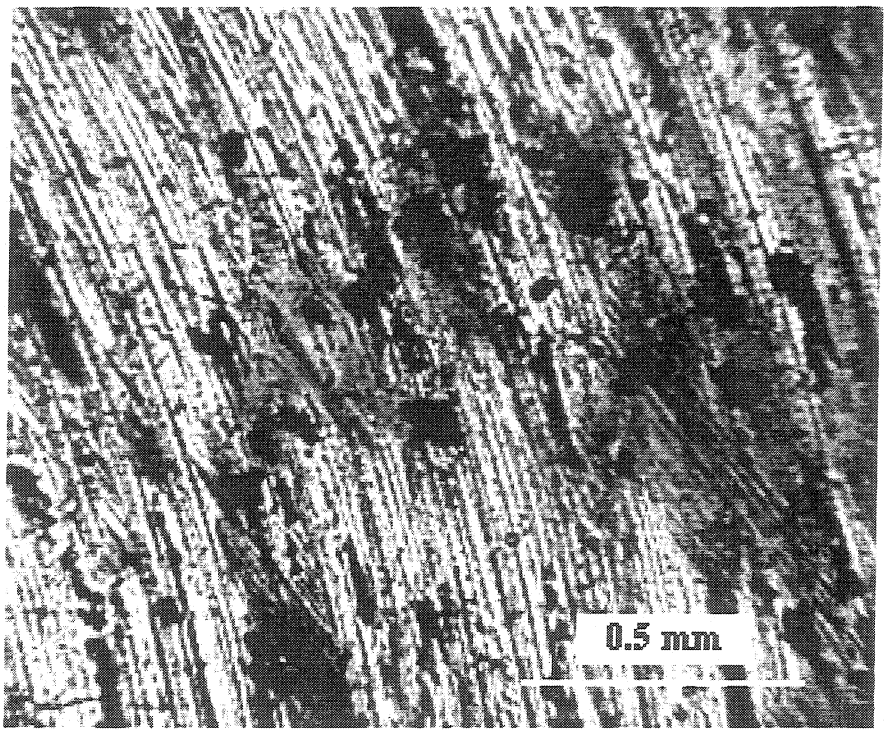

Fig. 4.11 - Surface of 390-T6 Al after 20 minute at one load step below scuffing

For the data presented up to now, a step duration of 15 seconds was used since a steady state temperature condition is reached after approximately 10 seconds under starved lubrication conditions. However, it is possible that scuffing data can be affected by the step duration. In the second series of tests, scuffing data were obtained using a single step immediate loading, and a 0.25 minute, 1 minute and 2 minutes steps. As indicated in Fig. 4.12, the lowest scuffing load is obtained with the immediate loading. This indicates the beneficial effect of running-in of machine components. The results also show that the average scuffing load reaches a plateau if the step duration is higher than 1 minute. The increase of the scuffing load with step duration is attributed to the formation of protective films and surface smoothening, as previously noted. Typical surfaces of pin specimens for both 0.25 and 2.0 minute-step tests, at the given P and V, are shown in Fig. 4.13. This figure clearly shows that the size of the locally-deformed areas (black patches) increases as the step

duration increases. Even though not shown, more surface smoothening is also obtained as the step duration increases.

As previously indicated, a step duration of 15 seconds was used in this study since, under starved lubrication conditions, a steady state temperature is reached after approximately 10 seconds. Even though Fig. 4.12 shows that different results can be obtained if a different loading history is used, the data presented in this study are still valid because it is a comparative study and it is also believed that actual failure of a component cannot be easily characterized in time-history fashion.

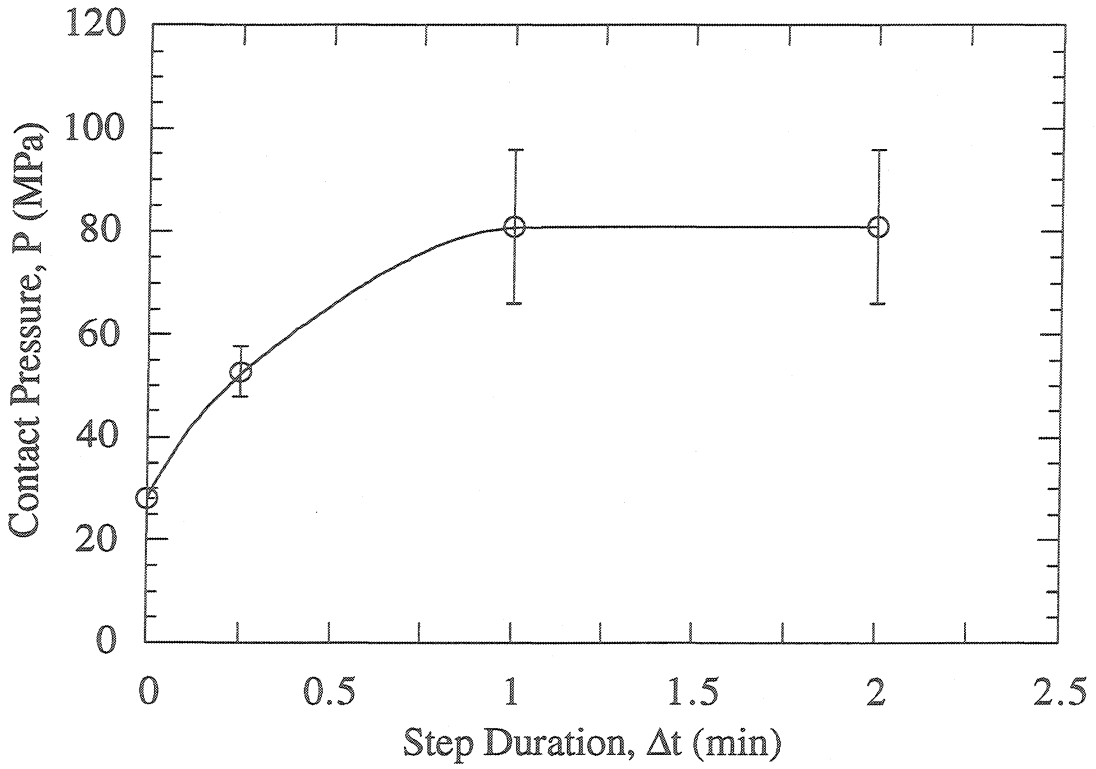

Fig. 4.12 - Effect of loading history on scuffing of 390-T6 Al alloy

LSR = 50 mg/min, V = 1.86 m/s

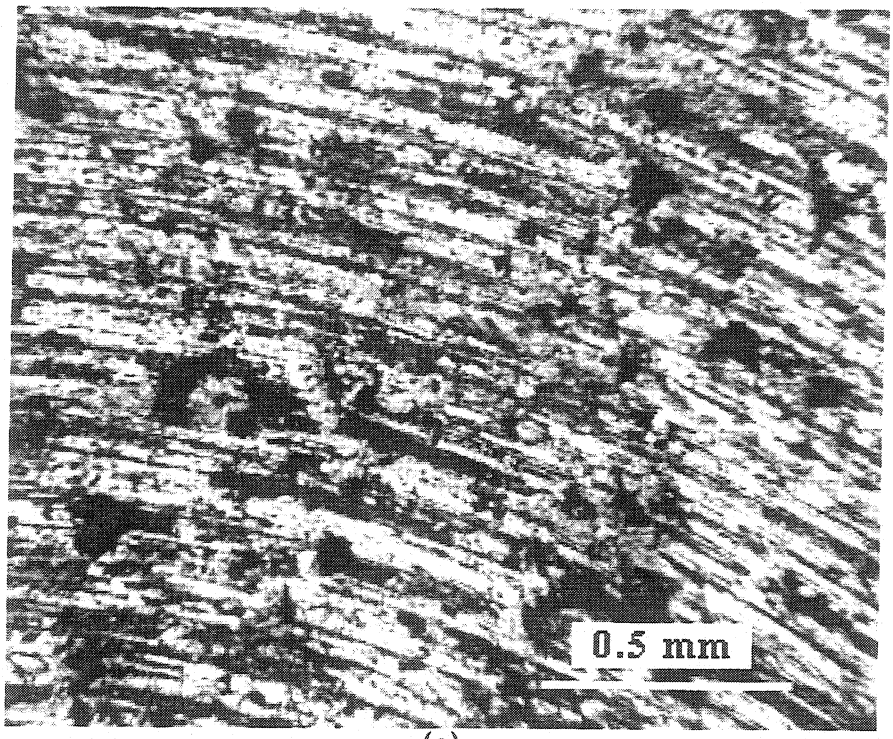

(a)

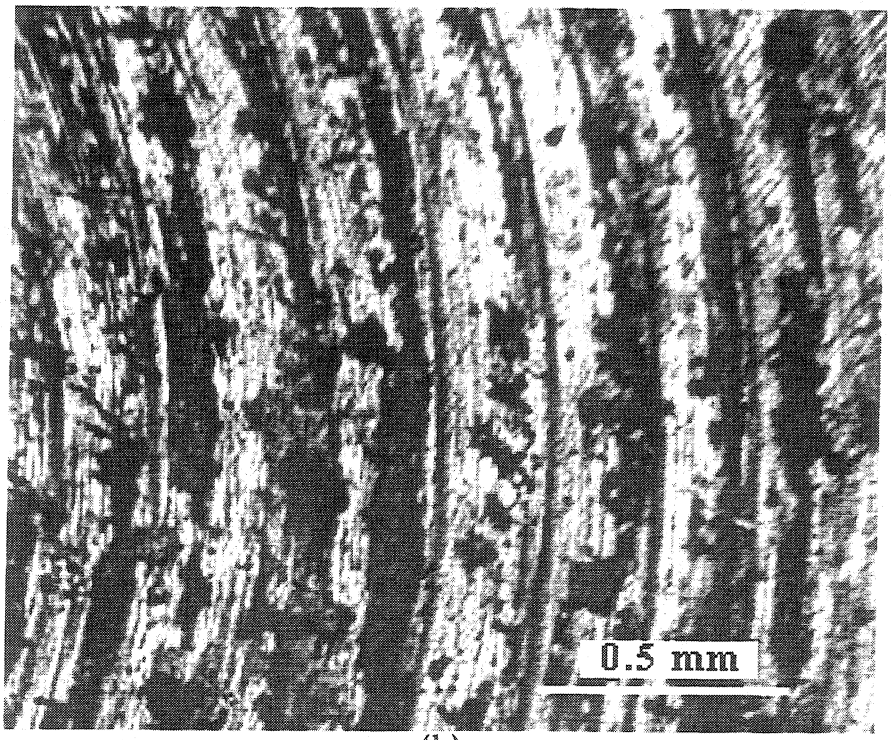

(b)

Fig. 4.13 - The surfaces of 390-T6 pin specimens at one load step below scuffing

(a) 0.25 minute-step, (b) 2.0 minute-step

P = 42.2 MPa, V = 1.86 m/s, LSR = 50 mg/min

In general, it is known that running-in can improve the scuffing resistance of sliding components. The running-in process is a rather complex problem because it is affected by many variables such as run-in load, sliding velocity, initial surface roughness, lubricant used, lubrication condition, etc. The purpose of the third series of tests is to examine the effect of initial running-in time on scuffing. For these tests, the load was maintained constant at 445 N (30 % of a scuffing load) for 0.25, 10 and 20 minutes, and then increased again stepwise until scuffing occurs. A typical result is shown in Fig. 4.14.

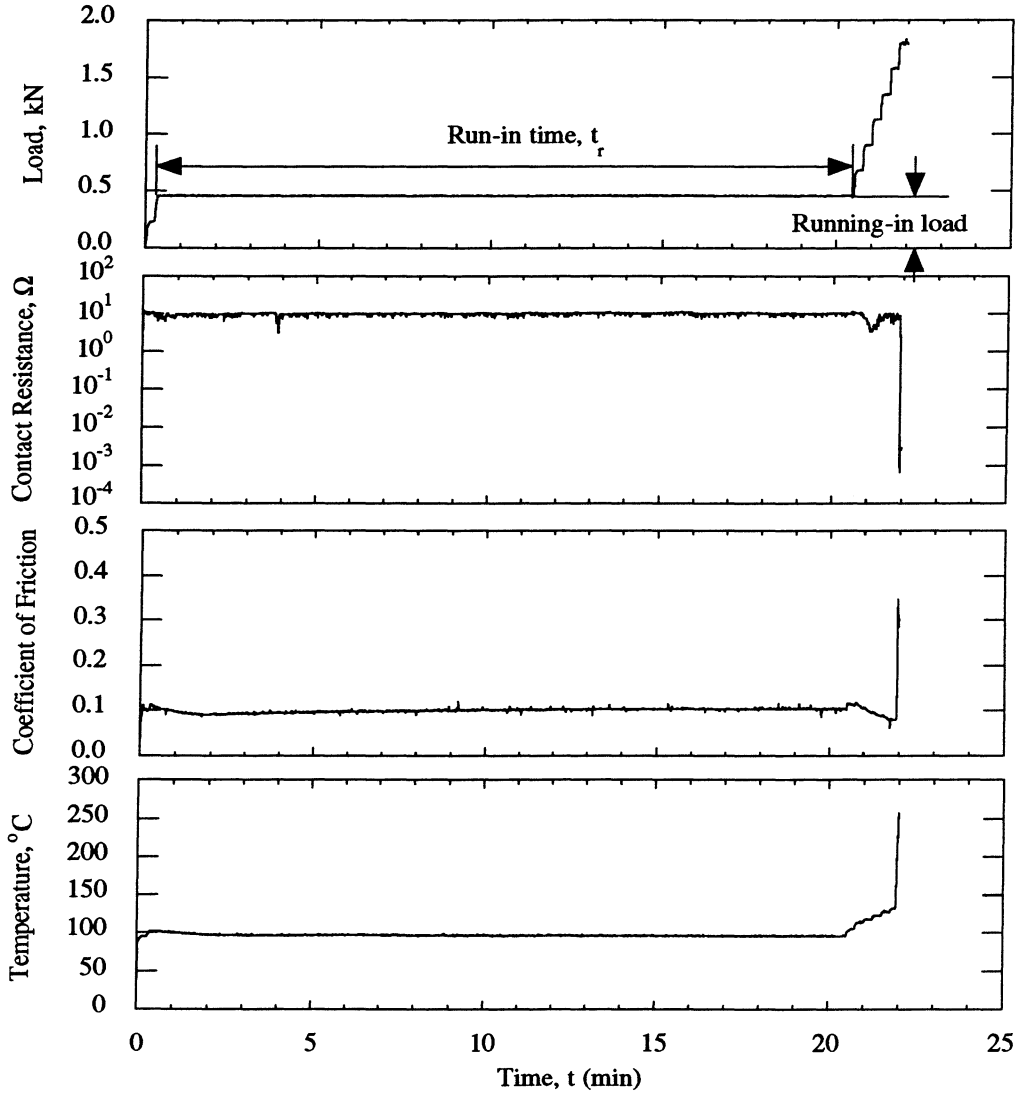

Fig. 4.14 - Typical test data for the run-in effect on scuffing of 390-T6 Al

Run-in load = 445 N, LSR = 50 mg/min, V = 1.86 m/s

As shown in Fig. 4.15, for given test conditions, the scuffing pressure increases as the time duration at a constant load (445 N) increases. Again, this can be due to the formation of a relatively uniform protective surface film (black areas) and surface smoothening during a long step duration, as shown in Fig. 4.16. Note that scuffing data tend to have increased scatter with increased run-in time. It is hypothesized that, if the run-in time is long enough, damage to the sliding surface can be initiated by the removal of protective surface films by wear. It is possible that, with a longer run-in time, there is a competing process between the formation and removal of the protective surface films, resulting in increased scatter of the scuffing data.

For given test conditions, the results obtained for loading history effects suggest that a gradual accumulation of damage is not responsible for scuffing under starved lubrication conditions. It is possible that the scuffing mechanisms under starved lubrication conditions might be different from those hypothesized by Sheiretov [57] under dry sliding conditions.

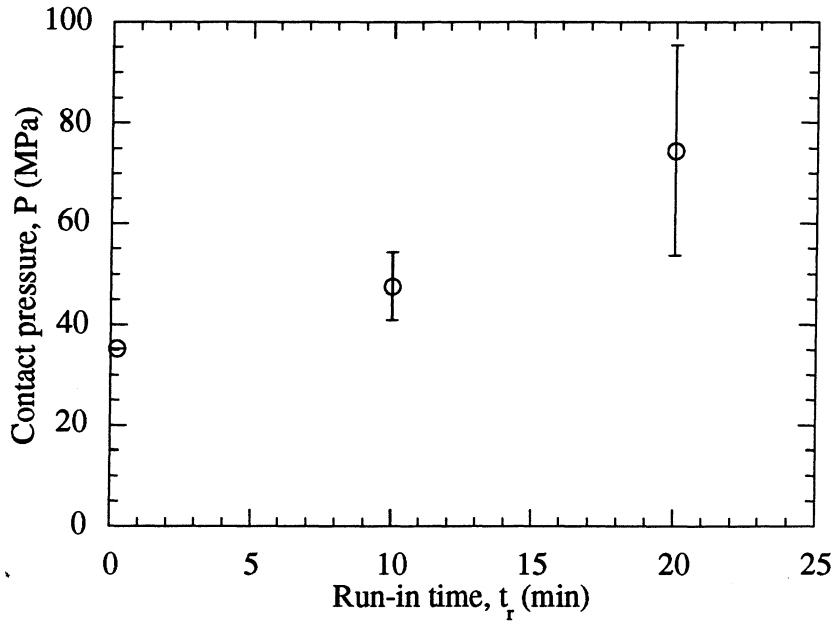

Fig. 4.15 - Effect of run-in on scuffing of 390-T6 Al alloy

Run-in load = 445 N, LSR = 50 mg/min, V = 1.86 m/s

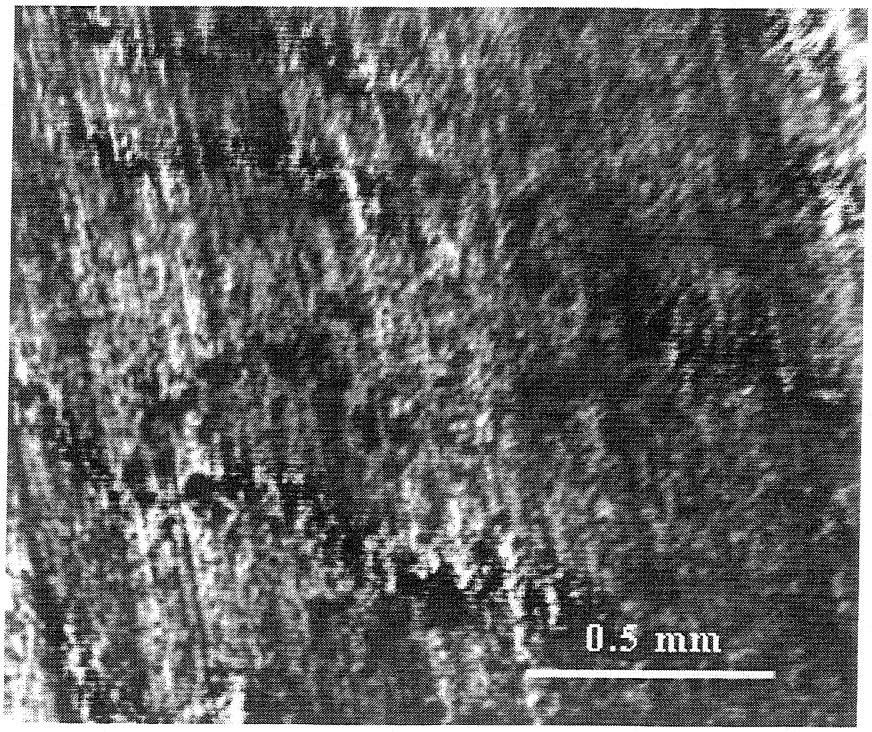

Fig. 4.16 - The surface of a 390-T6 Al pin specimen just before scuffing

Run-in duration = 20 minutes, P = 70.3 MPa, V = 1.86 m/s, LSR = 50 mg/min

4.4 Transition Characteristics of 390-T6 Aluminum Alloys

The scuffing data obtained with a pin-on-disc geometry were based on initial transitions of the contact resistance, friction coefficient and subsurface temperature of the pin specimens. However, it was found that, for a certain range of the lubricant supply rates, a second transition occurs if the load is further increased. Typical load and friction coefficient plots which show the two transitions are given in Fig. 4.17. Upon examining the scuffed surfaces of the pin specimens, it was seen that a dark surface layer is formed on the surface of the pin after the first transition occurs. An Auger chemical analysis, which will be discussed in the following chapter, shows that this layer contains oxygen, carbon and iron. The presence of oxygen in this layer indicates the formation of oxides and the presence of carbon and iron suggests that wear particles from the steel disc counterface were transferred to the pin surface due to local asperity

failures during the first transition. This layer continues to protect the surface until a second transition occurs, at which point, the layer is completely destroyed, leading to higher material removal rates due to macroscopic adhesion.

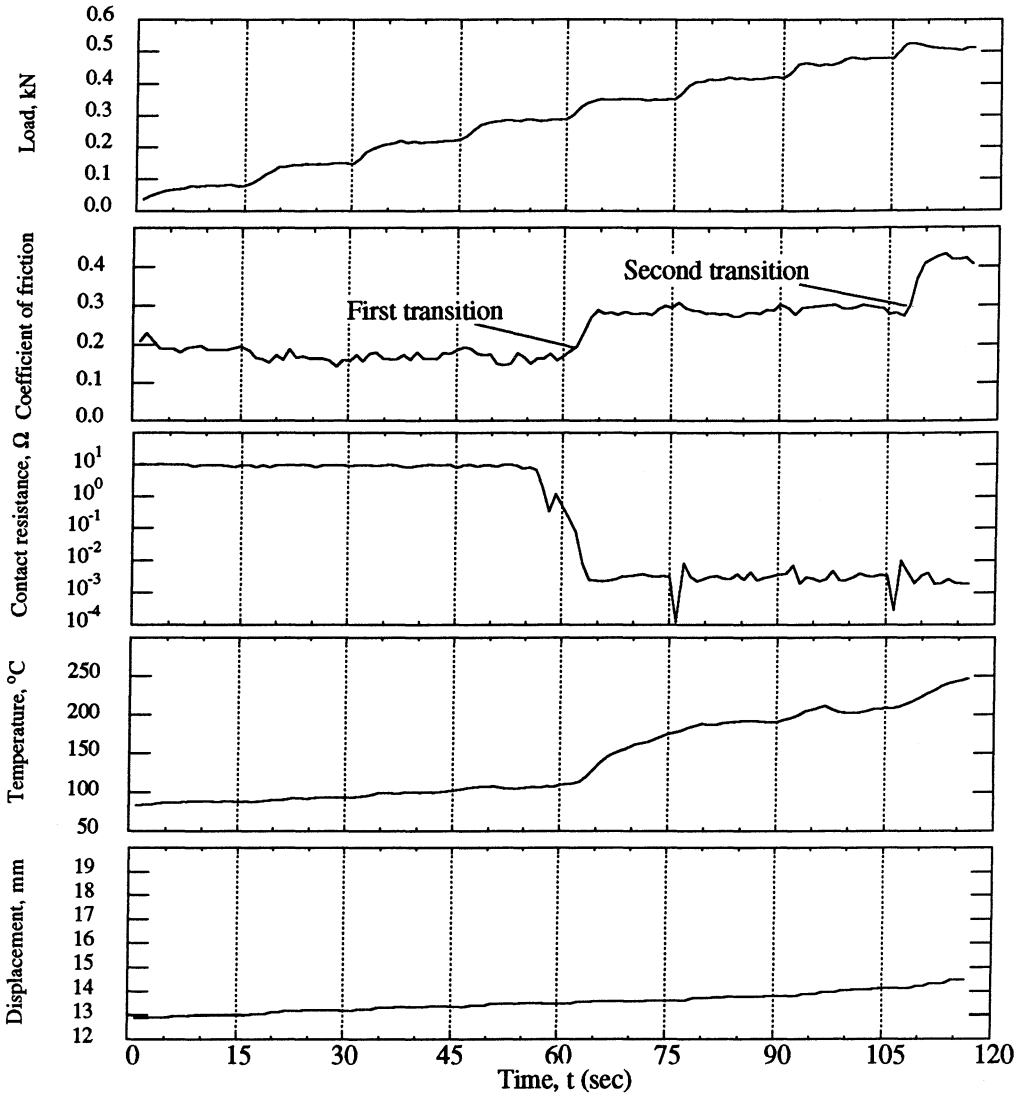

Fig. 4.17 - Load and friction coefficient plots showing first and second transitions under starved lubrication conditions

LSR = 18 mg/min, V = 1.86 m/s

In order to further examine the transition behavior of 390-T6 aluminum alloy as a function of the lubricant supply rate, a set of scuffing data was obtained as shown in Fig. 4.18. These data were obtained with a base PAG/R134a mixture. The plot shows three characteristic regions (I, II and III). The condition of the sliding surfaces in region I is characterized by a friction coefficient of about 0.1. There is no observable material transfer in this region. However, there is surface smoothening on the pin due to asperity deformation. For a given sliding velocity, if the load is further increased for LSR $\leq$ 60 mg/min, region II is reached. This region is characterized by a friction coefficient of about 0.3. Some material transfer from the aluminum pin to the steel disc and the formation of a transformed layer similar to that observed in dry contact [57] are common in this region. Finally, in region III, a friction coefficient of about 0.4 and higher wear rate are observed. It should be noted that, for high lubricant supply rates ($\geq$ 60 mg/min), a direct transition from region I to region III takes place. This might be due to much higher stresses experienced by the material when this transition occurs. Typical test data at high lubricant supply rate, which show a direct transition from region I to region III, are given in Fig. 4.19.

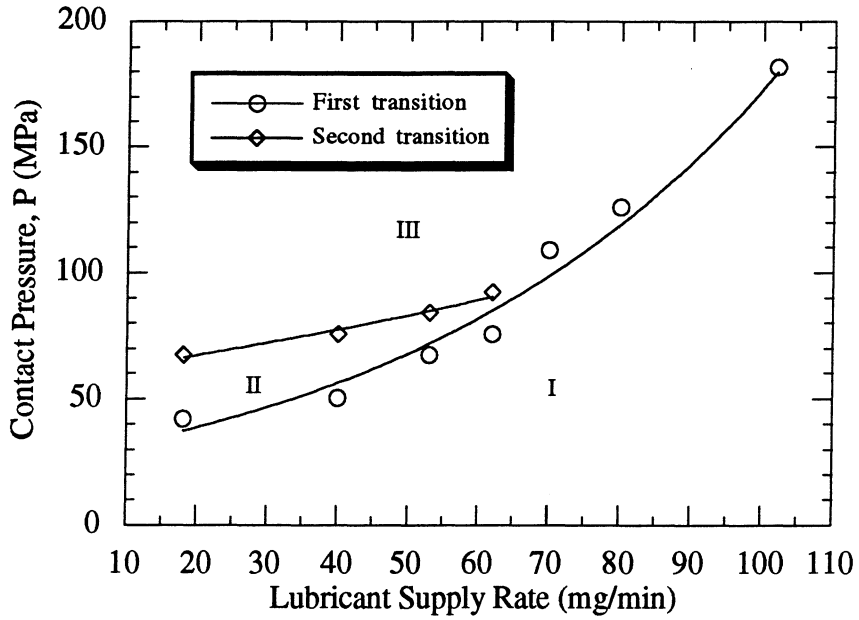

Fig. 4.18 - Scuffing results for 390-T6 Al alloys under various lubricant supply rates Pin diameter = 0.125 in., Lubricant refrigerant mixture: PAG/R134a, V = 1.86 m/s.

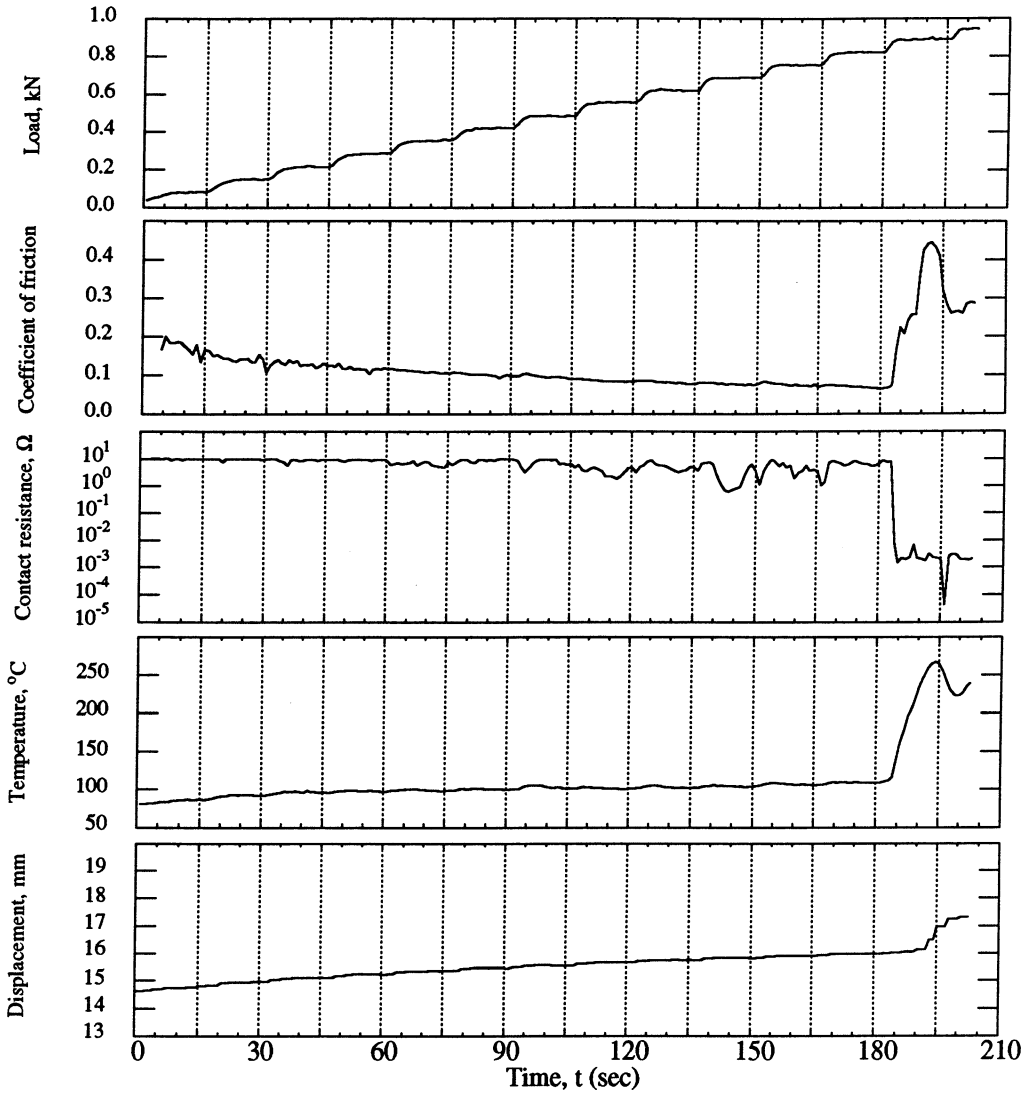

Fig. 4.19 - Typical scuffing test data at high lubricant supply rate

LSR = 80 mg/min, V = 1.86 m/s

CHAPTER 5

EXAMINATION OF SCUFFED SURFACES AND SUBSURFACES

Various mechanisms have been proposed to characterize the scuffing failure over the past few decades. Scuffing failure is normally considered to be related to the breakdown of surface films, which include films of adsorbed lubricant molecules and metal oxides. However, the properties of the material itself form the last line of defense against scuffing failure. Therefore, in order to better understand the processes and failure mechanisms of scuffing, the scuffed surfaces and subsurfaces need to be examined. In this study, the surfaces of the test specimens are studied with an optical microscope, a surface profilometer, SEM (Scanning Electron Microscope) and AES (Auger Electron Spectroscopy). The subsurfaces are studied by sectioning the pin specimens tested under scuffing and non-scuffing conditions and examining the sections with SEM and AES.

Recall that scuffing of both shoe-on-disc and pin-on-disc geometries are examined in this research. Therefore, scuffed surfaces on both the aluminum disc and pin specimens were examined to see if the scuffing phenomenon for the two geometries is the same. Typical scuffed surfaces and their corresponding surface profiles for the aluminum disc and pin specimens are given in Fig. 5.1 and Fig. 5.2, respectively. Both scuffed surfaces show macroscopic material removal and local delamination accompanied by deep grooves. Since the scuffing phenomenon looks the same for both specimens, the examinations of the scuffed surfaces and subsurfaces in this chapter are based on the pin specimens tested in Chapter 4 since they can be more easily sectioned and examined.

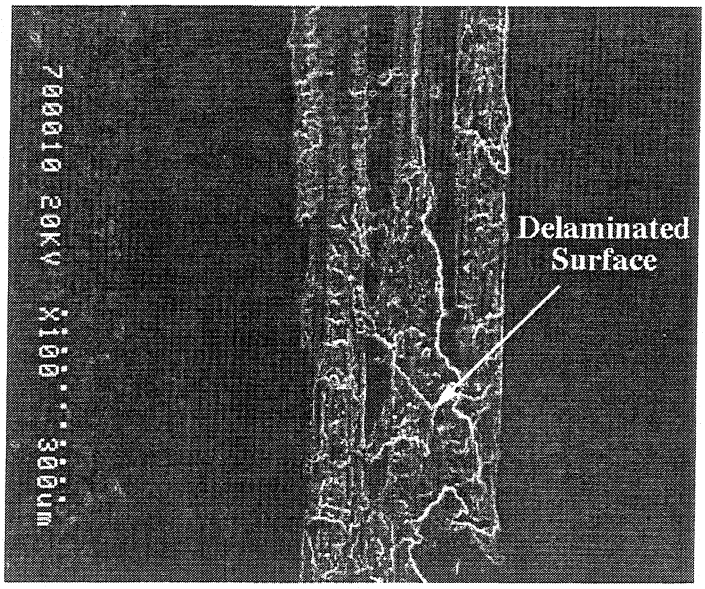

(a)

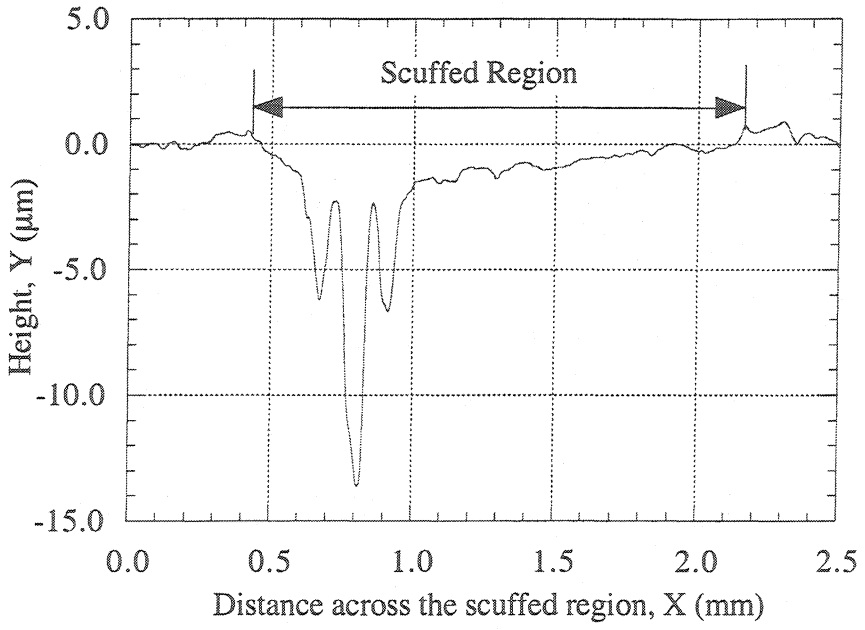

(b)

Fig. 5.1 - (a) Typical scuffed surface on the 390 Al disc and (b) its corresponding surface profile

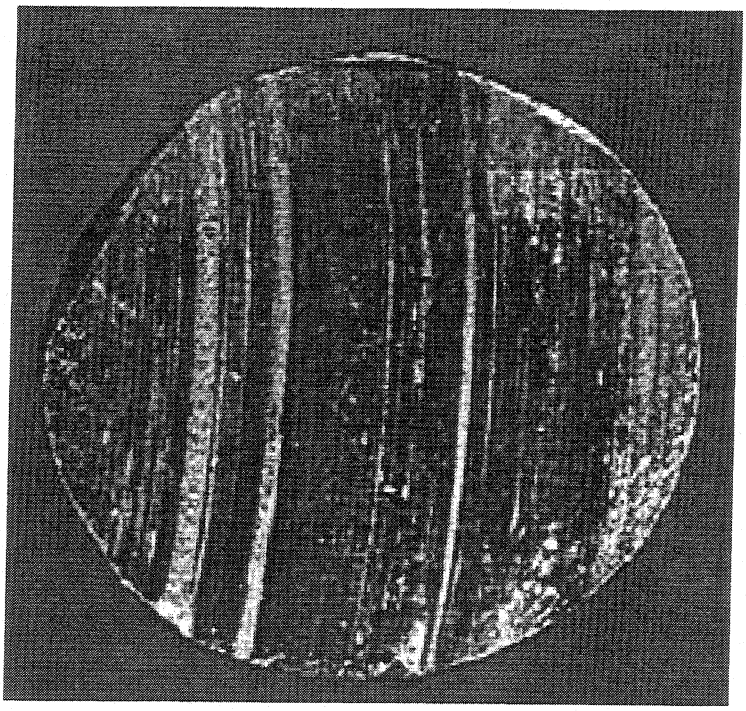

(a)

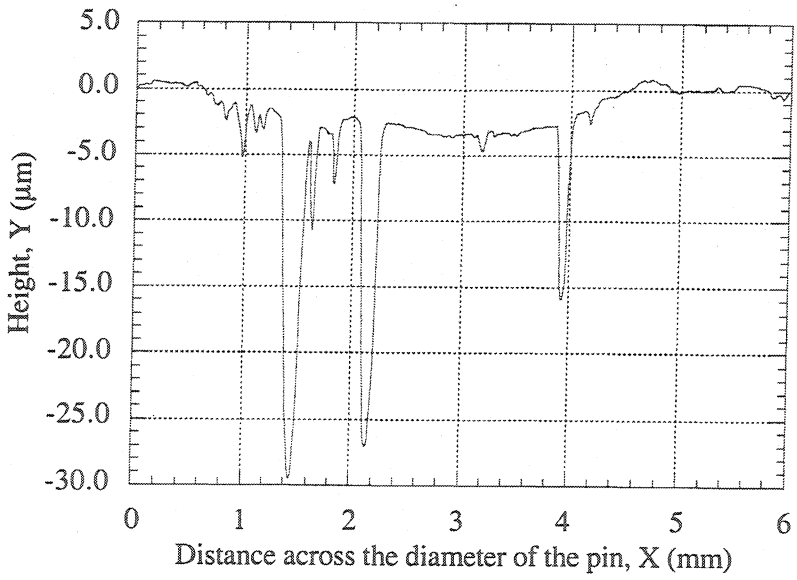

(b)

Fig. 5.2 - (a) Typical scuffed surface on the 390 Al pin and (b) its corresponding surface profile

5.1 Characteristics of the Scuffed Surfaces

The scuffed surface of a 390-T6 Al pin was examined with AES to determine its chemical compositions. The compositions are obtained after an initial sputtering to a depth of approximately 0.02 μm. A typical scuffed surface and its chemical compositions are given in Fig. 5.3. The scuffed surface of 390-T6 Al is characterized by dark and light regions. The AES analysis shows that the dark area has much more carbon, oxygen and iron compared to the light area. The presence of oxygen indicates the formation of oxides on the surface. A large percentage of carbon and iron suggests that wear particles from the carburized steel counterface were transferred to the surface of the pin during the scuffing process. The iron transfer is attributed to abrasion by hard silicon particles on the aluminum surface.

Typical scuffed surfaces for Si-Pb brass and gray cast iron are shown in Fig. 5.4. The scuffed surface of Si-Pb brass is smoother than those of aluminum and gray cast iron. As previously indicated, the smoothening is attributed to the soft lead in the brass, which tends to smear easily at the sliding interface. In contrast, due to the brittleness of gray cast iron, much more damage is observed when scuffing occurs, as shown in Fig. 5.4(b). A relatively large portion of the pin surface is destroyed, generating larger wear particles and material transfer.

5.2 Progression of Scuffing

The progression of scuffing is examined by stopping a test at the initial stage of scuffing and after scuffing, and the surfaces and subsurfaces are examined using a surface profilometer and SEM. The initial stage of scuffing and after scuffing are demonstrated in the typical coefficient of friction plot shown in Fig. 5.5. The progression of scuffing is demonstrated in Fig. 5.6. The picture given in Fig. 5.6(a) shows that scuffing is initiated locally (left side) where some of the surface material is removed to a depth of about 1 μm, as shown by the surface profile. Removal of this section of the load-bearing area increases the severity of the loading over the remaining area. This process self-accelerates and leads to the

fast removal of the remaining surface. In the final stage of scuffing, shown in Fig. 5.6(b), most of the original surface of the pin is removed to a depth of about 2-3 μm. It is also seen that local deep grooves are formed in the scuffed surface, as shown by the surface profile. This is considered subsequent damage, which follows the initiation of scuffing failure, and eventually leads to the complete seizure of the sliding surfaces.

The unscuffed and scuffed areas of the specimens shown in Fig. 5.6 are sectioned along the direction of sliding and the subsurfaces are examined. The SEM micrographs which show the difference in the subsurface damage in these specimens are given in Fig. 5.7. For the scuffed specimen (Fig. 5.7(b)), it is clear that both voids and cracks are formed in the subsurface. The voids and cracks seem to propagate in the direction of sliding. This can be attributed to severe plastic deformation on the sliding surface during the scuffing process. However, no cracks or voids could be observed in the subsurface of the unscuffed specimen. This indicates that the initial scuffing damage (~1 μm deep) shown in Fig. 5.6(a) is probably not caused by subsurface fatigue. Also, no observable plastic deformation is present in the subsurface. The subsurfaces of Si-Pb brass and gray cast iron obtained at one load step before scuffing are also examined with SEM. As shown in Fig. 5.8, they also show no observable subsurface damages. The black needle-like flakes in the cast iron structure are graphites, which resemble cracks.

It should be noted that the depth at which cracks are seen in Fig. 5.7(b) is approximately the same as the depth of the deep groove shown in Fig 5.6(b). This indicates that the formation of these deep grooves is a subsequent damage which follows the initial scuffing damage. Based on the observation of scuffed surface and subsurface, it is hypothesized that the material removal at the initiation of scuffing is caused by plastic shearing or smearing. Figure 5.9 shows that some material, removed by initial scuffing failure, is smeared to the counterface steel disc. Due to the higher tendency of adhesion between the same materials (aluminum on aluminum), large chunks of aluminum particles (probably caused by surface fatigue) are then adhered on top of the smeared aluminum, resulting in a

macroscopic cold weld. As shown in Fig. 3.16(b), similar material transfer is obtained on the shoe specimen from the shoe/disc geometry tests.

The chemical compositions of both scuffed (dark area) and unscuffed region of the specimen shown in Fig. 5.6(a) are analyzed using an AES. An AES depth profile of the virgin surface is also obtained for comparison purpose (Fig. 5.10). The oxygen plot indicates that the thickness of the nascent aluminum oxide is approximately 7.5 nanometer. The chemical compositions of both scuffed and unscuffed regions are plotted, as a function of depth, in Fig. 5.11. As previously noted, the presence of oxygen suggests that the oxides are formed on both unscuffed and scuffed regions. The percentage of oxygen present in both regions decreases as the depth from the surface increases. For the unscuffed region, the oxygen present on the surface can be detected only up to 1 μm deep. The carbon and iron can be detected up to a depth of about 0.5 μm. This indicates that a relatively thin transformed layer is formed on the aluminum surface before scuffing occurs. However, the presence of oxygen in the scuffed region (dark area) is detected at depths of up to 6 μm. Also, relatively large amounts of carbon (~ 17 %) and iron (~ 8 %) are present at a depth of 6 μm, indicating the formation of the thick transformed layer during the scuffing process. As previously indicated, the presence of carbon and iron in the relatively deep aluminum surface is due to wear particles transferred from the counterface steel disc and gross plastic deformation on the sliding surface during the scuffing process. This finding supports the view that the compaction of wear particles is important mechanisms for the formation of the transformed layer.

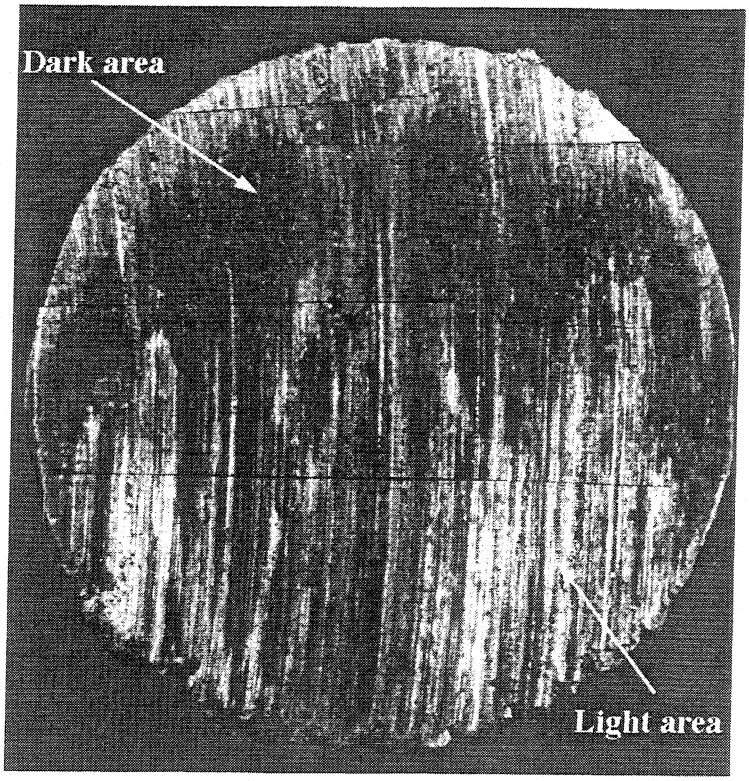

(a)

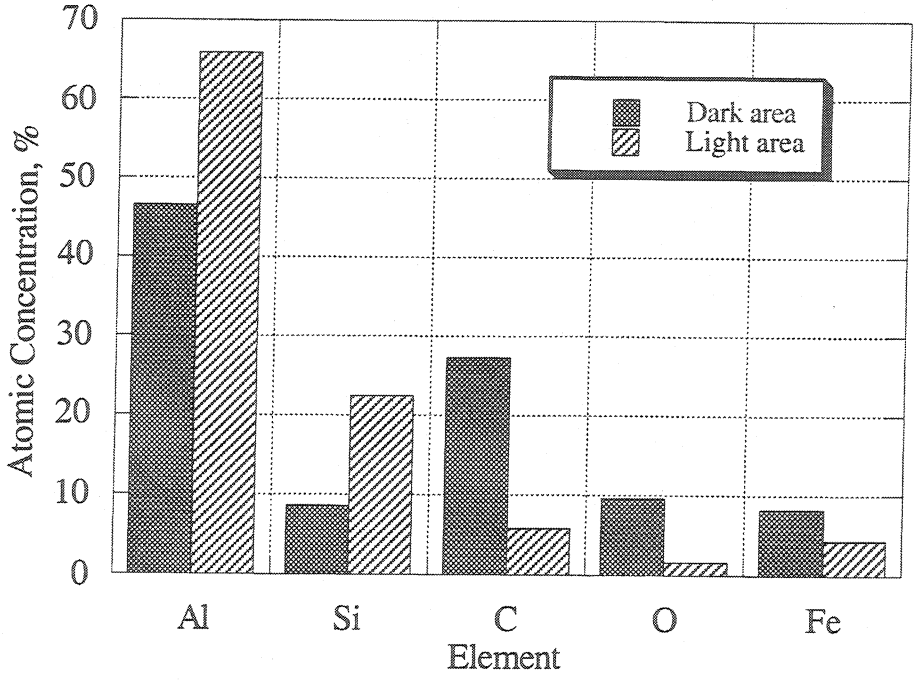

(b)

Fig. 5.3 - (a) Typical scuffed surface and (b) an AES analysis for a 390-T6 aluminum pin

The sliding direction of the scuffed surface is from top to bottom.

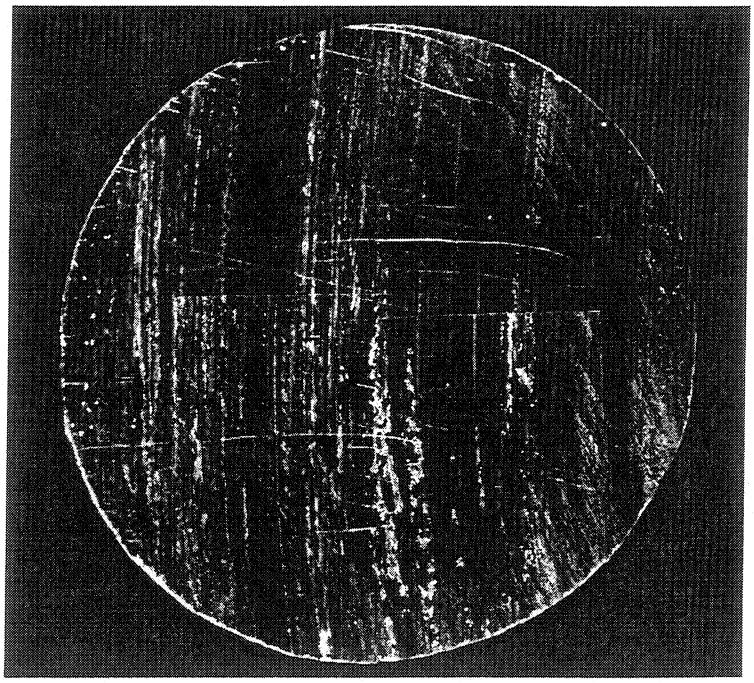

(a)

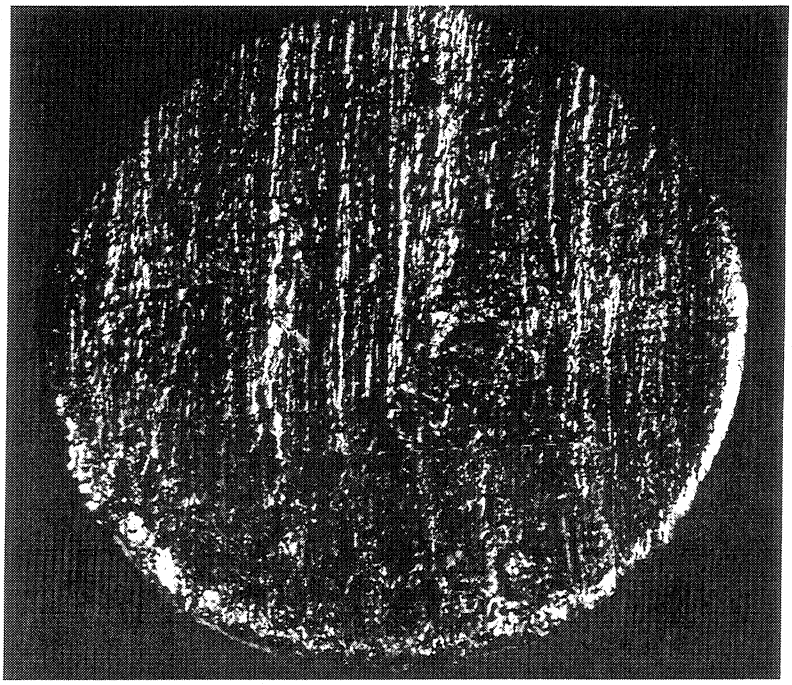

(b)

Fig. 5.4 - Typical scuffed surfaces for (a) the Si-Pb brass pin and (b) gray cast iron pin

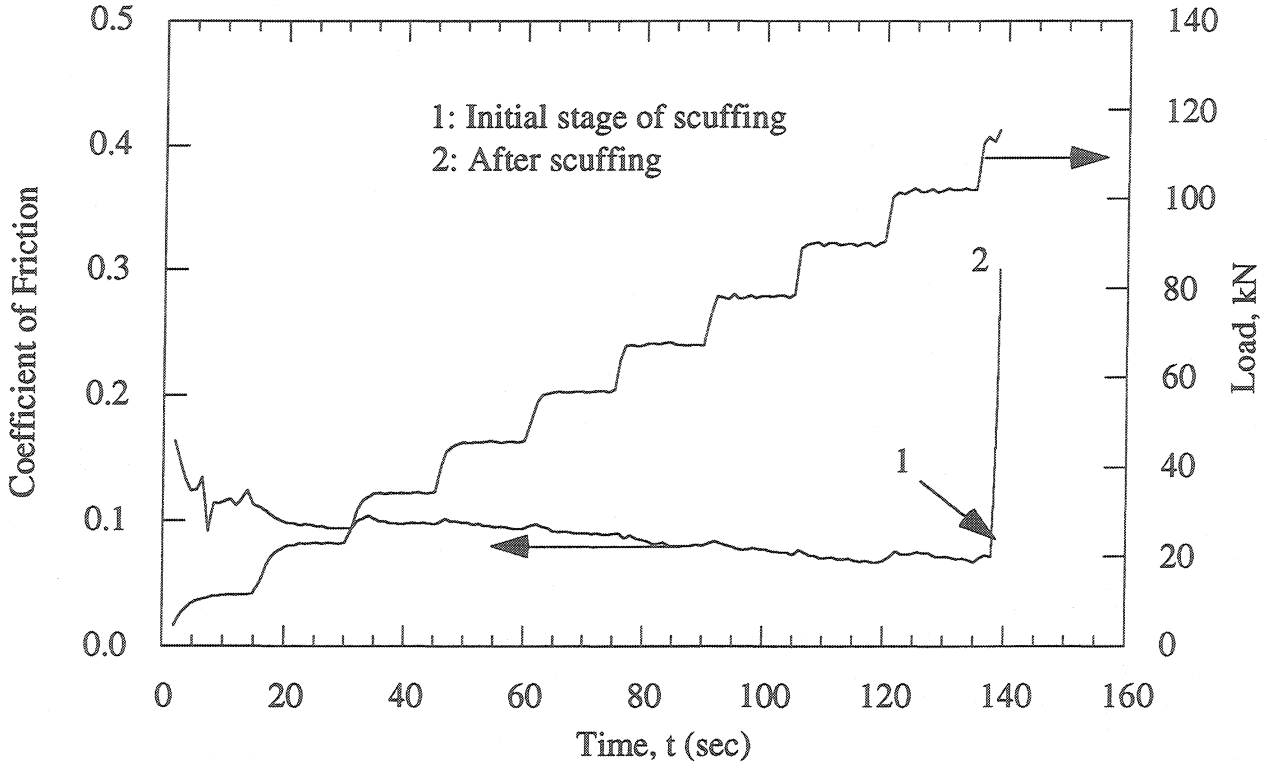

Fig. 5.5 - Typical coefficient of friction and load plots showing the initial stage of scuffing and after scuffing

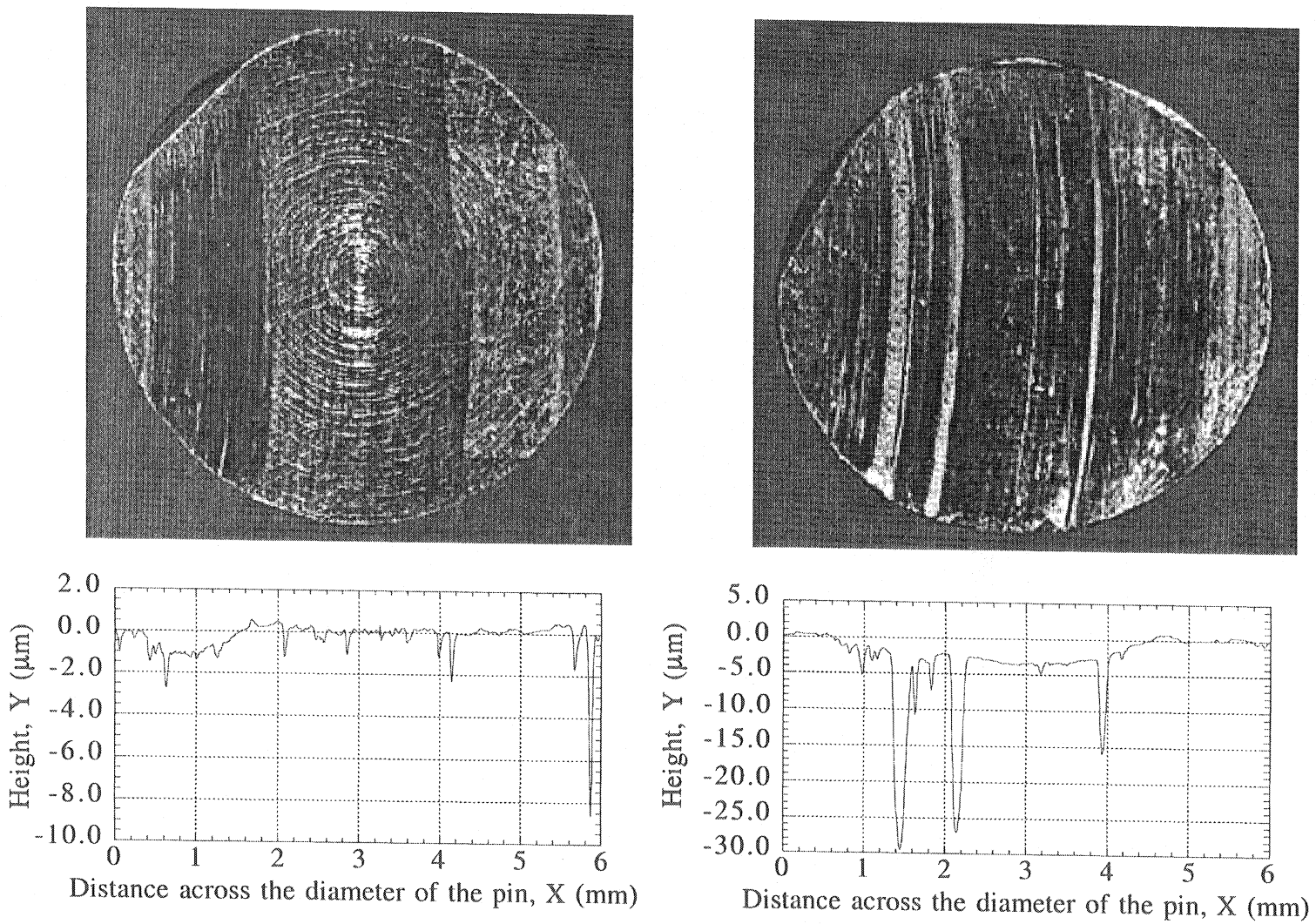

Fig. 5.6 - Progression of the scuffing process

(a) Pin surface at initiation of scuffing and its surface profile, P = 63.3 MPa, V = 1.4 m/s,

(b) Pin surface after scuffing and its surface profile, P = 70.3 MPa, V = 1.4 m/s

Environmental temp. = 121°C, LSR = 45 mg/min, Sliding direction: From top to bottom

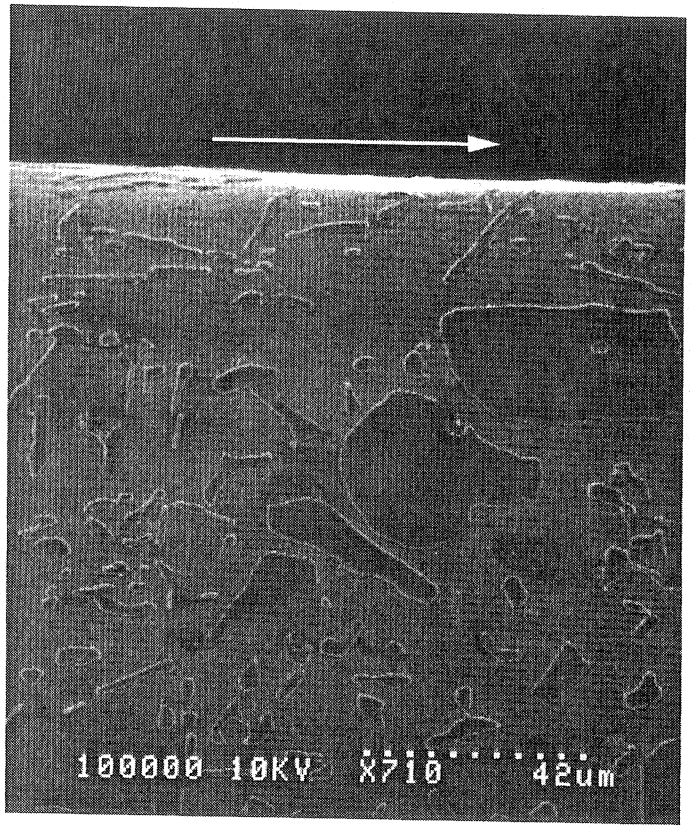

(a)

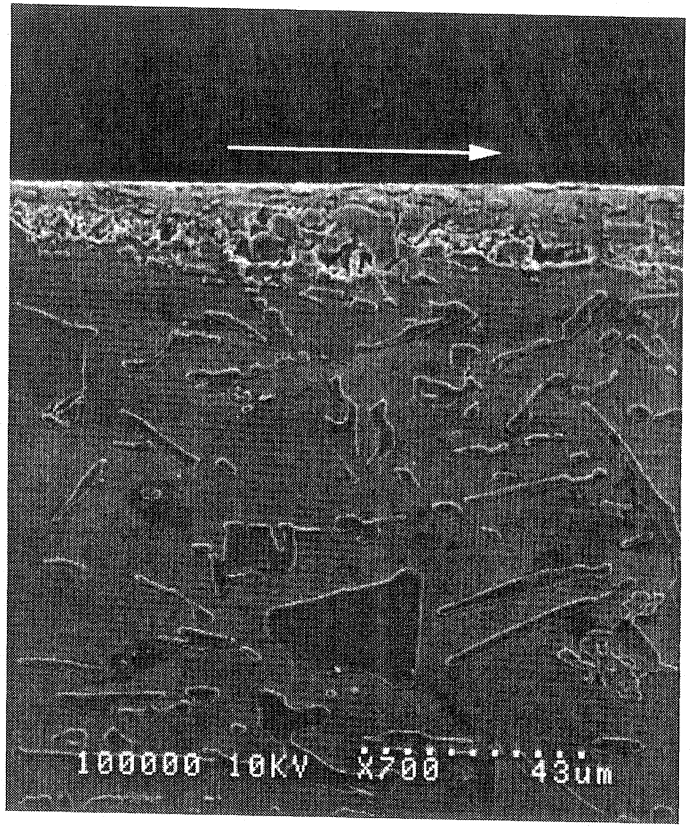

(b)

Fig. 5.7 - SEM micrographs of the subsurfaces

(a) Unscuffed area, P = 63.3 MPa, V = 1.4 m/s (b) Scuffed area, P = 70.3 MPa, V = 1.4 m/s

Environmental temp. = 121°C, LSR = 45 mg/min

The arrow on top indicates the direction of sliding

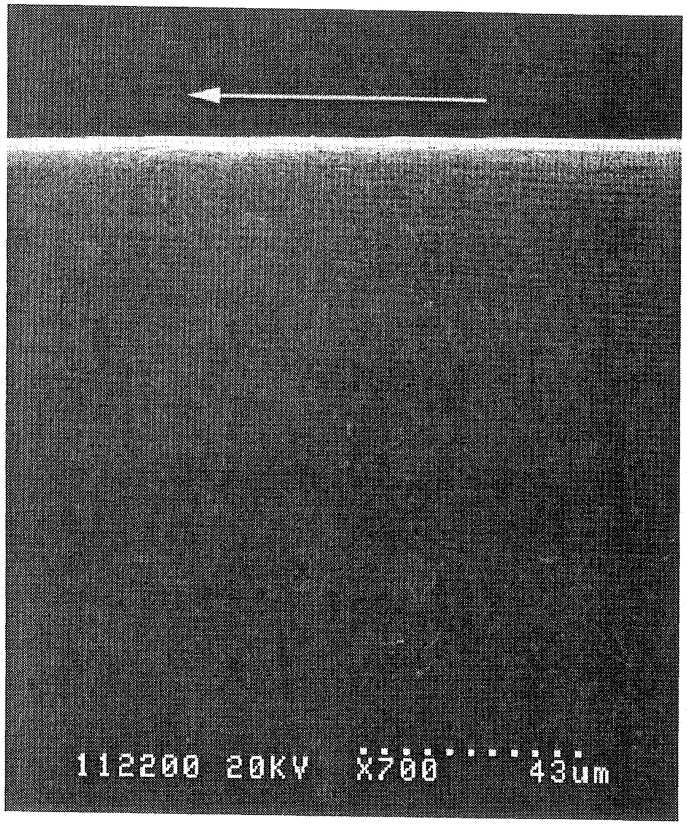

(a)

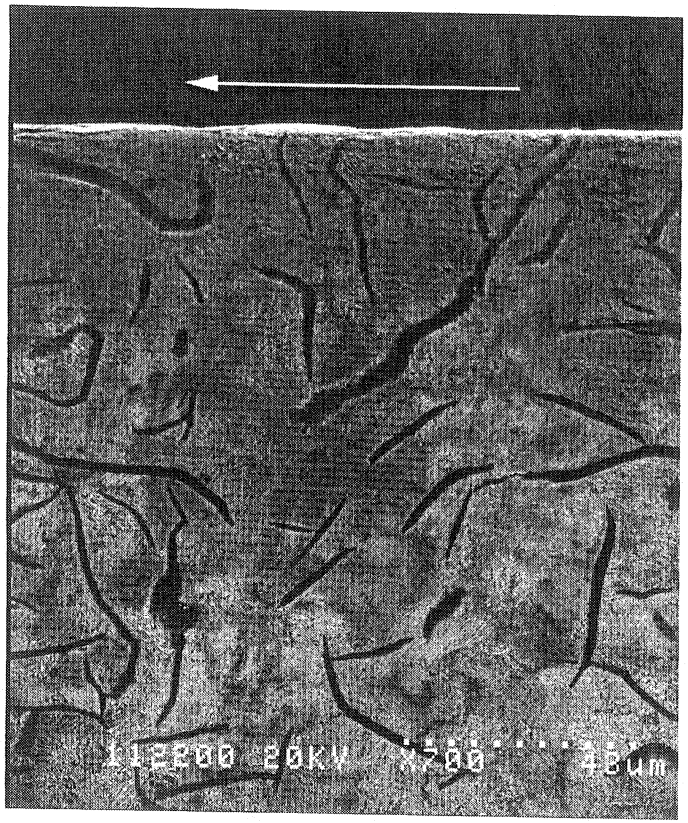

(b)

Fig. 5.8 - SEM micrographs of the subsurfaces of (a) Si-Pb brass and (b) gray cast iron

P = 35.2 MPa, V = 3.72 m/s, Environmental temp. = 121°C, LSR = 45 mg/min

The arrow on top indicates the direction of sliding

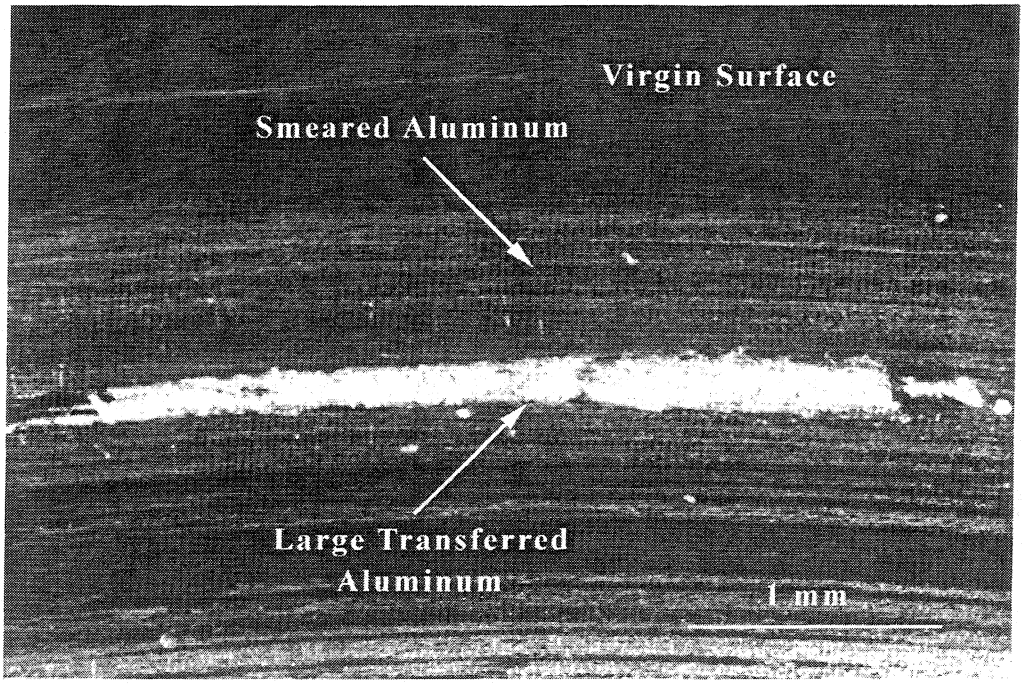

Fig. 5.9 - Typical aluminum material transfer on 1018 steel disc

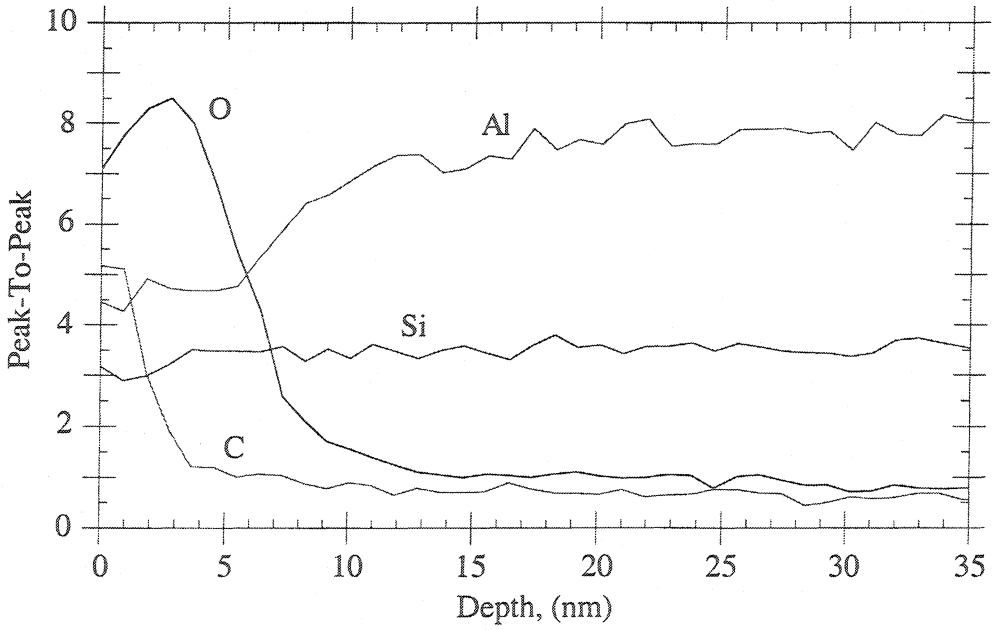

Fig. 5.10 - An AES depth profile of the virgin surface of 390-T6 Al pin

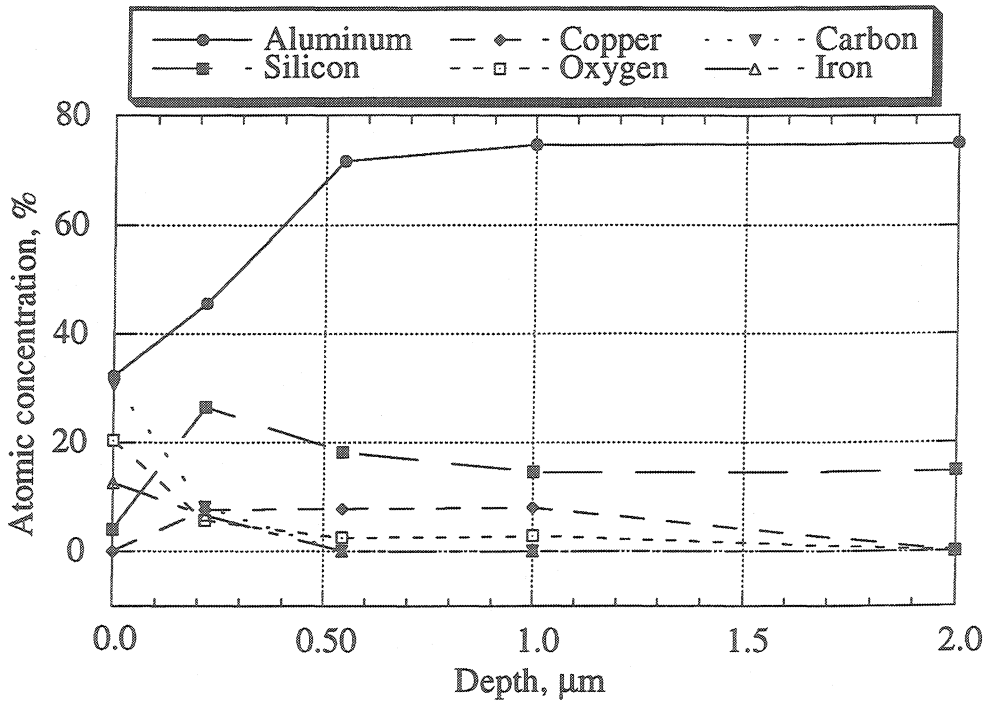

(a)

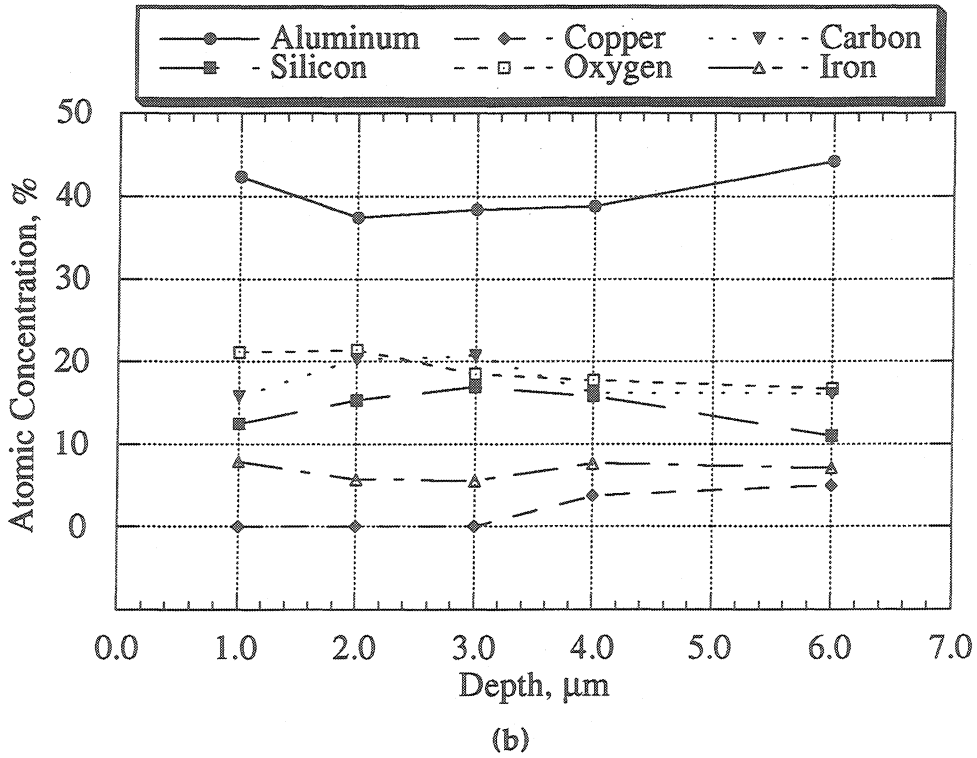

(b)

Fig. 5.11 - The chemical composition of the layers as a function of depth

(a) Unscuffed region, (b) scuffed region

P = 63.3 MPa, V = 1.4 m/s, Environmental temp. = 121℃, LSR = 45 mg/min

5.3 Structure of Subsurface Failures

In order to examine the structure of the subsurface, the scuffed surfaces are sectioned along the direction of sliding and their subsurfaces are examined. A SEM micrograph which shows a typical structure of the subsurface after scuffing is shown in Fig. 5.12. The subsurface shows three characteristic regions (transformed layer, plastically deformed region and elastically deformed or undisturbed region). It is known that oxidation is a dominant mechanism for the formation of the transformed layer. However, recent works [68,69] indicate that the compaction of wear particle and mechanical alloying are also important mechanisms. It is seen that large silicon particles are fragmented into smaller particles in this layer. This is attributed to the extremely high plastic strain within this layer [57]. The thickness of this layer is typically in the range of 5-10 μm under the conditions studied. It is also typical to have voids and cracks nucleated within the transformed layer.

Below the transformed layer, the plastically deformed region typically reaches a depth of 50-60 μm. Characteristics of this layer are the orientation of all the features in the direction of sliding and the fracture of silicon particles due to the large plastic deformation during the scuffing process.

The subsurface damage after scuffing, for the aluminum alloys and Si-Pb brass, are also examined with SEM. The gray cast iron pin specimens cannot be examined because its surface is completely destroyed when scuffing occurs, as noted previously. Typical scuffed 390-T6 and DHT3 Al alloys which show subsurface damages are given in Figs. 5.13 and 5.14, respectively. For 390-T6 alloy, a long crack is formed within the transformed layer and propagates along the direction of sliding. However, due to the relative ductility and low silicon content of the DHT3 alloy, both voids and cracks are formed in this material. It is assumed that voids are initially formed and eventually coalesced to form long cracks within the transformed layer. For Si-Pb brass, as shown in Fig. 5.15, no subsurface voids or cracks are observed. However, the layer formed on the sliding surface indicates that large plastic deformation occurs during scuffing. Material from one location on the specimen is often

displaced in the direction of motion by plastic flow, forming a layered structure, which includes oxides, strained harden and severely deformed material.

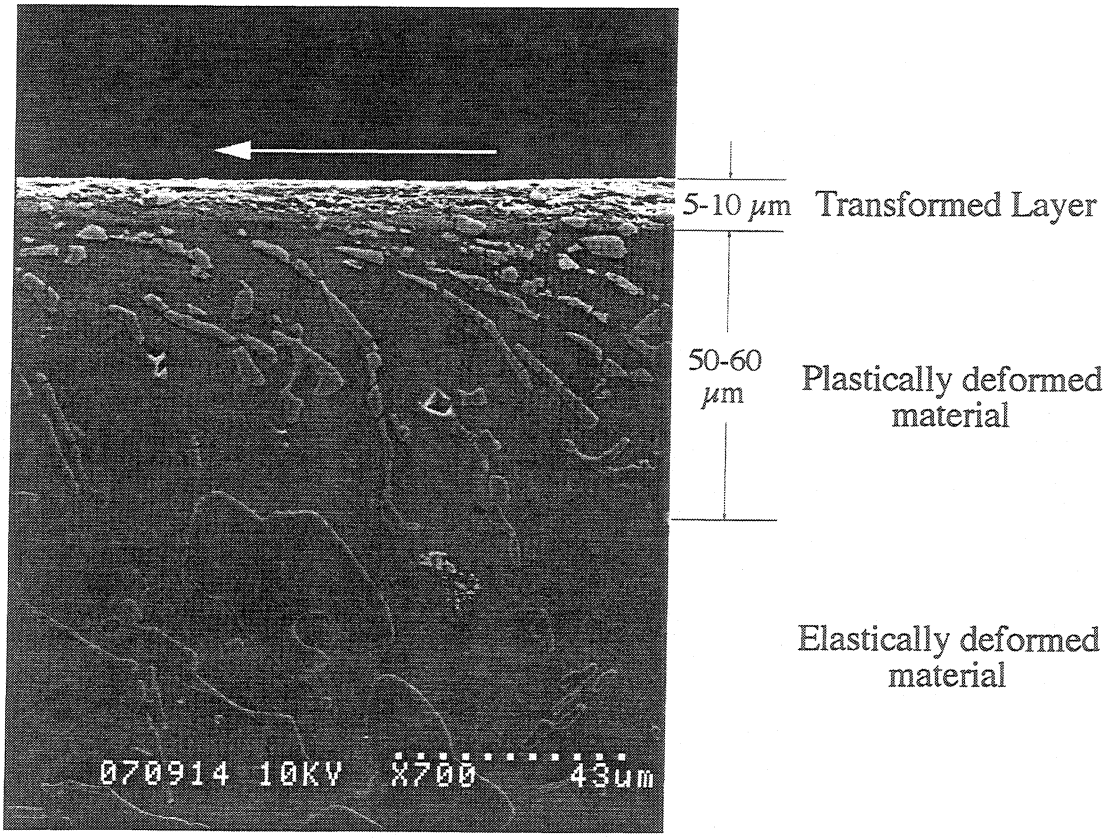

Fig. 5.12 - Structure of the subsurface after scuffing

P = 63.3 MPa, V = 1.4 m/s, Environmental temp. = 121°C, LSR = 45 mg/min

The arrow on top indicates the direction of sliding

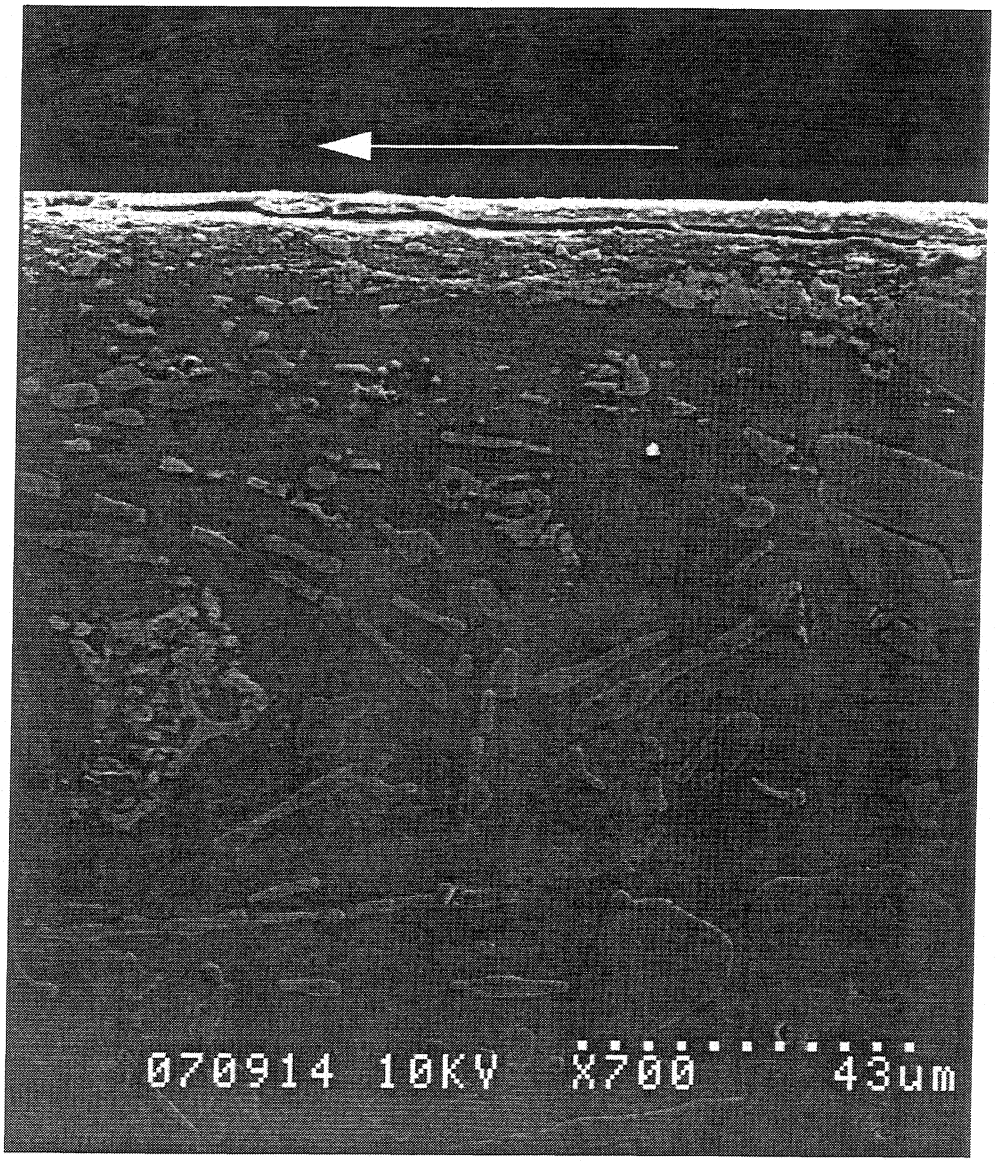

Fig. 5.13 - Subsurface damage of 390-T6 Al alloy after scuffing

P = 63.3 MPa, V = 1.4 m/s, Environmental temp. = 121°C, LSR = 45 mg/min

The arrow on top indicates the direction of sliding

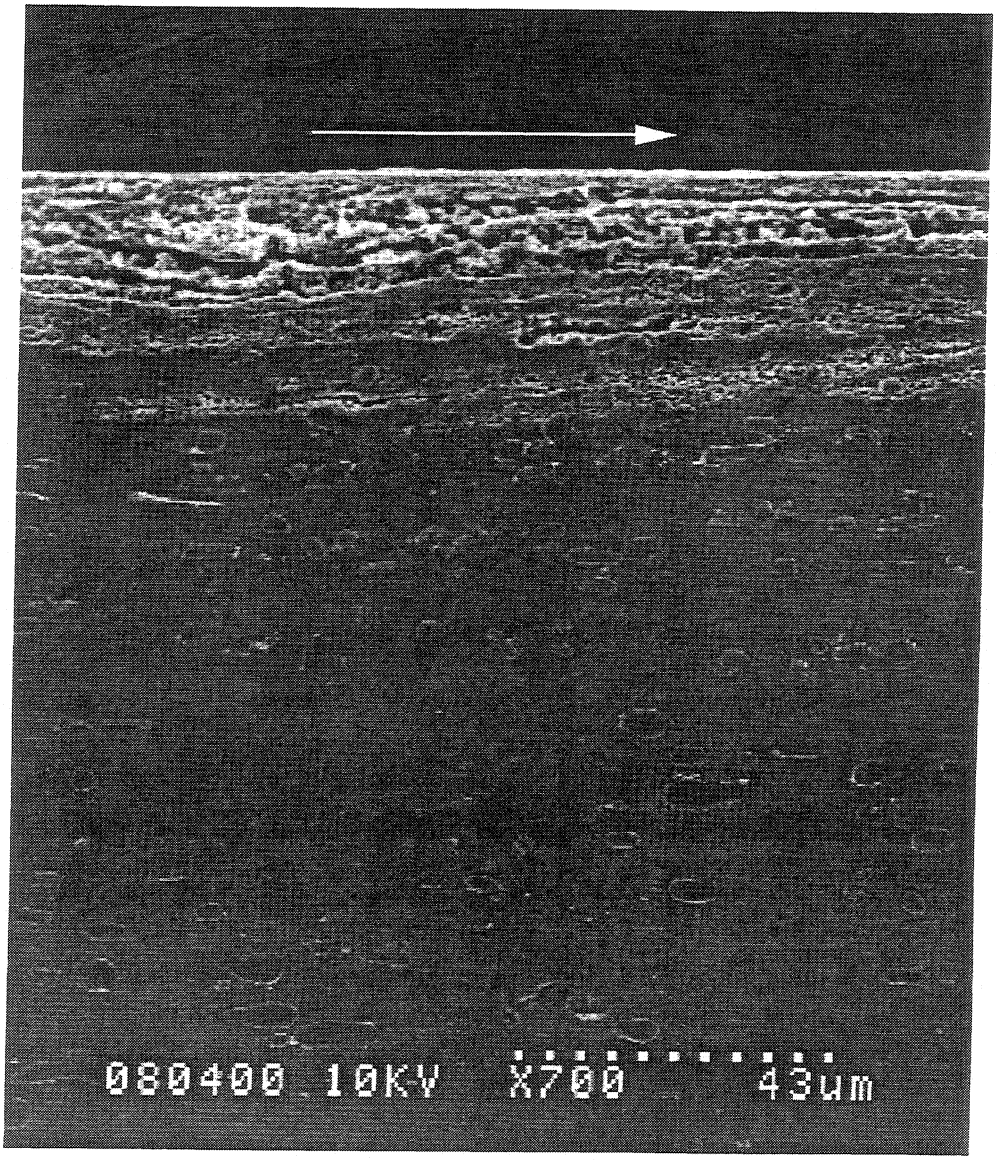

Fig. 5.14 - Subsurface damage of DHT3 Al alloy after scuffing

P = 14.1 MPa, V = 2.8 m/s, Environmental temp. = 121°C, LSR = 45 mg/min

The arrow on top indicates the direction of sliding

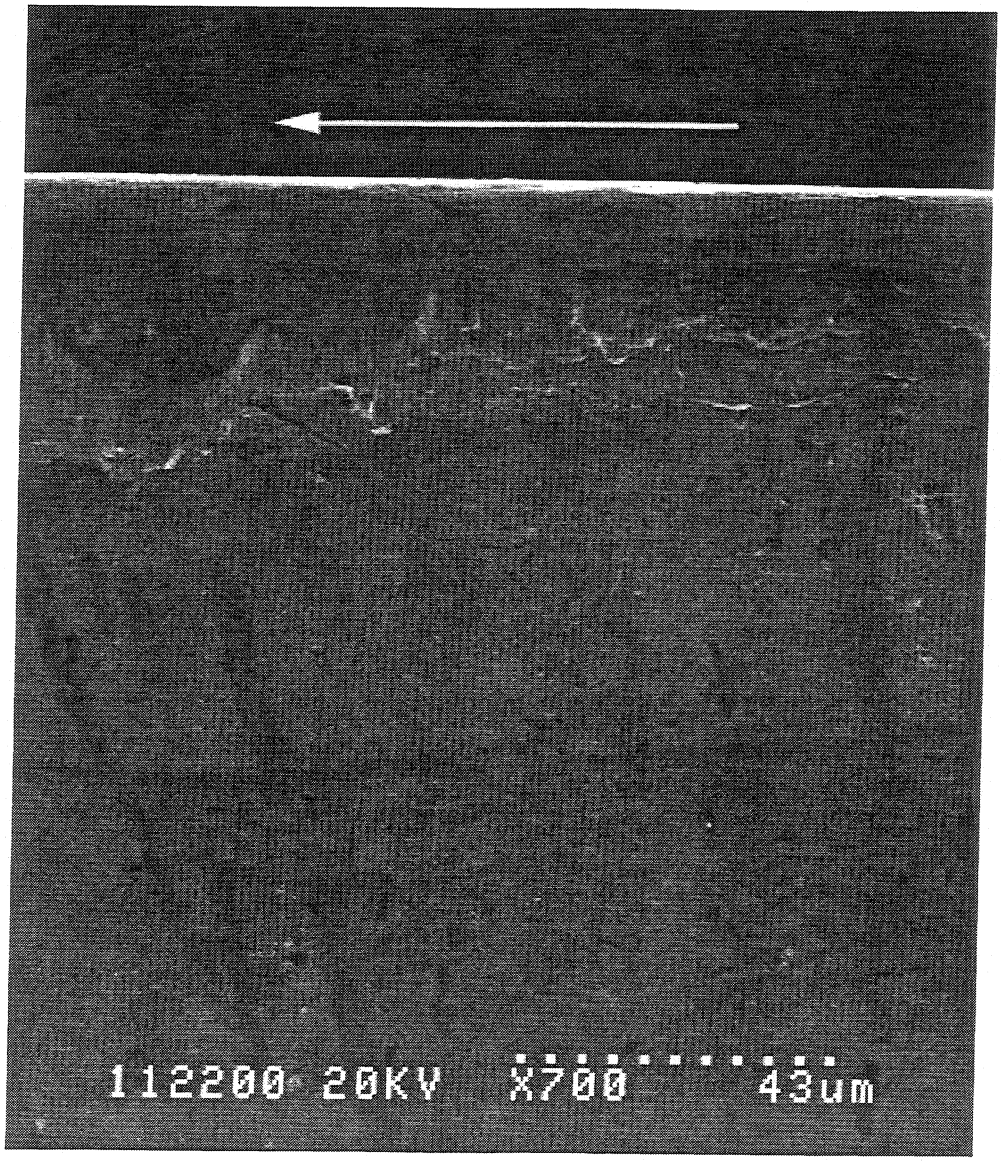

Fig. 5.15 - Subsurface damage of Si-Pb brass after scuffing

P = 42.2 MPa, V = 2.8 m/s, Environmental temp. = 121°C, LSR = 45 mg/min

The arrow on top indicates the direction of sliding

CHAPTER 6

EVALUATION OF THE EXISTING HYPOTHESES FOR SCUFFING

Several scuffing hypotheses have been proposed in the literature over the past sixty years. However, none of the existing hypotheses and criteria for scuffing can explain adequately all the experimental results and observations. Also, most of the proposed criteria are condition criteria in that they specify critical conditions (loads, sliding speeds, and temperature, etc.) beyond which scuffing will occur.

The hypotheses for scuffing can be subdivided into three major groups. The first is mainly based on the assumption that scuffing occurs if some critical thermal conditions are reached at the sliding contact surfaces. The second is based on the breakdown of the main elastohydrodynamic lubrication films in sliding contacts. The third group of hypotheses is based on bulk material failure. These hypotheses assume that if a critical condition on or under the surface of the contacting bodies is reached, surface films or bulk material failures occur, which consequently leads to scuffing. Based on experimental observations obtained both in the literature and the present study, some of the more important of these hypotheses are evaluated below.

6.1 Hypotheses Based on Critical Thermal Conditions

6.1.1 Critical Surface Temperature Hypothesis

In 1937, Blok proposed that scuffing occurs when a critical surface temperature is reached. Blok's hypothesis for scuffing is still the most widely used. As indicated in Chapter 1, this hypothesis suggests that a system will scuff if the surface temperature (T_S) exceeds a certain critical value (T_C). In a simplified form, this hypothesis is given by:

$$T_s = \left(T_o + C_t \mu A_o PV + T_f\right) \geq T_c \tag{6.1}$$

where T_0 is the environmental temperature, $(C_t \mu A_o PV)$ is the temperature rise due to frictional heating and T_f is the flash temperature. In the expression for the frictional heating, μ is the coefficient of friction, A_0 is the apparent area of contact, and C_t is a constant characterizing the thermal dissipation properties of the system. The flash temperature is difficult to measure since it is of very short duration and decays rapidly, both with time after the surface has left the contact and with depth below the surface. Therefore, in most cases, the flash temperature must be estimated. It is often calculated based on the analytical works of Blok [19] and Jaeger [70] for stationary and moving heat sources over a semi-infinite half-space. Their analyses relates the flash temperature to the friction coefficient, the load, the surface velocities, and the thermal properties of the bodies in contact.

This hypothesis can easily explain the effects of the environmental temperature on scuffing, which has been experimentally observed in many studies, including those under dry sliding conditions [57]. However, the surface temperature at scuffing is also affected by the size of the specimen and the test environment [57]. Many researchers have also found that the surface temperature reached just before scuffing is, in fact, not constant but varies with lubricant, materials and other factors [15, 44, 71-73]. The other limitation of this hypothesis is that failure is not related to the temperature effects on the materials properties in the conjunction. The data presented in this thesis also show some deviations from the constant surface temperature condition at scuffing, as shown in Table 6.1. In this Table, the flash temperatures are based on the model developed by He [74]. A detail description of this model and flash temperature calculations are given in the following chapter. Since the flash temperature increases as the sliding velocity increases, the variation in the calculated surface temperatures at scuffing becomes larger than the measured variations in bulk temperature. In fact, a constant critical bulk temperature criterion seems to be a better fit for the data given in Table 6.1.

Table 6.1 - Typical surface temperatures at scuffing for aluminum alloys tested

Material	P (MPa)	V (m/s)	PV (MPa•m/s)	$^{\dagger}T_b$ (°C)	T_f (μ=0.30) (°C)	T_s (°C)
390-T6 Al	112.5	0.93	104.6	147	81.2	228.2
	63.3	1.40	88.6	142	106.8	248.8
	42.2	1.86	78.5	150	123.0	273.0
	21.1	2.79	58.9	145	142.9	287.9
	14.1	4.65	65.6	150	181.6	331.6
DHT3 Al	112.5	0.47	52.8	120	43.3	163.3
	56.2	0.93	52.3	130	72.1	202.1
	35.2	1.40	49.3	131	95.7	226.7
	14.1	2.79	39.3	126	129.4	255.4
	10.5	4.65	48.8	130	152.8	282.8

† Experimentally measured; $T_b = T_o + C_t \mu PV$

6.1.2 Critical Frictional Power Intensity Hypothesis

The critical frictional power intensity hypothesis, initially suggested by Matveevsky [22], is an alternative hypothesis relating scuffing to some critical thermal condition. The frictional power intensity is defined as the ratio of the generated frictional power to the nominal contact area. It is equal to the product of coefficient of friction, nominal contact pressure and sliding velocity. The frictional power intensity hypothesis gives the heat flux generated at the sliding contact. Scuffing failure occurs when this heat flux reaches a critical value. This hypothesis is based on the experimental observation that scuffing often occurs along the curves described by PV = *constant* relationship, where P and V are the contact pressure and the sliding velocity, respectively. Many experimental works have been conducted to validate this hypothesis [24, 44-45, 71]. Even though the results are controversial, some experimental data show that, for given material/lubricant combinations,

the frictional power intensity at scuffing is approximately constant over a certain velocity range [24, 71]. As shown in Fig. 6.1, for all materials tested, the experimental data obtained from this study also show that the frictional power intensities at scuffing are approximately constant for the velocity range studied. However, for given materials, the critical frictional power intensity at scuffing is affected by the contact geometry, the test environment and lubricant supply rate. In reference [57], it was found that, for given sliding velocities, the scuffing *PV*'s under dry sliding conditions increase as the size of the specimens decreases. Since μ is approximately the same for both geometries, the frictional power intensities at scuffing for smaller diameter pin specimens are higher than those of larger pin specimens. Also, the scuffing *PV* under a R134a environment deviates significantly from *PV* = constant behavior which is obtained in an air environment [57]. This indicates that the critical frictional power intensities can be affected by the test environment.

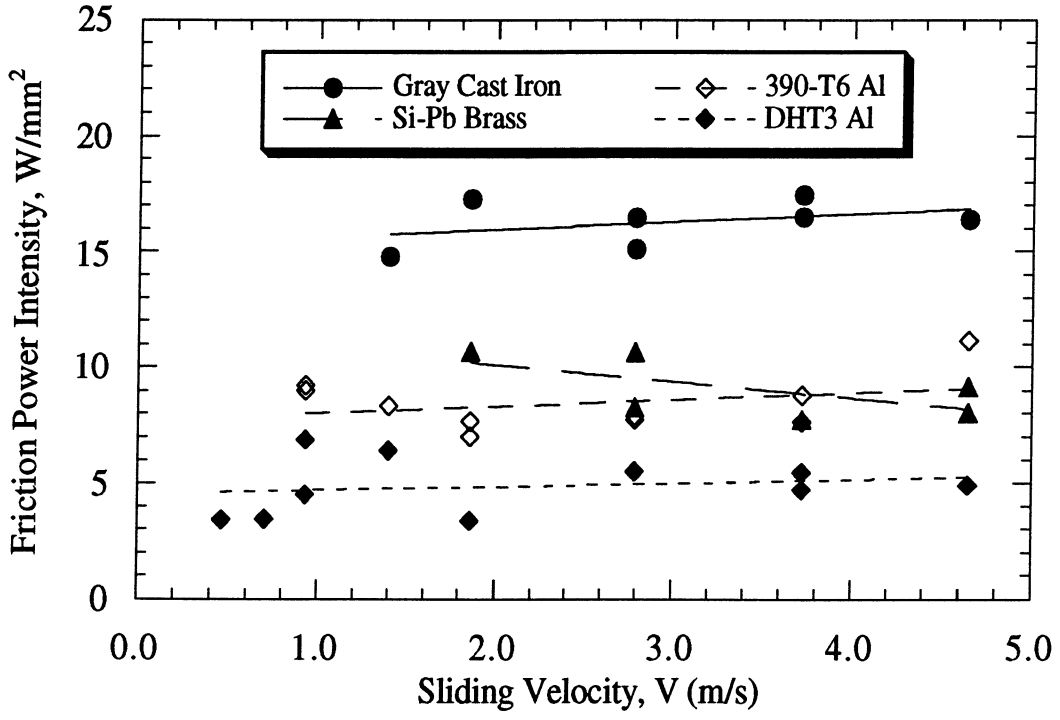

Fig. 6.1 - Frictional power intensities of various materials as a function of sliding velocity

The experimental results from this study (Fig. 4.2) show that the critical frictional power intensity also depends on the lubricant supply rate as shown in Fig. 6.2. As with the critical temperature criterion, this hypothesis does not relate the scuffing process to material failure. In addition, it does not consider the heat dissipating characteristics of the system.

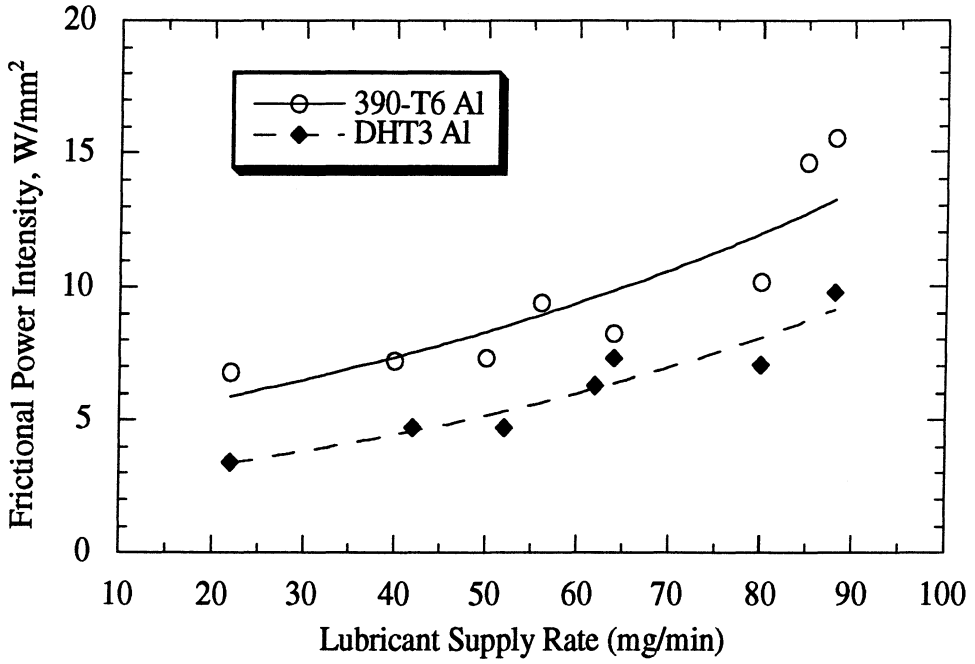

Fig. 6.2 - Frictional power intensity of Al alloys as a function of the lubricant supply rate

6.1.3 Thermoelastic Instability Hypothesis

The thermoelastic instability hypothesis also relates scuffing to a critical temperature condition reached at the surface. The suggested mechanism responsible for scuffing is asperity expansion. As one asperity on one surface collides with other asperities on the counterface, the asperity heats up and expands. It then stands above its previous height, causing more thermal expansion. This sequence of events is indirectly verified in experiments where metal pins slide against glass. Hot spots are observed within the contact region. If an expanded asperity does not wear away, it may adhere to another, initiating scuffing. Based on this concept, Johnson, Dow, and Zhang [75] presented an analysis of

thermoelastic instability in a simple sliding contact as an explanation for scuffing failure. For a sliding contact of crowned cylinders, their analysis yielded a predictive theoretical scuff boundary based on system parameters and materials having the same bulk properties as follows:

$$W = \frac{144(A+B)}{E^2(1-\nu^2)}\left(\frac{\pi m_t^2 n_t K(1-\nu)}{\mu V m \alpha}\right)^3 \tag{6.2}$$

where W is the transition load above which scuffing will occur, A and B describe the curvatures of the cylinders in the point of contact, E and ν are Young's modulus and Poisson's ratio, respectively, m_t and n_t are coefficients characterizing the change of shape of the contact due to thermal loading, K is the thermal conductivity of the material, μ is the coefficient of friction, V is the sliding velocity, m is a constant which relates the load to the size of a Hertzian contact and α is the coefficient of thermal expansion.

This model predicts that scuffing depends on contact load, sliding velocity, coefficient of friction, geometrical parameters, and thermal and material properties of the contacting surfaces. However, it should be noted that, for a similar contact geometry, load, sliding velocity and coefficient of friction, this model predicts the same scuffing load for all aluminum alloys, irrespective of their composition, because they have approximately the same elastic and thermal properties. This clearly contradicts the experimental data obtained from both the scuffing study under dry sliding conditions [57] and the present study. Furthermore, the above model is based on the Hertzian contact, therefore, the applicability of the model for area contacts needs to be examined.

6.2 Hypothesis Based on Failure of Lubricant and Surface Films

The hypothesis based on failure of lubricant films was first proposed by Dyson [24]. Based on this hypothesis, scuffing was explained as a collapse of the hydrodynamic and elastohydrodynamic lubricant films which, under normal operating conditions, separate the

sliding surfaces completely. If films collapse, some asperities come into contact with asperities from the counterface which results in high local pressures and temperatures. These high local temperatures may lead to local reduction of the viscosity of the lubricant, more contacts, and further increase in temperature. Therefore, attention was drawn to the comparison of lubricant film thickness with the average height of asperities. In this hypothesis, the condition for scuffing is usually related to the Λ ratio, which is defined as:

$$\Lambda = \frac{h}{\sigma} \tag{6.3}$$

where h is the fluid film thickness based on smooth surfaces and σ is the composite rms surface roughness of sliding surfaces 1 and 2, defined as:

$$\sigma = \sqrt{\left(\sigma_1^2 + \sigma_2^2\right)} \tag{6.4}$$

Based on this hypothesis, if the fluid film thickness can be maintained to a dimension greater than that of the asperity heights on the sliding surfaces, there should be no scuffing. There is some validity to the Λ criterion, but this hypothesis has a serious limitation because the collapse of lubricant films does not always lead to scuffing. In practical machinery there are many examples of surfaces that survive values of Λ as low as 0.3 [76]. Obviously, lubricant films are the first line of defense against scuffing, however, if contact conditions are severe enough, these films cease to be effective and the protection of the surfaces may rely on films formed by physical or chemical reaction between the surface and the lubricant, or a chemical reaction between the surface and the environment. The failure of lubricant films represents only a necessary condition for scuffing. Lee and Ludema [76] also noted that surface failure could not be predicted by using the Λ ratio except when chemically inert lubricants are used. They found that the protective layers on

sliding surfaces, which are formed by chemical reaction with the lubricant, reduced the surface roughening and increased the scuffing load.

Another difficulty of this approach is that, under isothermal conditions, the equation of elastohydrodynamics for elliptical contacts predicts that the lubricant film thickness increases with the sliding velocity as follows [76]:

$$\frac{h_{\min}}{R'} = 3.63\left(\frac{V\eta_o}{E'R'}\right)^{0.68}(\alpha E')^{0.49}\left(\frac{W}{E'R'^2}\right)^{-0.073}\left(1-e^{-0.68k}\right) \tag{6.5}$$

where

$h_{\min}$: minimum film thickness

V: $\frac{V_1+V_2}{2}$, entraining surface velocity

V_1, V_2: velocities of surfaces 1 and 2

η_o: viscosity of the lubricant at atmospheric pressure

E': $2\left(\frac{1-\upsilon_1^2}{E_1}+\frac{1-\upsilon_2^2}{E_2}\right)^{-1}$, combined Young's modulus for surfaces 1 and 2

R': $\left(\frac{1}{R_1}+\frac{1}{R_2}\right)^{-1}$, equivalent radius of curvature for surfaces 1 and 2

α: pressure-viscosity coefficient

W: normal load

k: ellipticity parameter

Therefore, for the given load, the tendency of scuffing should be lower at higher velocities. However, the experimental data of the IRG studies show that scuffing resistance decreases as sliding speed increases. Hence, the effect of decreasing film thickness due to the higher temperature must dominate the effect of increasing film thickness due to the higher velocity. The same trend was also observed from the experimental data obtained in this study, both with shoe-on-disc and pin-on-disc geometries. It should also be noted that the Λ criterion does not consider material properties. Ludema [58] indicated that the

critical value of Λ is different for every type of surface topography, substrate microstructure, lubricant, and break-in process. Furthermore, these four variables are interdependent. The conclusion is that this hypothesis provides some correlation with the experimental data in some cases, but scuffing predictions cannot be based on the Λ values.

An extensive amount of research [7-8, 20-21] has been conducted in the area of adsorption to explain the critical conditions for scuffing. Frewing [78] initially suggested that desorption of the surface-active material from the metal is responsible for the friction transition. This idea was extended by Askwith, Crouch and Cameron [20] who analyzed their data using Langmuir's adsorption theory. They suggested that the critical temperature of 150°C obtained with a mineral oil was due to desorption of the surface-active compounds in the oil. This has led to the formulation of the desorption hypothesis [7] for scuffing. The major assumption of this hypothesis is that scuffing occurs when the layer of polar molecules adsorbed on the surfaces becomes critically depleted or disoriented. Lee and Cheng [8] further developed this hypothesis and proposed a theoretical temperature-pressure theory for scuffing using the following adsorption/desorption formula [21]:

$$\theta = \frac{F}{F + \frac{K_b T}{h}\frac{2\pi m_a K_b T}{h^2}\exp\left(\frac{-\Delta H}{K_b T}\right)} \tag{6.6}$$

where

F: $\dfrac{p}{\sqrt{2\pi m_a K_b T}}$

p: bulk lubricant pressure

m_a: mass of the adsorbate

K_b: Baltzmann's constant

ΔH: heat of adsorption

h: Plank's constant

θ: fractional adsorbate coverage

T: surface temperature

The critical temperature-pressure theory is based on the thermal adsorption/desorption behavior of the protective lubricant film interposed between the interacting surfaces. This theory predicts the breakdown point of the lubricant surface film as a function of the hydrodynamically-generated pressure and the frictionally-generated contact temperature. When the temperature is increased, the thermal excitation of adsorbed lubricant molecules becomes greater, increasing their possibility of escape from the surface. In contrast, increasing the pressure keeps the adsorbates from leaving the surfaces by the "caging effect". Therefore, the concentration of the adsorbed surface film is determined by a competition between the pressure and temperature. Spikes and Cameron [7] in 1974 found that a friction transition occurs when the fractional adsorbate coverage (θ) is about 0.5. Based on this critical adsorbate concentration, Lee and Cheng [8] obtained a theoretical critical temperature-pressure curve for a PAO (Poly α olefin) oil as shown in Fig. 6.3.

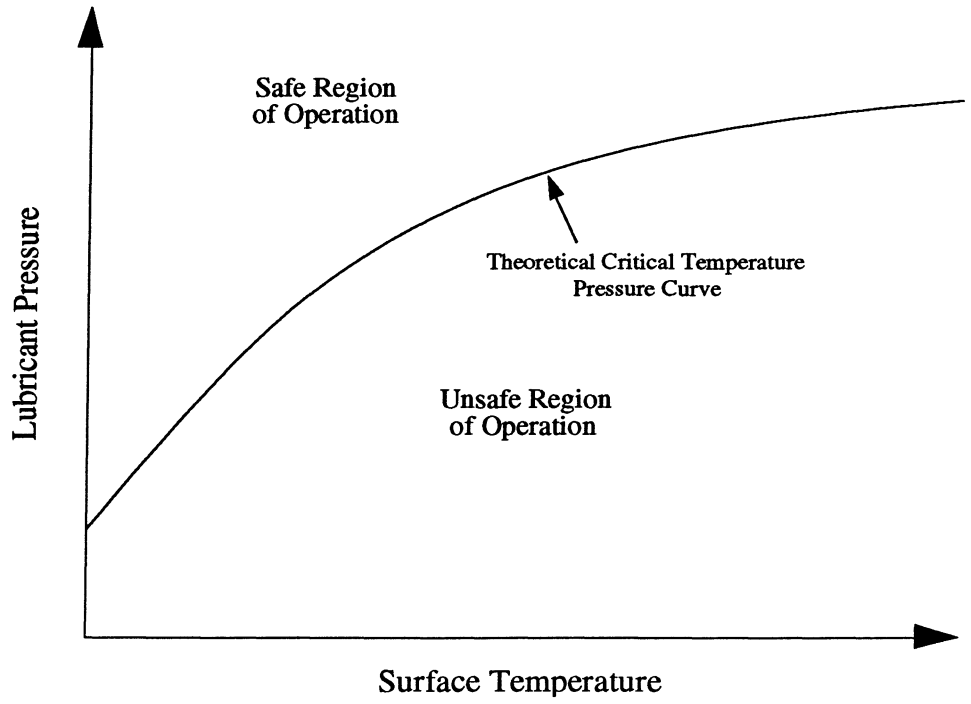

Fig 6.3 - Schematic form of the theoretical critical pressure-temperature curve at 50 percent adsorbate concentration. Ref. [8]

Based on this theory, if any sliding system operates above the critical temperature pressure curve it is safe from scuffing failure while operating below the curve will result in scuffing failure. There seems to be a correlation between experimental scuffing data and this critical temperature and pressure theory [21]. However, this hypothesis has difficulties explaining the effect of materials which is of primary importance for the scuffing process. In this hypothesis, the heat of adsorption for a particular lubricant-metal system is one of the controlling factors in characterizing scuffing failure. However, our scuffing data (Fig. 4.4) show that the scuffing pressure of 390-T6 aluminum alloy is higher than that of DHT3 aluminum alloy. The heat of adsorption for these materials with a PAG lubricant should not be significantly different. In addition, Lee and Ludema [76] argued that the desorption process for surface films formed by chemical reactions is reaction-rate related and therefore time dependent. Hence, the dynamics of their formation and destruction cannot be described by a simple static equation. As stated before, the critical temperature-pressure theory indicates that, as the surface temperature increases, the adsorbate concentration on the surfaces decreases resulting in scuffing failure. However, during sliding, it is also known that oxide films are formed and they can further protect sliding surfaces from scuffing after desorption of the adsorbed films occurs. Therefore, a complete modeling of scuffing would also require the characterization of oxides formed on the surfaces. Ludema also noted that if scuff initiation takes place on a microscopic scale, then all microscopic entities must be thoroughly characterized, including oxides. For these reasons, some hypotheses related to the breakdown of the oxide films were proposed and are discussed in detail below.

A model for predicting scuffing failure based on the competitive kinetics of oxide formation and removal was developed by Cutiongco and Chung [9]. This hypothesis assumes that the oxide removal rate will be greater than the oxide formation rate at a certain critical temperature, leading to eventual metal-to-metal contact, and hence, scuffing failure. This seems to be another hypothesis which relates scuffing to surface temperature.

However, this hypothesis can provide an explanation for the physical nature of the critical temperature condition.

In this hypothesis, the rates of oxide formation and removal are expressed as Arrhenius-type relations:

$$R_f = v_f \exp\left(-\frac{E_f}{RT}\right) \tag{6.7}$$

and

$$R_r = v_r \exp\left(-\frac{E_r}{RT}\right) \tag{6.8}$$

where R_f and R_r are the rates of oxide formation and removal respectively, v_f and v_r are the corresponding pre-exponential factors, E_f and E_r are the activation energies, R is the gas constant and T is the absolute temperature. The critical scuffing condition is expressed as:

$$R_r \geq R_f \tag{6.9}$$

This model was applied to scuffing data with some success by Shen et al. [79]. However, in this hypothesis, data for the rate of oxide growth are taken from static oxidation tests at temperatures in the range of 140-250°C. The rates of oxides removal are obtained from wear tests in vacuum. It has been experimentally proven [69] that static oxidation rates cannot be used to predict the thickness of the oxide layer in a sliding contact. From scuffing study under dry sliding condition [57], the thickness of transformed layers observed are orders of magnitude thicker than layers found using static oxidation rates. As was indicated in Chapter 5, there are other mechanisms involved in the formation of a transformed (oxide) layer.

Since it is generally accepted that scuffing will occur if the rate of removal of the protective surface layers exceeds the rate of their formation, the concept behind this hypothesis still remains valid. However, more experimental and theoretical work on the dynamics of the protective layer formation and destruction are necessary.

6.3 Hypotheses Based on Material Failure

6.3.1 Critical Plastic Deformation Hypotheses

The major problem with the above hypotheses is that the effect of the mechanical properties of the contacting surfaces is not taken into account. A large amount of surface and subsurface plastic deformation is often present at scuffing. Therefore, the plasticity index, originally proposed by Greenwood and Williamson [12], has been proposed as a possible indicator of scuffing . The plasticity index is a measure of the amount of surface plastic deformation due to the contact between the asperities. It was postulated that scuffing will occur at some critical value of surface plastic deformation, which would lead to the destruction of the protective surface layers. The plasticity index is defined as:

$$\psi = (E'/H)\sqrt{\sigma/\beta}, \quad \text{then}$$

if $\psi < 0.6$ elastic contact, and

if $\psi > 1$ plastic contact

where E' is the equivalent elastic modulus, H is the hardness of the softer material, β is the average asperity tip radius, and σ is the composite surface roughness of the two bodies in contact. Even though this hypothesis was experimentally verified in the work of Hirst and Hollander [13], the experimental results of Park and Ludema [28] showed that the plasticity index for predicting scuffing is not a useful indicator. They repeated the tests of Hirst and Hollander and investigated the validity of the plasticity index for a large range of

surface roughness, test conditions and material properties. They found that the plasticity index hypothesis deviate significantly from the experiments.

In another hypothesis proposed by Xue and Ludema [29], scuffing is based on a critical amount of accumulated plastic strain in the sliding track. The proposed criterion is formulated as:

$$\frac{\varepsilon_c}{\varepsilon_o} \propto \frac{\tau_i WV}{H^2} \tag{6.10}$$

where ε_c is the critical strain, ε_o is the ductility of the material in terms of reduction in area at fracture, and τ_i/H is the ratio of the strength of the surface films to the bulk hardness of the material. In this hypothesis, scuffing failure is related to the damage in the surface caused by extensive plastic deformation. However, there are no experimental data for the plastic deformation in the original paper, therefore, the validity of this concept has not been proven.

6.3.2 Subsurface Fatigue Hypothesis

Although subsurface fatigue is widely recognized as one of the major wear mechanisms, the possibility that the same process could be responsible for scuffing has not been investigated in much details. Kim and Ludema [30] made the first attempt to relate scuffing to bulk low cycle fatigue. They found a good correlation between scuffing of steel/steel contacts under lubricated conditions and low cycle fatigue. However, this idea has not been developed to the point where the mechanism of scuffing can be explained.

Recently, Sheiretov [57] proposed a subsurface fatigue hypothesis for scuffing under dry sliding conditions. Based on this hypothesis, scuffing is due to the accumulation of plastic deformation and fatigue damage in the subsurface. A criterion for scuffing based on the proposed hypothesis is also developed. The criterion involves several functional relationships between the macroscopic loading parameters, the local stresses and

temperatures, and the local material properties. The proposed criterion can explain the experimentally observed phenomena such as the effect of the material, PV = *constant* relationship, temperature dependence, size and loading history effects. However, the proposed hypothesis is based on the experimental data obtained under dry sliding conditions. In the present study, no subsurface damage is observed in the specimens until scuffing occurs (Figs. 5.7(a) and 5.8). Also, the results obtained for loading history effects presented in Figs. 4.12 and 4.15 of Chapter 4, suggest that a gradual accumulation of damage is not responsible for scuffing under starved lubrication conditions. Therefore, for the starved lubrication conditions considered in this work, this hypothesis does not seem to be directly applicable.

6.3.3 Critical Subsurface Shear Stress Hypothesis

The critical subsurface stress hypothesis was proposed by Somi Reddy et al. [17] to describe the large-scale subsurface failure of aluminum-silicon alloys, which was observed at scuffing under dry sliding conditions. Based on this hypothesis, ductile rupture of the subsurface is the mechanism responsible for scuffing. This hypothesis states that scuffing occurs when the shear stress (τ) at a critical depth under the surface exceed the temperature-dependent shear strength of the bulk material (S_m) at this depth. The critical condition for scuffing is simply described as:

$$\tau \geq S_m(T) \tag{6.11}$$

The subsurface failure mechanism for scuffing is supported by the experimental observations in their previous paper [31]. This hypothesis is also supported by the fact that the stronger aluminum alloys scuffed at higher PV's. The temperature effects can also be easily incorporated in the hypothesis through the dependence of the shear strength on temperature. However, Sheiretov [57] has shown that this criterion for subsurface failure is

not satisfied for the conditions that he studied. He compared the shear strength of 390-T6 Al at the measured bulk temperature to the calculated subsurface equivalent shear stresses at the critical depths and found that the shear stresses at those depths are not high enough to cause the predicted bulk shear failure. Also, this hypothesis needs to be verified for lubricated contacts.

CHAPTER 7

PROPOSED SCUFFING HYPOTHESIS UNDER STARVED LUBRICATION CONDITIONS

As shown in the previous chapter, the scuffing hypotheses in the literature are based on very different physical processes which make their generalization to a single theory of scuffing very difficult. The only common feature of these hypotheses seems to be the destruction of protective films, although each hypothesis deals with films of very different physical and chemical nature. In general, it seems that the key to understanding scuffing is the dynamics of protective films formation and destruction. In most lubricated contacts, films of various nature may be present at the sliding interface, building several lines of defense against scuffing, as shown in Fig. 7.1.

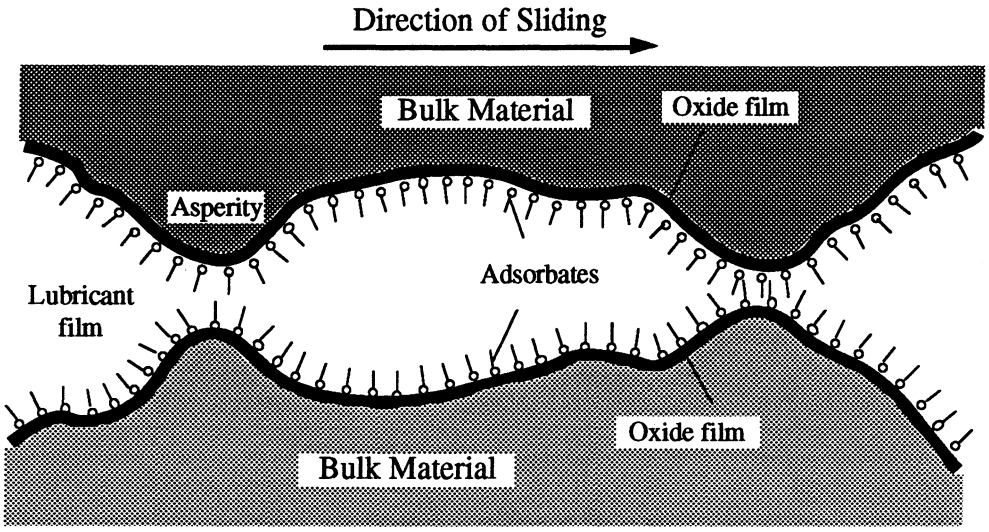

Fig. 7.1 - Schematic of various surface protective films in a lubricated contact

The bulk lubricant film protects the surfaces by limiting asperity interactions and distributing the load more evenly over the whole contact area. In general, the adsorbed films have low shear strength characteristics so that they can reduce the local temperature rise.

The oxide films also have low shear strength characteristics and they protect surfaces from adhesions by preventing exposure of the bare metal. All the lines of defense must be removed for scuffing to occur. This view can be expressed in terms of necessary and sufficient conditions for scuffing, as suggested by Lee and Cheng [21]. The failure of lubricant and adsorbed films represent only necessary conditions for scuffing. In the present study, it is suggested that the sufficient condition for scuffing is given by the destruction of the oxide films due to plastic deformation of asperities. The strength of the material is a important parameter characterizing the scuffing process since it makes the surface more resistant to plastic deformation. The mechanism of failure of the surface and/or subsurface material is one of the least studied and understood aspects of scuffing. Therefore, the present study concentrates on these aspects of the process. A hypothesis and its corresponding criterion for scuffing are proposed based on the experimental results obtained in this study.

7.1 Description of the Proposed Scuffing Hypothesis

In this study, only scuffing under starved lubrication conditions is considered. However, it is believed that the scuffing process and failure mechanism of the material are the same for fully lubricated contacts. In the proposed hypothesis, it is assumed that all the protective surface films must be removed for scuffing to occur. It was shown in Fig. 5.9 that macroscopic adhesions are formed at the sliding interface, resulting in the formation of cold welds. Also, based on a progression study of the scuffing process in Chapter 5 (Figs. 5.6 and 5.7), initiation of scuffing failure seems to be caused by plastic shearing. Based on these assumption and findings, it is proposed in this study that the formation of macroscopic adhesions leading to plastic shearing of the bulk material is responsible for scuffing. This concept was first addressed in a study by Somi Reddy et al. [17]. As previously described, they proposed that scuffing under dry sliding conditions occurs if the shear stress at a critical depth under the surface exceeds the temperature-dependent shear

strength of the bulk material at this depth. However, they did not develop this idea any further for lubricated contacts and did not provide a detail description of the scuffing process.

In the present study, it is hypothesized that, when scuffing occurs, the local surface tangential traction at the sliding interface is higher than the bulk strength of the softer material. The softer material is then sheared and transferred to the harder counterface, as shown in Fig. 5.9. During the sliding process, the surface is initially protected by various surface protective films formed at the tips of asperities. These films prevent large-scale adhesion between the sliding surfaces. However, at certain critical conditions, these films can be locally removed mainly due to high local pressures and temperatures, exposing bare metals which can cause local microscopic adhesions. The bulk material failure due to plastic shearing, caused by the formation of extensive adhesions at the sliding interface, is considered as the final stage of the scuffing process. A detail description of probable mechanisms of the scuffing process is given below. A generalized view of events leading to scuffing is schematically illustrated in Fig. 7.2.

(1) Local breakdown of the lubricant and adsorbed films.

In mixed or boundary lubrication conditions, due to local high pressures and temperatures, lubricant breakdown can occur as the result of asperity interactions. The surfaces can still be continuously protected by chemically or physically-formed adsorbed films. However, if the local temperature is high enough, the thermal excitation of adsorbates increases resulting in a higher probability of their detachment from the surface, as proposed in the adsorption theory [7]. This condition is schematically shown in Fig. 7.2(a). As indicated previously, the breakdown of these films is only the necessary condition for the occurrence of scuffing.

(2) Breakdown of the protective oxide films due to plastic deformation of asperities.

After breakdown of the lubricant and adsorbed films, the oxide films can still protect the surface from scuffing. If the contacts are under relatively light load at a given speed, the oxide films are generally not destroyed, and relatively weak adhesion between these oxides occurs. This is the condition where the oxidative wear is dominant. However, if the load is increased, the elastic limit of the softer material can be reached locally, resulting in plastic deformation of asperities under the oxide. This plastic deformation destabilizes the protective oxide films formed on top of the asperities, and eventually causes shearing or chipping-off of these films as shown in Fig. 7.2(b).

(3) Local exposure of the bare metal and formation of microscopic cold welds.

The removal of the local surface protective films expose the bare metal. The contact of this bare metal with the counterface will result in the formation of microscopic adhesions. It is known that, for aluminum/steel contacts, when the nascent aluminum makes contact with the steel, whether it is the steel itself or the oxide present on the steel surface, the adhesion is extremely strong because aluminum bare metal is very reactive and bonds very strongly to the oxygen of the iron oxide or to the elemental iron itself [80]. If, due to microscopic adhesion, the local surface tractions mainly shear off the tips of the asperities, mild adhesive wear occurs or sometimes also referred to as microscopic scuffing.

(4) Formation of macroscopic adhesions leading to plastic shearing of the bulk material.

As the load is further increased, the accumulation of microscopic cold welds eventually leads to the formation of macroscopic adhesions. It is generally observed that, when two dissimilar metals are brought into contact, the interfacial bonding between them is stronger than the cohesive bonds of the weaker metal. Upon application of separating forces to the adhered junction, failure occurs in the cohesively weaker metal, and this allows the cohesively weaker to be transferred to the cohesively stronger [80]. With surface traction, these adhesions can cause subsurface shear failures. The depth at which these

failures occur depends on the mechanical and thermal properties of the near surface layer. For the conditions studied in this research, shear failures often occurred at a depth of about 1-2 μm (Fig. 5.6(a)). When this happens, the surface traction at the interface will increase sharply.

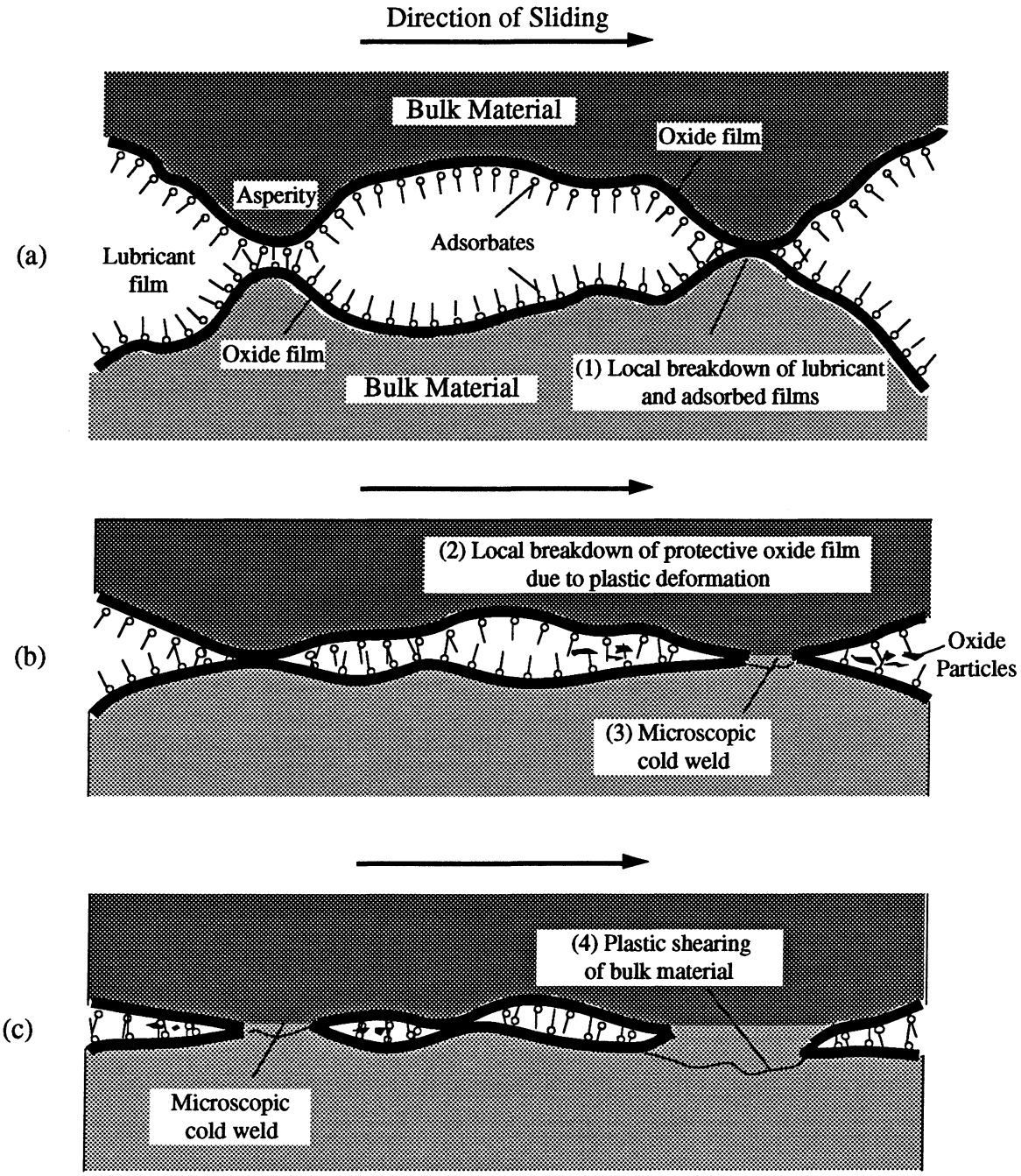

Fig. 7.2 - A descriptive model for the scuffing process under starved lubrication conditions

7.2 Proposed Criterion for Scuffing

Based on the above hypothesis, scuffing occurs when the surface tangential traction ($\mu P_{\max}$) at the interface exceeds the temperature-dependent bulk shear strength (τ_s) of the material. This criterion can be expressed as:

$$\mu P_{\max} \geq \tau_s(T) \tag{7.1}$$

where μ is the coefficient of friction and P_{max} is the maximum asperity contact pressure.

Contact between solid bodies at normal operating loads is limited to small areas of true contact between the high asperities of either surfaces. The maximum asperity contact pressures, therefore, are very high and can result in localized plastic deformation. Since this pressure increases with increased nominal contact pressure, the surface tangential traction increases as the nominal contact pressure increases. However, at the given speed, the near-surface shear strength of the material decreases as the contact pressure increases since the surface temperature increases with the increased contact pressure. Therefore, as the contact pressure increases at the given speed, a critical point is reached where the surface tangential traction equals the near-surface shear strength of the material. This critical condition for scuffing is schematically illustrated in Fig. 7.3 for a step loading history.

7.2.1 Shear Strength of the Materials

To evaluate the proposed criterion for scuffing, the shear strength data for the materials tested need to be obtained at various temperatures. These data are obtained according to the ASTM B 565-94 procedure. Typical load-displacement curves obtained with this procedure are given in Figs. 7.4 and 7.5. From these data, the shear strengths of the materials as a function of temperature are obtained, as shown in Fig. 7.6. It should be noted that, except for 150 ℃, the shear strengths of 390-T6 and DHT3 Al alloys are approximately the same even though the hardness of 390-T6 Al (72 HRB) is much higher than that of DHT3 Al (46 HRB). The 390-T6 and DHT3 Al alloys are fabricated by casting

and extrusion processes, respectively. It is believed that the lower than expected bulk shear strength of the 390-T6 Al alloys is due to the large amount of porosity generated during the casting process. It is also interesting to note that the shear strengths of gray cast iron and Si-Pb brass are approximately the same up to 300 ℃, and that of Si-Pb brass sharply decreases if the temperature is higher than 300 ℃, as shown in Fig. 7.6.

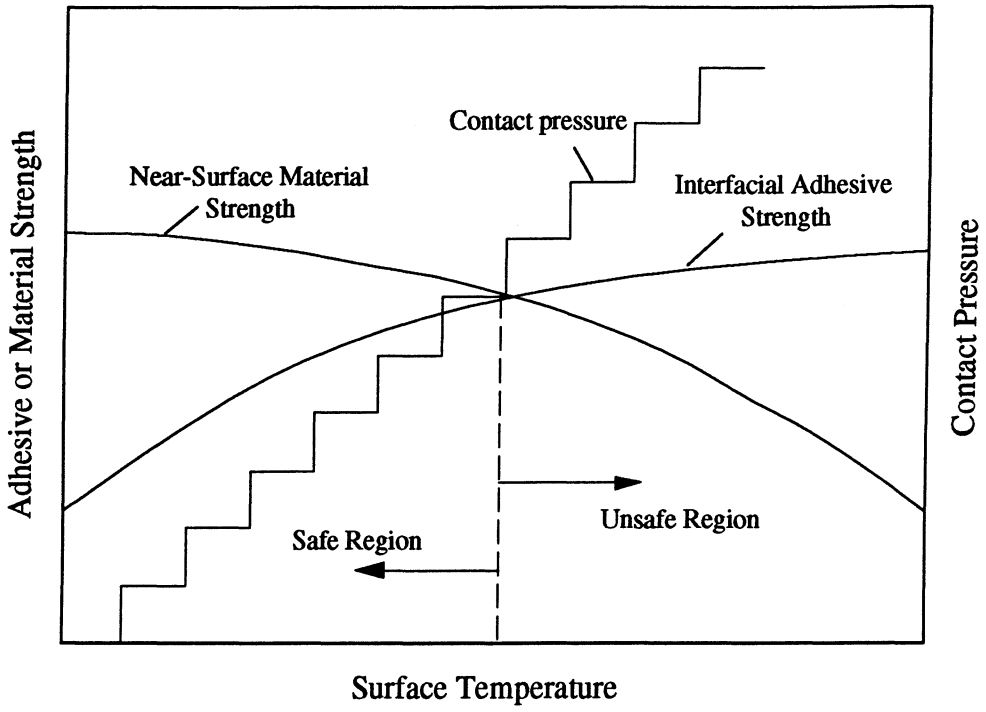

Fig. 7.3 - Illustration of the critical condition for scuffing at the given speed

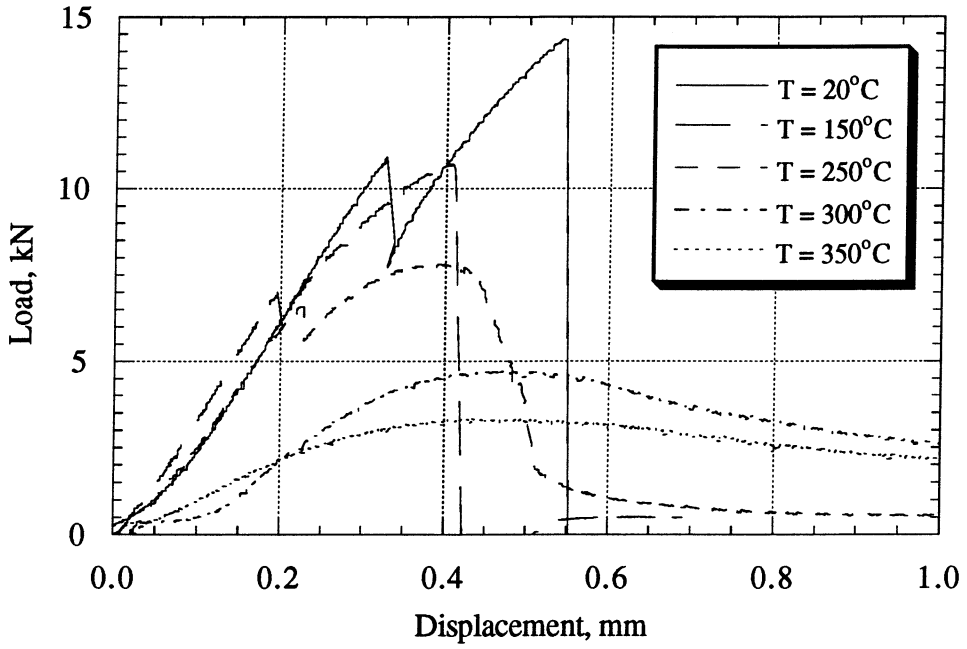

(a)

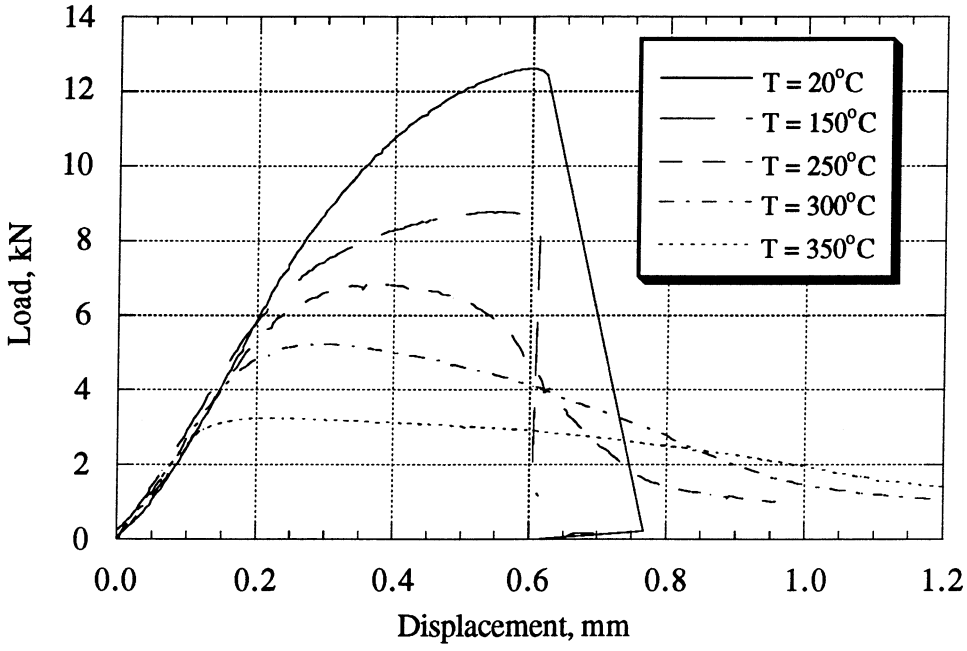

(b)

Fig. 7.4 - Typical load-displacement curves for (a) 390-T6 Al and (b) DHT3 Al

Shear displacement rate = 0.05 mm/s

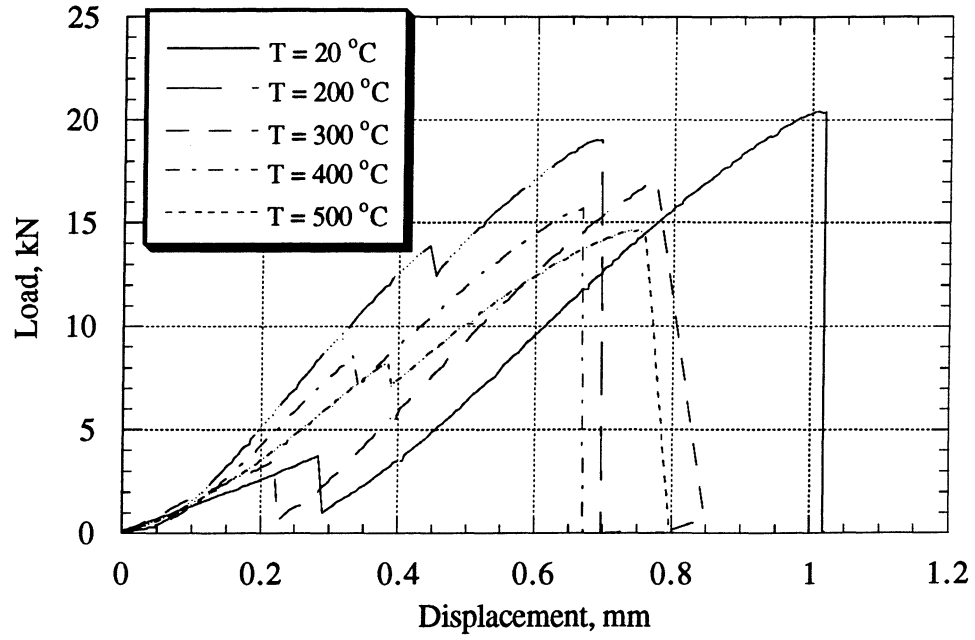

(a)

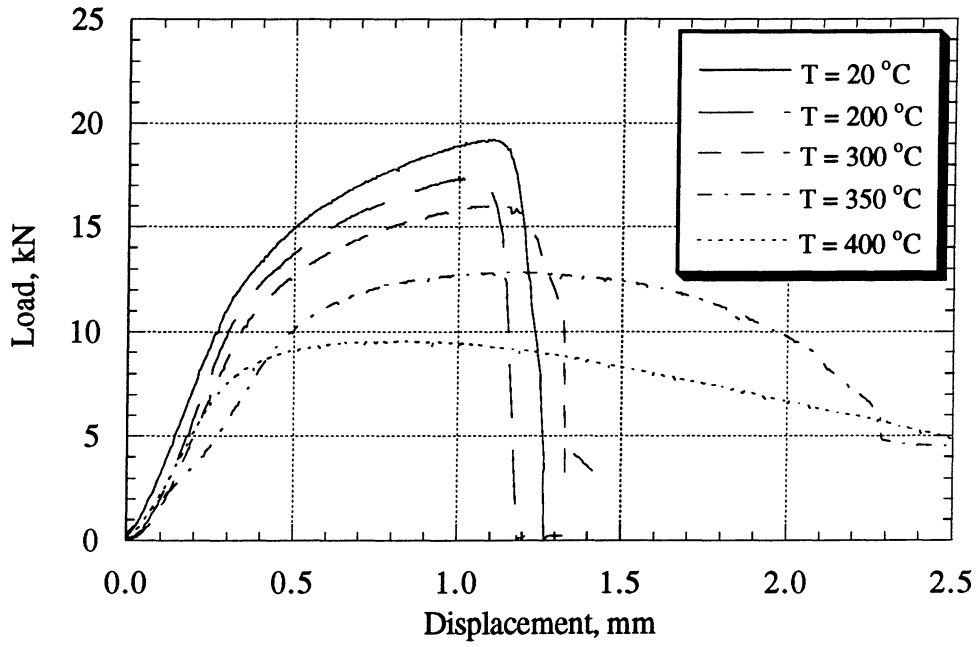

(b)

Fig. 7.5 - Typical load-displacement curves for (a) Gray Cast Iron and (b) Si-Pb Brass

Shear displacement rate = 0.05 mm/s

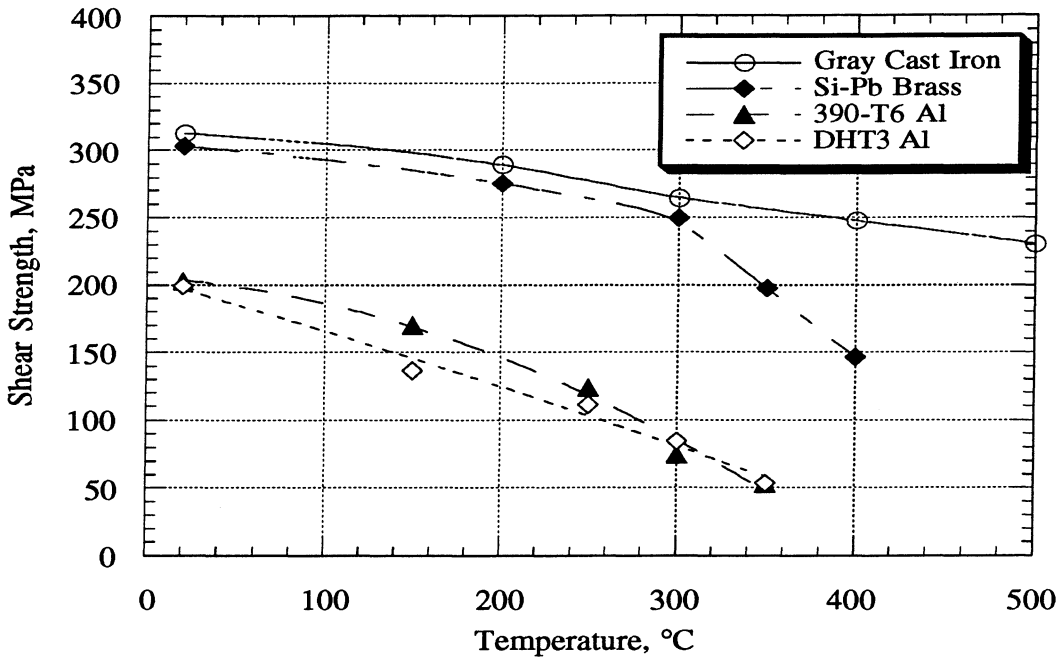

Fig. 7.6 - Bulk shear strength of gray cast iron, Si-Pb brass, 390-T6 and DHT3 Al alloys as a function of temperature

Shear displacement rate = 0.05 mm/s

7.2.2 Asperity Contact Pressure

As previously stated, when two rough surfaces are pressed together, discrete contact regions are produced. The total area of these contact is known as the real area of contact. This area is much smaller than the nominal area of contact. Therefore, the contact pressures at the tips of the contacting asperities are much greater than the average nominal contact pressure. These pressures are important parameters since they affect the local plastic deformation and temperature rise. To examine the proposed criterion for scuffing, these pressures need to be obtained. Unfortunately, these parameters cannot be measured. Hence, their determination is based on models for the contact of rough surfaces.

In this study, the asperity contact pressures are estimated using the analytical model developed by He [74]. This model is based on a 3-D contact simulation of rough surfaces developed by Ren and Lee [81]. Their contact simulation assumes that the contact

deformation is purely elastic. The rough surface profiles of two contacting bodies are combined to form one equivalent rough surface (with an appropriately adjusted elastic modulus) in contact with a rigid plane. Ren and Lee used the following Boussinesq's solutions for the normal elastic displacement d of an arbitrary point on the surface with coordinates (x, y) due to a point force p(s, t)dsdt applied at (s, t):

$$d(x,y)=\frac{2}{\pi E'}\iint_{\Omega_c}\frac{p(s,t)}{\sqrt{(s-x)^2+(t-y)^2}}dsdt \tag{7.2}$$

where

E': $2\left(\frac{1-\upsilon_1^2}{E_1}+\frac{1-\upsilon_2^2}{E_2}\right)^{-1}$, equivalent Young's modulus of bodies 1 and 2

Ω_c: real area of contact

As shown in Fig. 7.7, the gap between the rigid plane and deformed surface, h is written as:

$$h(x,y)=h_o(x,y)+h_r(x,y)+d(x,y) \tag{7.3}$$

where h_o and h_r are the original undeformed surface profile height measured from the mean line and the vertical distance from the rigid plane to the undeformed mean line, respectively.

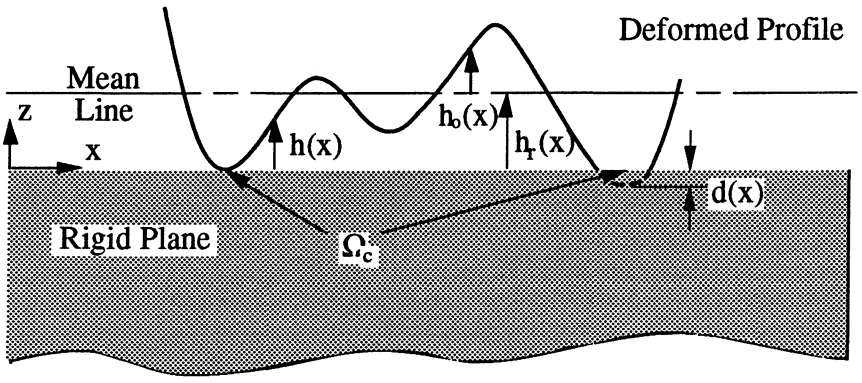

Fig. 7.7 - Contact between an elastic half-space and a rigid plane

If it is assumed that the asperities have spherical tips, then, using the following non-dimensional parameters,

$$X = \frac{x}{a} \qquad Y = \frac{y}{a} \qquad P = \frac{p}{p_H} \qquad H = \frac{hR}{a^2} \tag{7.4}$$

where

$$p_H = \frac{2}{3}\frac{w}{\pi a^2} \qquad a = \frac{2}{3}\left(\frac{wR}{E'}\right)^{1/3} \tag{7.5}$$

a: Hertzian contact radius

p: contact pressure

p_H: maximum Hertzian contact pressure

R: sphere radius

w: applied load

equations (7.2) and (7.3) can be written as:

$$D(X,Y) = \frac{2}{\pi^2}\iint_{\Omega_C} \frac{P(\xi,\lambda)}{\sqrt{(\xi - X)^2 + (\lambda - Y)^2}} d\xi d\lambda \tag{7.6}$$

$$H(X,Y) = H_o + H_r(X,Y) + D(X,Y) \tag{7.7}$$

The boundary conditions are given as:

$H(X,Y) = 0$, $P(X,Y) > 0$; when point (X,Y) in Ω_c

$H(X,Y) > 0$, $P(X,Y) = 0$; when point (X,Y) not in Ω_c

where

D(X,Y): non-dimensional normal elastic displacement;

P(X,Y): non-dimensional contact pressure;

H(X,Y): non-dimensional gap between the rigid plane and deformed surface;

Equation (7.6) is written in a discrete form with the use of biquadratic polynomial interpolating functions (C_{ij}) for relating contact pressures to deformations:

$$\{D\} = [C]\{P\}, \text{ or } D_i = \sum_{j=1}^{N} C_{ij} P_j, \quad i = 1, \cdots, N \tag{7.8}$$

where $\{D\}$ and $\{P\}$ are the deformation and pressure vectors, respectively, and $[C]$ is the deformation matrix which is only a function of the grid geometry. Since neither the contact pressures nor the deformations are initially known, iterations are needed to modify the pressure distribution based on the assumed deformed surface profile. These processes are continued until all the boundary conditions are satisfied. A more detail description of this method is given in [81].

Based on Ren and Lee's contact simulation, He [74] obtained maximum asperity contact pressures (P_{max}) for Al-Si alloy/steel contacts. These pressures are based on asperities of the same heights using the following sinusoidal surface profiles:

Longitudinal roughness profile: $z(x,y) = R\sin(2\pi y/\lambda)$

Transverse roughness profile: $z(x,y) = R\sin(2\pi x/\lambda)$

Isotropic roughness profile: $z(x,y) = R\sin(2\pi x/\lambda)\sin(2\pi y/\lambda)$

A constant wave length of 0.17 mm was used in the simulations since typical wave length of actual surface profiles for his test specimens just before scuffing was approximately 0.17 mm. Different asperity heights were used to generate various surface roughness values. A large number of maximum asperity contact pressures is generated as a function of nominal pressures and surface roughness values. Through a series of curve fittings based on these data, the following close-form expressions for P_{max} are obtained:

For the longitudinal and transverse roughness profiles:

$$P_{max} = 12.46\sigma^{0.07}P \quad \text{(MPa)} \quad P < 5MPa \tag{7.9}$$

$$P_{max} = -0.0000232\sigma^{-1.11}P^2 + 5.08\sigma^{-0.11}P + 7.81\ln\sigma + 39.32 \quad \text{(MPa)} \tag{7.10}$$

$$5 \le P < 35MPa \qquad \text{for } \sigma = 0.0005 \sim 0.003mm$$

$$5 \le P < 40MPa \qquad \text{for } \sigma = 0.003 \sim 0.006mm$$

$$5 \le P < 50MPa \qquad \text{for } \sigma > 0.006mm$$

$$P_{max} = 92.43 \ln \sigma + 50.56 \sigma^{-0.13} \ln P + 495.77 \quad \text{(MPa)} \tag{7.11}$$

$$P \ge 35MPa \qquad \text{for } \sigma = 0.0005 \sim 0.003mm$$

$$P \ge 40MPa \qquad \text{for } \sigma = 0.003 \sim 0.006mm$$

$$P \ge 50MPa \qquad \text{for } \sigma > 0.006mm$$

For the isotropic roughness profile:

$$P_{max} = 17.03P \quad \text{(MPa)} \qquad P < 5MPa \tag{7.12}$$

$$P_{max} = (0.0475 \ln \sigma + 0.23)P^2 + 12.39\sigma^{-0.07}P + 3.22 \ln \sigma + 15.81 \quad \text{(MPa)} \tag{7.13}$$

$$5 < P \le 30MPa$$

$$P_{max} = 40.98\sigma^{-0.04} \ln P + 426.57\sigma^{0.04} \quad \text{(MPa)} \tag{7.14}$$

$$P > 30MPa$$

where P is the nominal contact pressure and σ is the combined rms roughness of two surfaces.

To estimate the asperity contact pressures at scuffing using the above equations, the surface roughnesses of the specimens just before scuffing are needed. However, it is very difficult to stop the test just prior to scuffing since scuffing occurs very fast and without warning. Therefore, the surface roughness values at one load step before scuffing, given in Table 7.1, are used.

Table 7.1 - Surface roughnesses for Al/steel contact pairs at one load step before scuffing

Material	P (MPa)	V (m/s)	PV (MPa•m/s)	σ_1 (μm rms) Al pins	σ_2 (μm rms) Steel discs	† σ (μm rms)
390-T6 Al	105.5	0.93	98.1	0.08	0.059	0.10
	56.2	1.40	78.7	0.16	0.058	0.17
	35.2	1.86	65.5	0.18	0.055	0.19
	14.1	2.79	39.3	0.23	0.045	0.23
	7.03	4.65	32.7	0.25	0.035	0.25
DHT3 Al	105.5	0.47	49.6	0.05	0.062	0.08
	42.2	0.93	39.2	0.08	0.056	0.10
	28.1	1.40	39.3	0.17	0.047	0.18
	14.1	2.79	39.3	0.24	0.028	0.24
	7.03	4.65	32.7	0.44	0.028	0.44

† Composite surface roughness; $\sigma = \sqrt{\sigma_1^2 + \sigma_2^2}$

The wave lengths of the surface profiles of the aluminum alloys tested are in the range of 0.13 - 0.16 mm. A typical surface profile, showing the wave length of DHT3 Al at one load step before scuffing, is shown in Fig. 7.8. The plot also shows that the asperity heights are approximately constant. Therefore, the above equations can be used to estimate the maximum asperity contact pressures for the aluminum alloys tested. Data for Si-Pb brass and gray cast iron are not obtained because the models for these materials are not available. In this study, it is assumed that the surface roughnesses of the specimens are isotropic because the contact spots observed one load step before scuffing are randomly distributed on the sliding surfaces as shown in Fig. 7.9. Using equations (7.12)-(7.14), a typical asperity contact pressure, as a function of the nominal contact pressure, for a surface roughness of 0.2 μm is shown in Fig. 7.10 Using the combined rms surface

roughnesses σ (Table 6) and the scuffing PV data given in Fig. 4.4, the maximum contact pressure for the aluminum alloys at scuffing is plotted in Fig. 7.11.

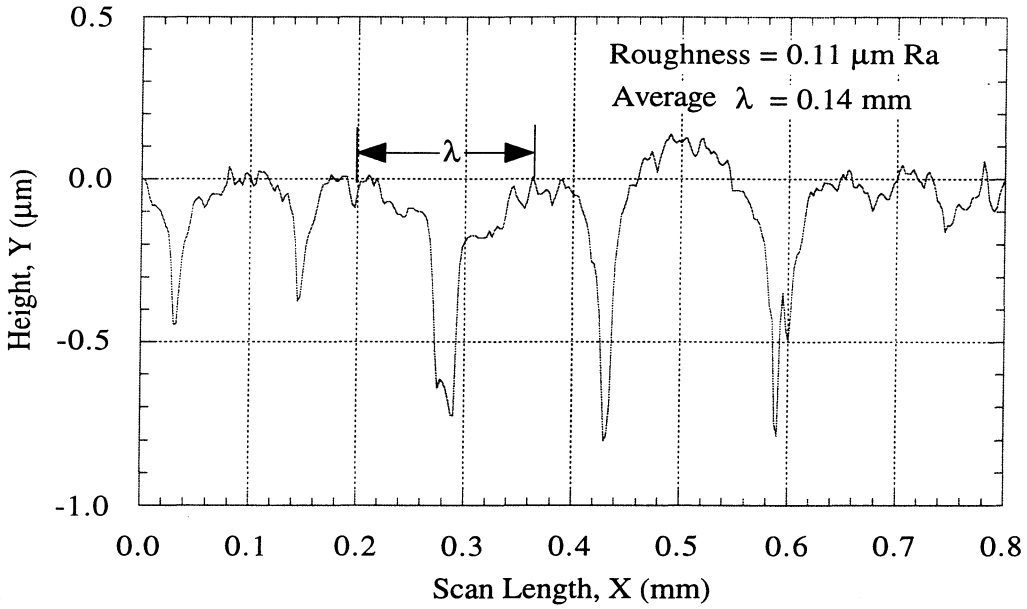

Fig. 7.8 - Typical wave length of DHT3 Al surface profile at one load step before scuffing

P = 42.2 MPa, V = 0.93 m/s

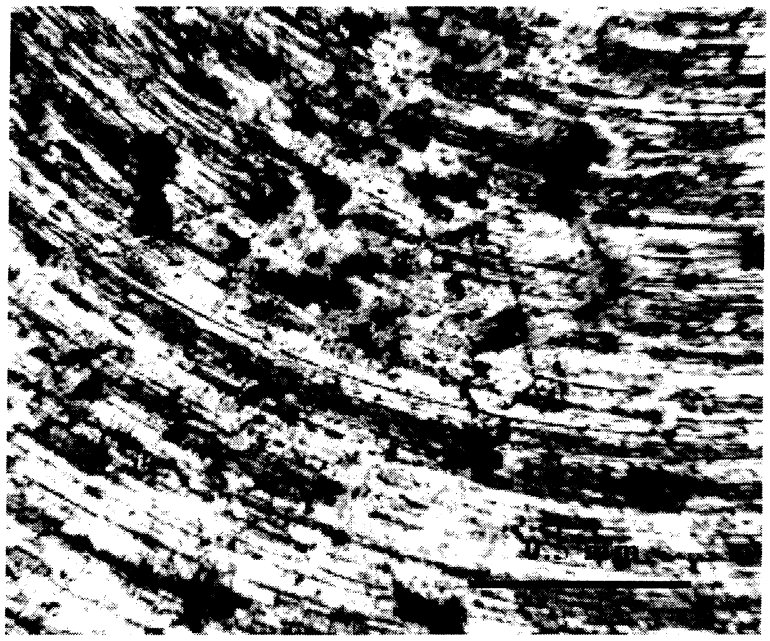

Fig. 7.9 - Typical surface of 390-T6 Al pin at one load step below scuffing

P = 42.2 MPa, V = 1.86 m/s

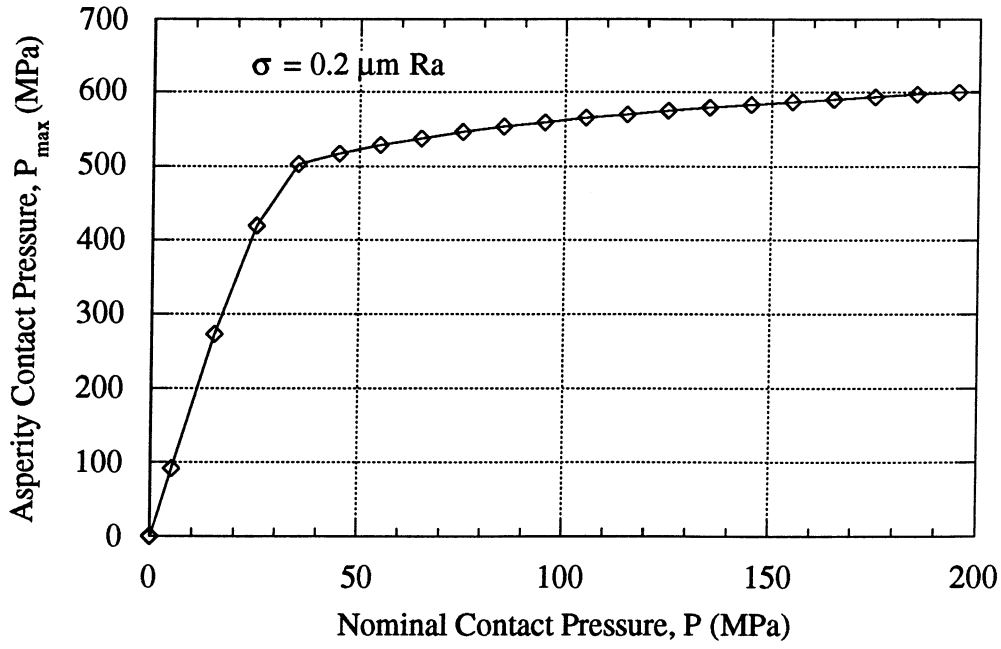

Fig. 7.10 - Asperity contact pressure as a function of the nominal contact pressure

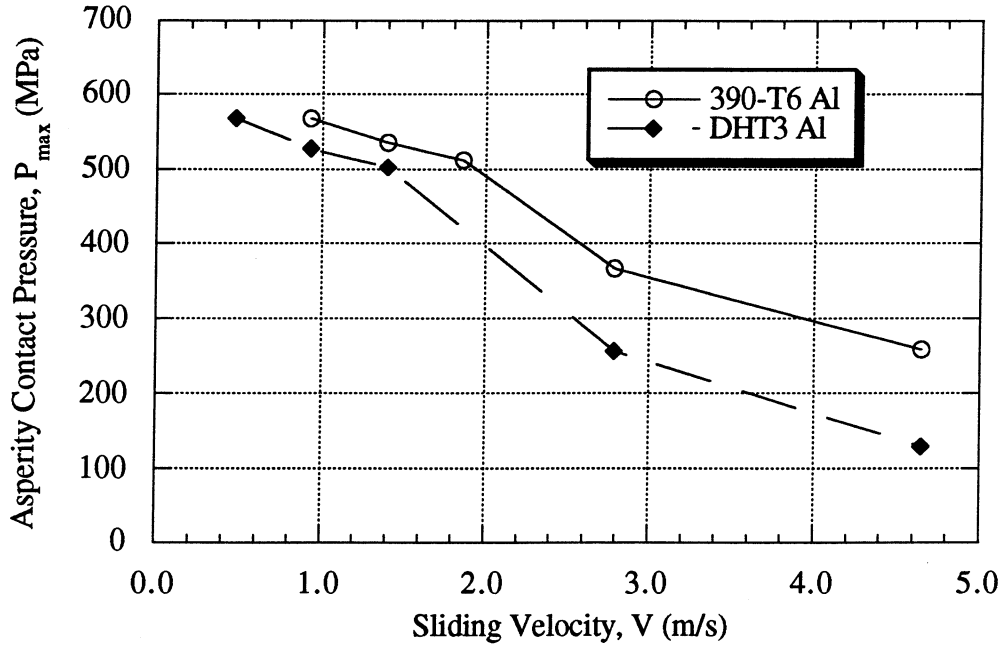

Fig. 7.11 - Asperity contact pressure for aluminum alloys at scuffing

7.2.3 Asperity Contact Temperature

As previously stated, the surface temperature consists of two components. The first component is the bulk temperature of the material and the second is the asperity contact temperature (the flash temperature). As with the asperity contact pressure, the asperity contact temperature is a very important parameter to characterize the interfacial conditions at the sliding surfaces. As indicated previously, since the real area of contact between opposing asperities is always considerably smaller than the apparent area of contact, the frictional energy and resulting heat at these contacts become highly concentrated with a correspondingly large temperature rise. This temperature rise, however, is very difficult to obtain experimentally. Hence, estimates for the asperity contact temperature also have to rely on thermal models.

The most popular of the thermal models is that of Blok's [19], which has been further developed by the theoretical work of Jaeger [70]. The model is based on the analytical solution for a point heat source acting on an infinite half-space. Results for circular and square stationary and moving heat sources have been derived. This model works very well for concentrated contacts. The reason is that the actual distribution of the real contact spots within the Hertzian contact area does not have a significant influence on the thermal resistance of the whole contact [82]. Thus, it can be assumed that the whole Hertzian contact area contributes to the conduction of heat, which avoids the solution of the problem for the actual distribution of the contact spots. However, these approximations do not give good results for area contacts.

Recently, Qiu and Cheng [83] developed a numerical simulation of the temperature rise between a three-dimensional rough surface against a smooth surface in a lubricated contact. As shown in Fig. 7.12, the contact area is considered to be fixed in the coordinate system and two half-space surfaces move across the contact along the x-axis with velocities V_1 and V_2, respectively.

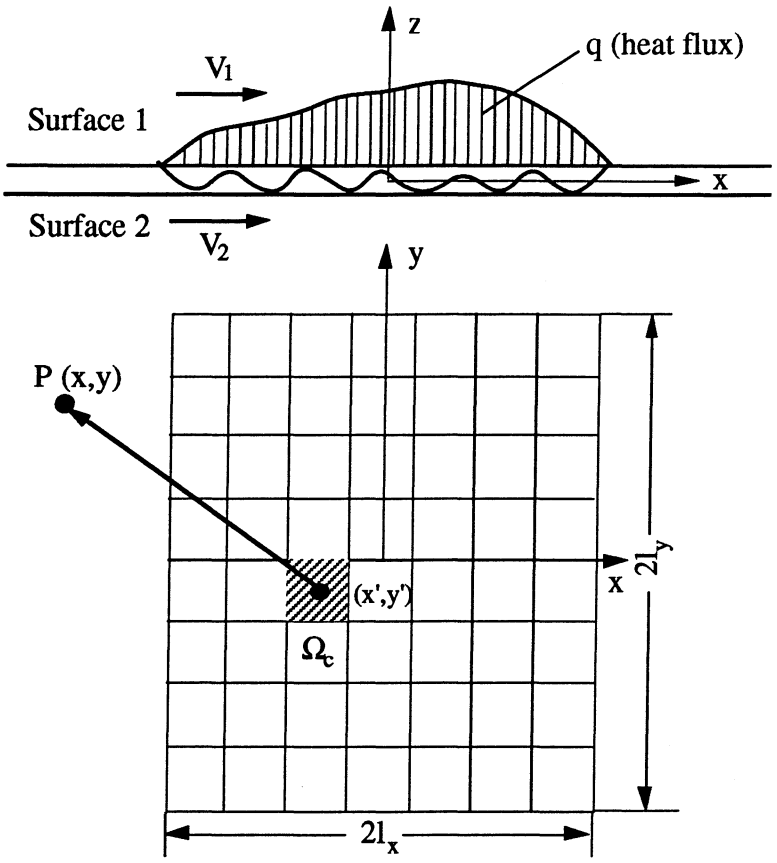

Fig. 7.12 - Schematic of sliding surfaces and contact area for temperature calculation

The equations which govern the surface temperature of the two moving surfaces, as functions of position and time, are derived as follows. If there is no heat loss from the surfaces, the temperature increment at a point P (x,y) on either of the two surfaces at any time due to an instantaneous heat source of strength q (x',y',0,t')dx'dy'dt' at x', y', and t' was calculated by the following equation given by Carslaw and Jaeger [84]:

$$dT = \frac{q(x',y',0,t')dx'dy'dt'}{4\rho c\left[\pi\alpha(t-t')\right]^{3/2}} \exp\left[-\frac{(x-x')^2+(y-y')^2}{4\alpha(t-t')}\right] \tag{7.15}$$

where ρ is the density of solids, c is their specific heat, and α is the thermal diffusivity of solids.

Using the following non-dimensional parameters:

$$\bar{x}=\frac{x}{l_x} \qquad \bar{y}=\frac{y}{l_x} \qquad \bar{t}=\frac{4\alpha}{l_x^2}t \qquad \bar{p}=\frac{p}{p_m} \qquad \bar{V}_i=\frac{V_i l_x}{4\alpha}$$

$$\sigma=\frac{l_x^2}{R} \qquad P_m=\frac{\pi E'\sigma}{2l_x} \qquad \bar{q}=\mu\bar{p}\bar{V}_s \qquad \bar{T}=\frac{\pi^{3/2}\rho c}{2P_m}T \qquad (7.16)$$

where

l_x: half contact length along moving direction x

p_m: reference pressure

V_s: $V_1 - V_2$, sliding speed

R: $\left(\frac{1}{R_1}+\frac{1}{R_2}\right)^{-1}$, equivalent radius

μ: coefficient of friction

σ: $\sqrt{\sigma_1^2+\sigma_2^2}$, composite surface roughness

Equation (7.15) can be written as:

$$d\bar{T}=\frac{\bar{q}(\bar{x}',\bar{y}',0,\bar{t}')d\bar{x}'d\bar{y}'d\bar{t}'}{(\bar{t}-\bar{t}')^{3/2}}\exp\left[-\frac{(\bar{x}-\bar{x}')^2+(\bar{y}-\bar{y}')^2}{(\bar{t}-\bar{t}')}\right] \qquad (7.17)$$

The total heat generated at the interface is partitioned according to a partition factor f (x,y,t), which represents the fraction of heat flux conducted into surface 1. The temperature rise formulations for the surfaces acted on by a single heat source at time t' are then given as follows:

Temperature rise on surface 1 is:

$$d\bar{T}_1=f(\bar{x}',\bar{y}',\bar{t}')\frac{\bar{q}(\bar{x}',\bar{y}',0,\bar{t}')d\bar{x}'d\bar{y}'d\bar{t}'}{(\bar{t}_1-\bar{t}')^{3/2}}\exp\left\{-\frac{\left[(\bar{x}-\bar{x}')-\bar{V}_1(\bar{t}_1-\bar{t}')\right]^2+(\bar{y}-\bar{y}')^2}{(\bar{t}_1-\bar{t}')}\right\} \qquad (7.18)$$

Temperature rise on surface 2 is:

$$d\bar{T}_2 = \left[1 - f(\bar{x}', \bar{y}', \bar{t}')\right] \frac{\bar{q}(\bar{x}', \bar{y}', 0, \bar{t}') d\bar{x}' d\bar{y}' d\bar{t}'}{(\bar{t}_2 - \bar{t}')^{3/2}} \exp\left\{ - \frac{\left[(\bar{x} - \bar{x}') - \bar{V}_2(\bar{t}_2 - \bar{t}')\right]^2 + (\bar{y} - \bar{y}')^2}{(\bar{t}_2 - \bar{t}')} \right\} \qquad (7.19)$$

The surface temperature rise produced by all the frictional heat sources is calculated by integrating the above differential temperatures over the contact heat source area from time $\bar{t}' = 0$ to time $\bar{t}' = \bar{t}$. The surface temperature rise in the fixed coordinate system at time $\bar{t}$ over the contact area is expressed as follows:

$$\Delta\bar{T}_1(\bar{x}, \bar{y}, \bar{t}) = \int_0^{\bar{t}} \iint_{\Omega_c} d\bar{T}_1(\bar{x}', \bar{y}', \bar{t}') \qquad (7.20)$$

$$\Delta\bar{T}_2(\bar{x}, \bar{y}, \bar{t}) = \int_0^{\bar{t}} \iint_{\Omega_c} d\bar{T}_2(\bar{x}', \bar{y}', \bar{t}') \qquad (7.21)$$

As with the maximum asperity pressure calculations, He [74] used the same sinusoidal surface profiles for asperity contact temperature estimations. Based on this numerical simulation, the maximum asperity temperature data for Al-Si alloys with various combinations of the nominal pressure, sliding velocity and surface roughness values were obtained. The following close-form expressions for the maximum asperity temperature, T'_{max}, are obtained:

For 339 Al-Si alloy:

(1) Longitudinal roughness:

$$T'_{max} = \mu\sigma^{0.06}\left(177.2V^{0.93} \ln P - 258.7V^{0.93}\right) \qquad (7.22)$$

(2) Transverse roughness:

$$T'_{\max} = \mu\sigma^{0.06}\left(187.1V^{0.62}\ln P - 273.2V^{0.62}\right) \tag{7.23}$$

(3) Isotropic roughness:

$$T'_{\max} = \mu\sigma^{0.19}\left(224.1V^{0.92}\ln P - 143.6V^{0.92}\right) \tag{7.24}$$

For 390-T6 Al-Si alloy:

(1) Longitudinal roughness:

$$T'_{\max} = \mu\sigma^{0.058}\left(175.5V^{0.91}\ln P - 256.9V^{0.91}\right) \tag{7.25}$$

(2) Transverse roughness:

$$T'_{\max} = \mu\sigma^{0.056}\left(182.2V^{0.62}\ln P - 266.11V^{0.62}\right) \tag{7.26}$$

(3) Isotropic roughness:

$$T'_{\max} = \mu\sigma^{0.19}\left(235.8V^{0.88}\ln P - 151.4V^{0.88}\right) \tag{7.27}$$

where μ is the coefficient of friction, σ is the rms combined surface roughness, V is the sliding velocity, and P is the nominal contact pressure.

Equations (7.22) to (7.27) are obtained based on the nominal contact area of $2l_x = 0.0065m$ by $2l_y = 0.001m$. Since the surface temperature rise depends on the nominal contact area, more calculations with various rectangular contact areas were conducted by He to obtain more general expressions for the maximum asperity temperatures. The modified equations for both Al alloys are given as follows:

(1) Longitudinal roughness:

$$T_{\max} = T'_{\max} + (21.54\ln V + 47.01)\ln\left(\frac{2l_x}{0.0065}\right) + (6.20\ln V + 16.66)\ln\left(\frac{2l_y}{0.001}\right) \tag{7.28}$$

(2) Transverse roughness:

$$T_{max} = T'_{max} + (40.45 \ln V + 54.60) \ln\left(\frac{2l_x}{0.0065}\right) + (1.18 \ln V + 13.81) \ln\left(\frac{2l_y}{0.001}\right) \quad (7.29)$$

(3) Isotropic roughness:

$$T_{max} = T'_{max} + (37.75 \ln V + 54.16) \ln\left(\frac{2l_x}{0.0065}\right) + (15.50 \ln V + 25.69) \ln\left(\frac{2l_y}{0.001}\right) \quad (7.30)$$

T'_{max} in equations (7.28) to (7.30) is based on the $2l_x = 0.0065m$ and $2l_y = 0.001m$. The second and third parts are due to the increase or decrease of contact nominal size along the x and y-direction, respectively.

Since 0.00635 m diameter pins are used in the present study, the asperity contact temperatures are estimated based on $2l_x = 2l_y = 0.00563m$, giving the same nominal contact area as the pins. Using Eq. (7.30) with $2l_x = 2l_y = 0.00563m$, the asperity flash temperatures of the aluminum alloys at scuffing are estimated using three different friction coefficients as shown in Fig. 7.13. The range of 0.2 to 0.3 is considered since this is the typical range of coefficient of friction obtained when scuffing occurs. It is assumed that the local friction coefficient range, when scuffing is initiated, is approximately the same. It should be noted that the temperature data for DHT3 Al are based on the equations obtained for 339 Al. This approximation should be valid since their hardness values are approximately the same. The surface temperature data for the aluminum alloys are summarized in Table 7.2. These data show that the surface temperature is not constant at scuffing.

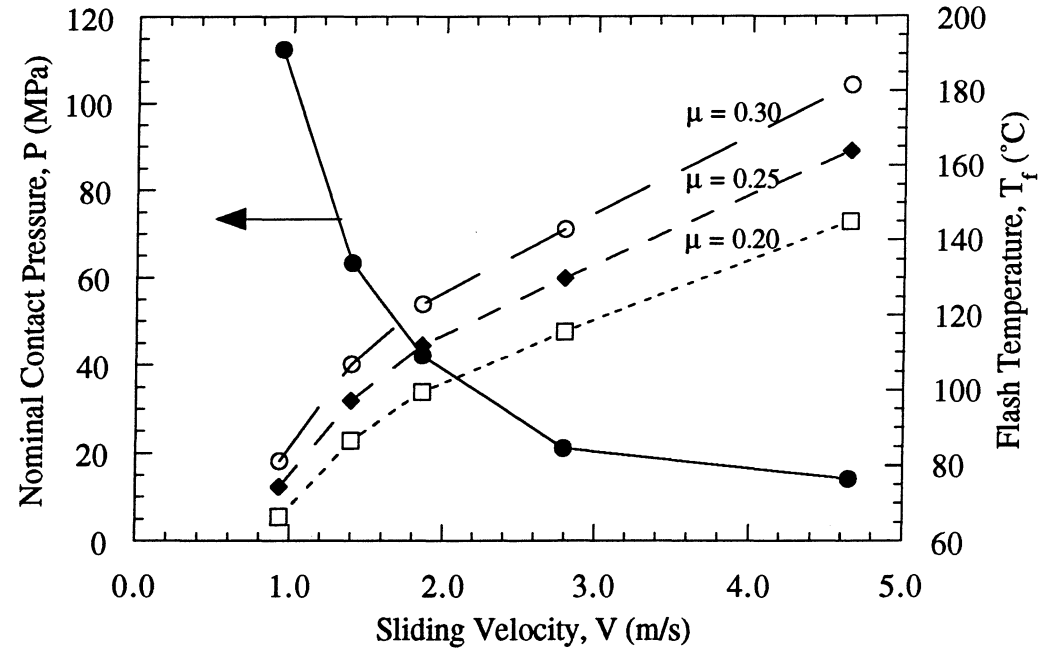

(a)

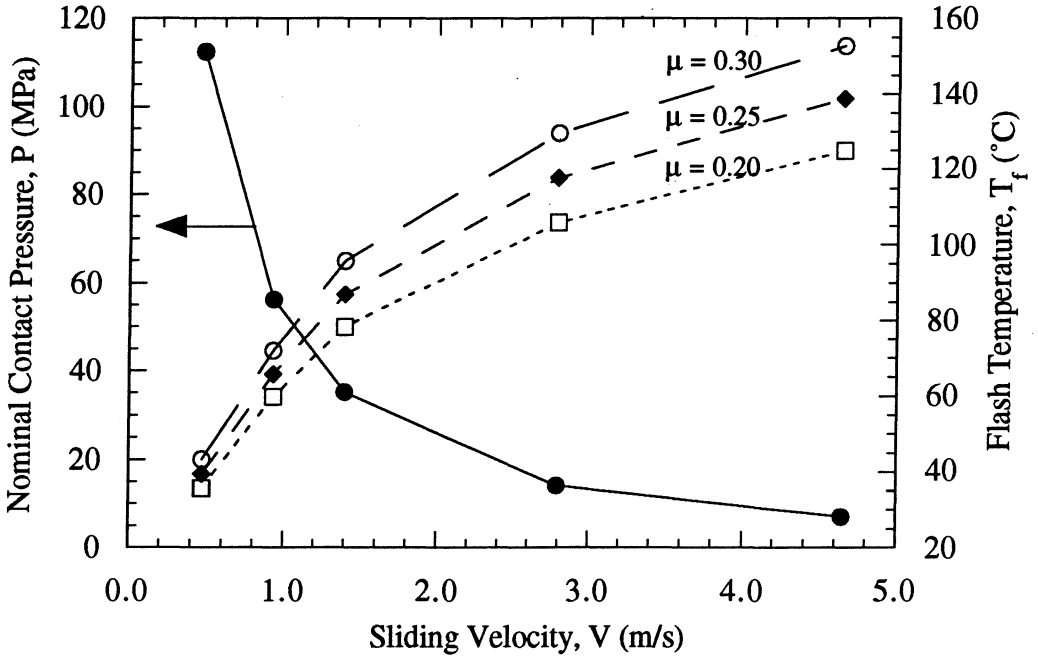

(b)

Fig. 7.13 - The flash temperatures for aluminum alloys at scuffing

(a) 390-T6 Al, (b) DHT3 Al

Table 7.2 - Surface temperature data at scuffing for aluminum alloys tested

Material	P (MPa)	V (m/s)	PV (MPa•m/s)	$^{\dagger}T_s$ (μ=0.2) (°C)	T_s (μ=0.25) (°C)	T_s (μ=0.30) (°C)
390-T6 Al	112.5	0.93	104.6	213.4	221.3	228.2
	63.3	1.40	88.6	228.5	239.2	248.8
	42.2	1.86	78.5	249.4	261.8	273.0
	21.1	2.79	58.9	260.5	274.8	287.9
	14.1	4.65	65.6	295.0	313.9	331.6
DHT3 Al	112.5	0.47	52.8	155.7	159.5	163.3
	56.2	0.93	52.3	189.7	195.9	202.1
	35.2	1.40	49.3	209.4	218.1	226.7
	14.1	2.79	39.3	231.9	243.8	255.4
	10.5	4.65	48.8	255.0	268.9	282.8

† $T_s = T_b + T_f$ = Surface temperature, T_b = Bulk temperature, $T_f = T_{max}$ = Flash temperature

Based on the surface temperature data given in Table 7.2, the near-surface shear strengths of the aluminum alloys are obtained using Fig. 7.6. The surface tangential tractions (μP_{max}) at scuffing are obtained using the asperity pressure data given in Fig. 7.11. In order to evaluate the proposed criterion, the ratios of the surface tangential tractions to the bulk shear strengths of the aluminum alloys at scuffing are plotted in Fig. 7.14. The results show that, for 390-T6 Al, data obtained with μ = 0.25 match well with the proposed criterion for every sliding velocities used. However, the surface tractions are higher for μ = 0.30 and lower for μ = 0.20 than the bulk shear strengths. A similar trend is observed with DHT3 alloy at lower speeds (V < 2 m/s), however, the surface tractions of DHT3 alloy are lower than the bulk shear strengths at higher speeds (> 2 m/s) for every friction coefficients used. As shown in Fig. 7.15(b), no observable protective films are formed on the specimen tested at 4.65 m/s since scuffing occurs within a very short time. The machining marks are still

present on the surface, indicating very little smoothening of the surface. The formation rate of protective films may be slower at a high speed/low load condition due to less asperity interactions on the sliding surfaces. In addition, there is more likelihood that any films formed are more readily worn since any material element is subjected to more cycles. This is hypothesized to be the reason why the specimens at high speeds failed earlier. In contrast, more surface smoothening is obtained with a low speed/high load, which results in the formation of a relatively uniform protective surface layer as shown in Fig. 7.15(a). The scuffing data for gray cast iron and Si-Pb brass cannot be evaluated based on the proposed criterion because the models for asperity contact pressures and temperatures for these materials are not available.

Considering the complexity of the scuffing process, it is not surprising that the shear criterion for scuffing may not be applicable over a wide range of operating conditions. As with other hypotheses, one of its main limitations is its independence of the dynamics of protective films. The mechanical and thermal properties of these films and their effects on the plastic deformation of the asperities are not known. An additional complexity involves the proper modeling of the surfaces just before scuffing so that better local estimations of asperity contact pressures and temperatures can be made. As shown in the results, the uncertainties associated with the coefficient of friction μ and composite RMS surface roughness σ just before scuffing hinders the proper evaluation of the proposed hypothesis. In spite of these limitations, the proposed hypothesis has some very attractive attributes. First, it describes the failure mechanism during the scuffing process for the materials tested. Secondly, it can explain the fact that stronger material scuffs at higher PV. The temperature effects obtained in a previous study [57] can also be easily incorporated in the hypothesis through the dependence of the shear strength on temperature (Fig. 7.6).

It should be noted that the proposed hypothesis is based on the evaluation of a few Al alloys under starved lubrication conditions. Additional experimentation for other

materials and operating conditions is necessary before the hypothesis can be effectively applied to predict scuffing.

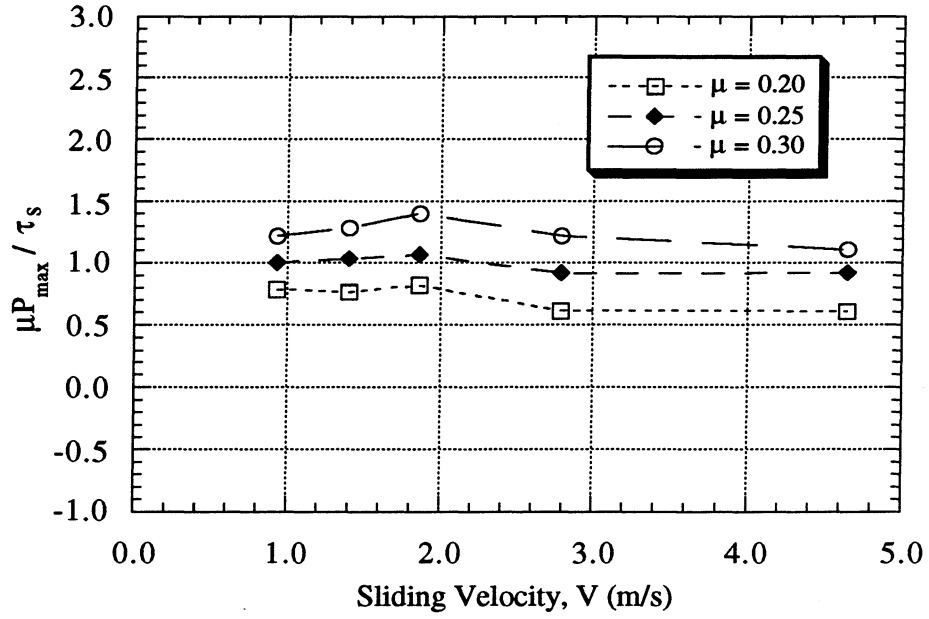

(a)

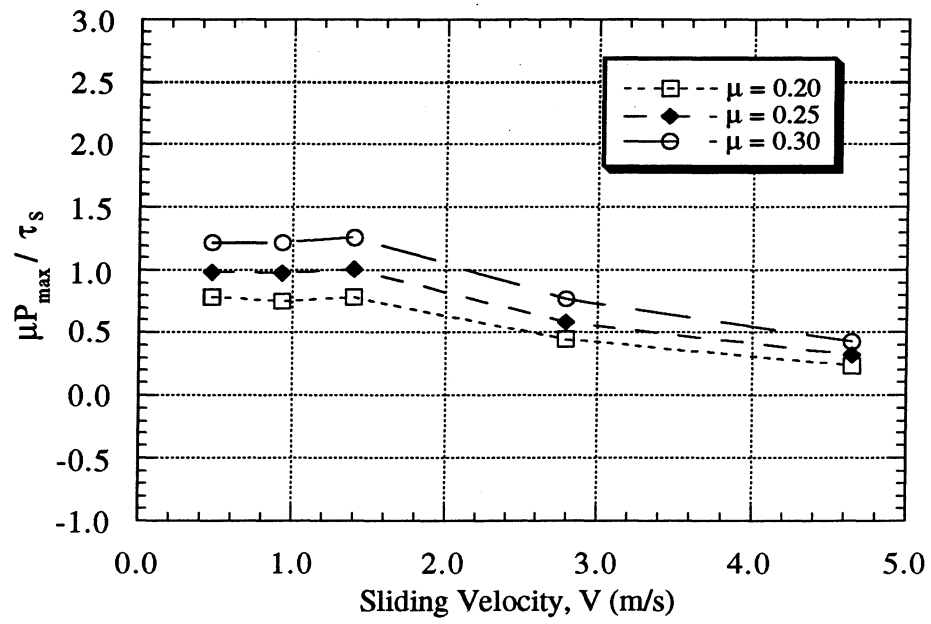

(b)

Fig. 7.14 - Ratios of the surface tangential traction to the shear strength of the aluminum alloys at scuffing
(a) 390-T6 Al, (b) DHT3 Al

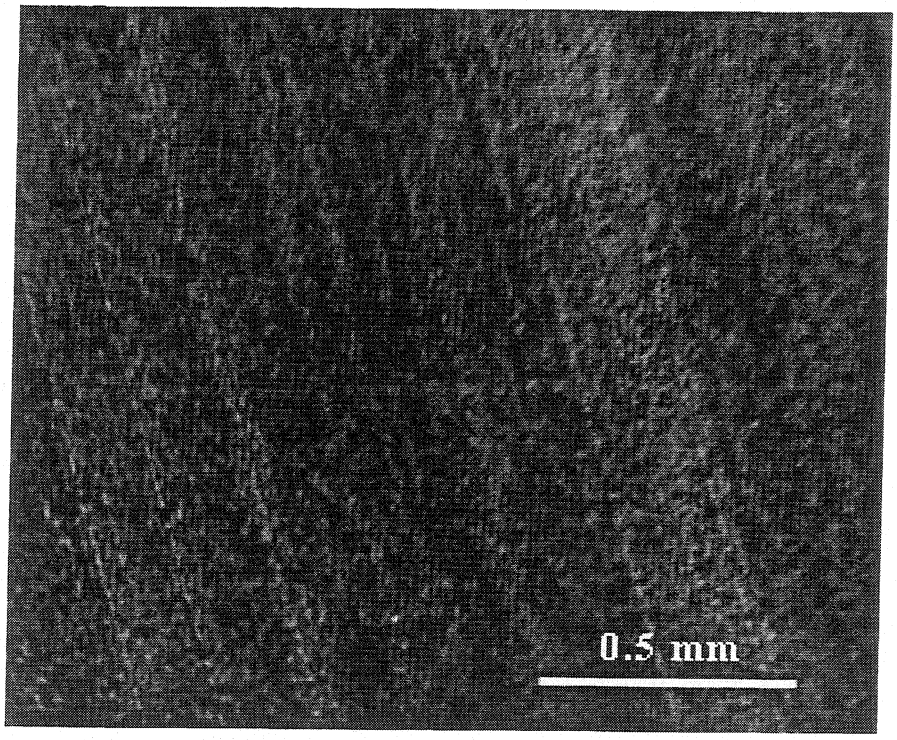

(a)

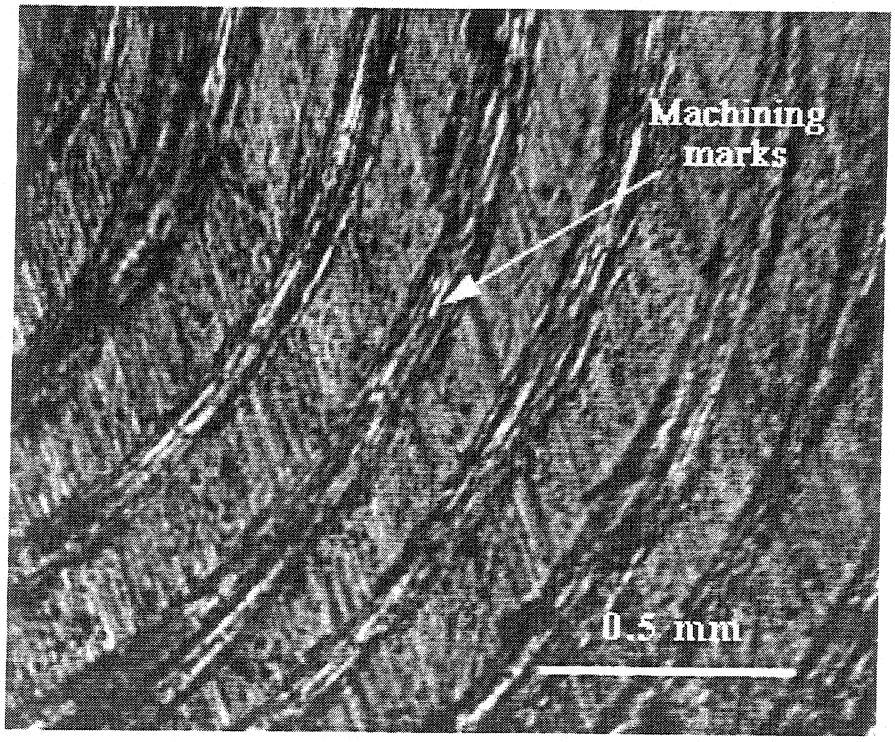

(b)

Fig. 7.15 - Surfaces of DHT3 Al pin obtained at one load step before scuffing
(a) P = 105.5 MPa, V = 0.47 m/s, Roughness = 0.05 μm Ra
(b) P = 7.03 MPa, V = 4.65 m/s, Roughness = 0.44 μm Ra

CHAPTER 8

CONCLUSIONS

Scuffing under lubricated conditions is very broad and complex since it involves mechanical, thermal and chemical interactions between the contacting bodies, the lubricant, the environment, and other species found at the sliding interface. This is the major reason why this phenomenon is still poorly understood, even though numerous studies have been conducted over the past sixty years. While there is an agreement that the formation of large areas of bare metal leading to macroscopic adhesions is one characteristic feature of the scuffing process, the processes leading to this condition and the failure mechanisms of the material are still not clearly understood. The present study concentrates primarily on this aspect of the process. In this study, a more complete set of experimental data for the scuffing behavior of area contacts, for various material pairs, is obtained under starved lubrication conditions. Based on the experimental observations, a probable mechanism of the scuffing process and its corresponding criterion are proposed.

8.1 Research Summary

The present research focuses on two major goals. The first is to obtain design data for swashplate compressors by examining the scuffing behavior of a 390 aluminum disc sliding against a 52100 steel shoe under starved lubrication conditions. The evaluation is based on a shoe-on-disc geometry which approximately simulates the swashplate/shoe contacts in an automotive swashplate compressor. All tests are conducted in a high pressure tribometer (HPT) under R134a environment with a base polyalkylene glycol (PAG) lubricant. The effects of degree of lubricant starvation, sliding velocity, geometry of contact, surface topography, a tin coating, and socket geometry supporting the shoe are evaluated. Data obtained from this study will help identify conditions under which scuffing problems may be reduced in swashplate compressors. The second goal is to study the processes and

mechanisms of the scuffing phenomenon under starved lubrication conditions. This study is based on a pin-on-disc geometry because a pin specimen is easier to section and instrument. The effects of material, lubricant/refrigerant mixture, and loading history on scuffing are examined. The transition behavior of a 390-T6 Al pin sliding against a 1018 carburized steel disc is also examined. To better understand the scuffing processes and the failure mechanisms of material, the surfaces of the test specimens are studied with an optical microscope, a surface profilometer, SEM (Scanning Electron Microscope) and AES (Auger Electron Spectroscopy). The subsurfaces are studied by sectioning the pin specimens tested under scuffing and non-scuffing conditions and examining the sections with SEM and AES. From these examinations, a scuffing hypothesis based on shear failure is proposed. The results obtained from the present study are summarized below:

Shoe/Disc Geometry

(1) For a given environmental temperature and specified contact geometry, the scuffing pressure increases as the lubricant supply rate increases and decreases as the sliding velocity increases.

(2) PV = *constant* relationship seems to characterize the scuffing behavior of 390-T6 Al plate/52100 steel shoe contacts. The value of this constant increases as the degree of lubricant starvation decreases.

(3) Scuffing is a function of crown height and the degree of lubricant starvation. Crowning is detrimental when the contact is severely starved.

(4) When the contact is severely starved, a dimple or groove is also detrimental.

(5) For the whole velocity range tested, the scuffing pressure of 390-T6 Al discs increases with improved surface finish.

(6) For the sliding velocity used, surface roughness effects are more significant as the lubricant supply rate increases, i.e., scuffing of the smoother specimen is affected to a greater degree than that of the rougher specimen.

(7) A skewness change from -0.34 to -1.26 for 390-T6 Al discs with the same surface roughness do not seem to improve their scuffing resistance.

(8) For a given lubricant supply rate, the scuffing pressure of tin-coated 390-T6 Al discs is about three times higher than that of the uncoated discs. It is hypothesized that scuffing of tin-coated 390-T6 Al discs is caused by the removal of the coating, which leads to the formation of macroscopic adhesions between the exposed Al substrate and the steel counterface.

(9) For the velocities and lubricant supply rates used, the effects of socket geometry supporting the shoe on scuffing are negligible.

Pin/Disc Geometry

(1) For any given lubricant supply rates and sliding velocities used, the scuffing resistance of 390-T6 aluminum alloy is better than that of DHT3 alloy (a bismuth-containing aluminum alloy).

(2) As with the results obtained with a shoe/disc geometry, for all materials tested, the scuffing pressure decreases as the sliding speed increases.

(3) At any given speed, the scuffing pressure of Si-Pb brass and gray cast iron is about the same and the scuffing resistance of these materials is better than that of the aluminum alloys tested.

(4) The scuffing pressures of 390-T6 aluminum alloy tested with both the POE base/R134a and the formulated PAG/R134a are higher than those of the aluminum alloy tested with the PAG base/R134a.

(5) For Al/steel contact considered, scuffing is a loading-history dependent phenomenon. The sudden application of the load is more detrimental than stepwise loading. For the run-in time durations considered, the scuffing pressure increases with run-in time.

(6) For 390-T6 Al alloys and for a certain range of the lubricant supply rates, two transitions to scuffing are observed.

(7) It is hypothesized that scuffing under starved lubrication conditions is due to macroscopic adhesions leading to plastic shearing of the bulk material. The processes leading to scuffing are described as follows:

(a) Local breakdown of the lubricant and adsorbed films.

(b) Breakdown of the protective oxide films due to plastic deformation of asperities.

(c) Local exposure of the bare metal and formation of microscopic cold welds.

(d) Formation of macroscopic adhesions leading to plastic shearing of the bulk material.

8.2 Major Accomplishments of the Present Study

Several accomplishments of this study contribute to a better understanding of the scuffing phenomenon. Very few scuffing studies for lubricated area contacts have been conducted in the past. Even fewer have been conducted under starved lubrication conditions. In the present study, a more complete picture of the effects of various parameters affecting scuffing is provided. Some of these factors are investigated for the first time. For the shoe-on-disc geometry, these include the effects of shoe geometries, surface roughness as a function of lubricant supply rates, and socket geometry supporting the shoe. This study also provides a better description of the scuffing processes and, more importantly, a possible failure mechanism of the contacting materials. Very few scuffing studies in the literature have addressed the mechanisms of material failure at scuffing under lubricated conditions. The major accomplishments of this study are discussed in more details below:

(1) Reliable reproduction and identification of scuffing under starved lubrication conditions.

The experimental data on scuffing reported in the literature are mainly based on dry or fully lubricated conditions. Even though many sliding components experience starved lubrication conditions, scuffing characteristics of these contacts, especially area contacts,

have not been fully examined. In this study, a test setup, which can reproduce starved lubrication conditions and used to identify scuffing for area contacts more reliably, has been developed.

(2) Experimental results for lubricated area contacts of various materials.

Historically, most scuffing studies have been conducted with counterformal contacts such as gear teeth, cams and followers, and ball or roller bearings. However, very limited scuffing data for lubricated area contacts are available in the literature. The present study provides a more complete set of experimental results for these contacts. Scuffing data were obtained with both shoe-on-disc and pin-on-disc geometries. A summary of the contributions of this study to the experimental database on scuffing is summarized below:

Shoe/Disc Geometry

(a) The degree of lubricant starvation on scuffing is examined as a function of sliding velocity.

(b) The effects of various shoe geometries on scuffing is examined for the first time.

(c) The effect of surface roughness on scuffing as a function of lubricant supply rates is examined for the first time.

(d) The effect of tin coating is examined and the scuffing mechanism for the tin-coated Al discs is proposed.

(e) The effect of socket geometry supporting the shoe on scuffing is examined for the first time.

Pin/Disc Geometry

(a) The scuffing behavior of the DHT3 Al is studied for the first time.

(b) Quantitative data for the loading history effects on scuffing are obtained.

(c) The transition behavior of 390-T6 Al as a function of the lubricant supply rate is examined for the first time.

(d) The scuffed surfaces and subsurfaces of the test specimens are extensively studied with SEM and AES.

(3) Proposed hypothesis and its corresponding criterion for scuffing.

Data obtained seem to support the hypothesis that scuffing is related to shear failure of the bulk material. This failure is caused by the formation of macroscopic adhesions at the sliding interface. Based on the hypothesis, the criterion for scuffing is given as:

$$\mu P_{\max} \geq \tau_s(T)$$

where μ is the coefficient of friction, P_{max} is the maximum asperity contact pressure and τ_s is the temperature-dependent bulk shear strength of the material. It is hypothesized that, when scuffing occurs, the local surface tangential traction ($\mu P_{\max}$) at the sliding interface is higher than the bulk strength of the softer material. The softer material is then sheared and transferred to the harder counterface.

As shown in Fig. 7.14, the proposed criterion does not accurately predict scuffing failures of the DHT3 Al over the entire velocity range. This was attributed to the following limitations: (a) as with other hypotheses, the proposed hypothesis is independent of the dynamics and properties of the protective surface films, (b) analytical models used to estimate asperity contact pressures and temperatures are based on simple sinusoidal surface profiles, and (c) accurate values of the coefficient of friction μ and the composite rms surface roughness σ just before scuffing are difficult to obtain.

8.3 Recommendations for Future Research

There are many possible areas of continued research in the scuffing area. As previously indicated, it seems that the major missing piece of information characterizing scuffing under lubricated conditions is the properties of surface films and the dynamics of films formation and destruction. Even though these films play an important role in the scuffing process, the effects of these films on scuffing are poorly understood. All the

existing models for the formation of protective films on contact surfaces are based on static oxidation or other static chemical reaction rates. The effects of macroscopic parameters such as contact pressure, sliding velocity and temperature on the rates of formation of these films has not been studied sufficiently. Therefore, this represents the vast area of future research.

The proposed shear criterion for scuffing should be more fully examined. Since the evaluation in this study is based on aluminum alloys tested and, furthermore, data do not match the criterion for the whole velocity range considered, the criterion needs to be fully explored for other materials and operating conditions. Also, the asperity contact pressures and temperatures are based on sinusoidal profiles which have asperities of the same height. Real surfaces obviously do not have such topography, therefore, more realistic contact models are necessary to consider more localized effects since scuffing initiation is a local rather than a global phenomenon.

REFERENCES

1 Tallian, T. E., "On Competing Failure Modes in Rolling Contact", *ASLE Transactions*, 10 (1967), 418-439.

2 Johnson, K. L., Greenwood, J. A., and Poon, S. Y., "A Simple Theory of Asperity Contact in Elastohydrodynamic Lubrication", *Wear*, 19 (1972), 91-108.

3 Cameron, A., "On a Generalized Theory of Scuffing", Proc. 12th Leeds-Lyon Symposium on Tribology, The Institut National des Sciences Appliquées, Lyon, France, 3-6 September 1985, 3-9.

4 Houpert, L. G. and Hamrock, B. J., "Elastohydrodynamic Lubrication Calculations Used as a Tool to Study Scuffing", Proc. 12th Leeds-Lyon Symposium on Tribology, The Institut National des Sciences Appliquées, Lyon, France, 3-6 September 1985, 146-155.

5 Andersson, S. and Salas-Russo, E., "The Influence of Surface Roughness and Oil Viscosity on the Transition in Mixed Lubricated Sliding Steel Contacts", *Wear*, 174 (1994), 71-79.

6 Evans, H. P. and Snidle, R. W., "A Model for Elastohydrodynamic Film Failure in Contacts Between Rough Surfaces Having Transverse Finish", *Transactions of the ASME, Journal of Tribology*, 118 (1996) 7, 847-857.

7 Spikes, H. A. and Cameron, A., "Scuffing as a Desorption Process - an Explanation of the Borsoff Effect", *ASLE Transactions*, 17 (1974), 92-96.

8 Lee, S. C. and Cheng, H. S., "Scuffing Theory Modeling and Experimental Correlations", *Transactions of the ASME, Journal of Tribology*, 113 (1991) 4, 237-334.

9 Cuotiongco, E. C. and Chung, Y. W., "Prediction of Scuffing Failure Based on Competitive Kinetics of Oxide Formation and Removal: Application to Lubricated Sliding of AISI 52100 Steel on Steel", *STLE, Tribology Transactions*, 37 (1994) 3, 622-628.

10 Barber, J. R., "The Influence of Thermal Expansion in the Friction and Wear Process", *Wear*, 10 (1967), 155-159.

11 Dow, T. A. and Burton, R. A., "The Role of Wear in the Initiation of Thermoelastic Instabilities of Rubbing Contact", *Journal of Lubrication Technology*, (1973), 71-75.

12 Greenwood, J. A. and Williamson, B. P., "Contact of Nominally Flat Surfaces", *Proc. R. Soc. London, Ser A*, 295 (1966), 300-319.

13 Hirst, W. and Hollander, A. E., "Surface Finish and Damage in Sliding", *Proc. R. Soc. London, Ser A*, 337 (1974), 379-394.

14 McCool, J. I. and Popgoshev, D., "Effect of Asperity Interaction on Scuffing", Proc. 12th Leeds-Lyon Symposium on Tribology, The Institut National des Sciences Appliquées, Lyon, France, 3-6 September 1985, 135-145.

15 Enthoven, J. and Spikes, H. A., "Infrared and Visual Study of the Mechanisms of Scuffing", *STLE Tribology Transactions*, 39 (1996) 2, 441-447.

16 Mishina, H. and Sasada, T., "Observation of Micro-Structure in Seized Portion and Mechanism of Seizure", *Transactions of the ASME, Journal of Tribology* 108 (1986) 1, 128-133.

17 Somi Reddy, A., Pramila Bai, B. N., Murthy, K. S. S., and Biswas, S. K., "Mechanism of Seizure of Aluminum-Silicon Alloys Dry Sliding Against Steel", *Wear*, 181-183 (1995), 658-667.

18 Wear Control Handbook, Peterson, and Winer editors, Glossary of Terms and Definitions in the Field of Friction, Wear and Lubrication, p. 1182.

19 Blok, H., "Theoretical Study of Temperature Rise at Surfaces of Actual Contact Under Oiliness Conditions", *Inst. Mech. Eng. General Discussion on Lubrication*, 2 (1937), 222-235.

20 Askwith, T. C., Cameron, A., and Crouch, R. F., "Chain Length of Additives in Relation to Lubricants in Thin Film and Boundary Lubrication", *Proc. Roy. Soc., London*, A 291 (1966), 500-519.

21 Lee, S. C. and Cheng, H., "Experimental Validation of the Critical Temperature-Pressure Theory of Scuffing", *STLE Tribology Transactions*, 38 (1995) 3, 738-742.

22 Matveevsky, R. M, "The Critical Temperature of Oil with Point and Line Contact Machines", *ASME Journal of Basic Engineering*, 87 (1965), 754-760.

23 Grubin, A. N., "Fundamentals of the Hydrodynamic Theory of Lubrication of Heavily Loaded Cylindrical Surfaces", in Investigation of the Contact Machine Components, Ketova, K. F. editor, Translation of Russian Book No. 30, Central Institute for Technology and Mechanical Engineering, Moscow, 1949.

24 Dyson, A., "The Failure of Elastohydrodynamic Lubrication of Circumferentially Ground Disks", *Proc. Inst. Mech. Eng.*, 190 (1976) 1, 52-76.

25 Cheng, H. S., "Micro-Elastohydrodynamic Lubrication", *NASA International Conference on Tribology in the 80's*, 2 (1984), 615-629.

26 Cheng, H. S. and Dyson, A., "Elastohydrodynamic Lubrication of Circumferentially Ground Disks", *ASLE Transactions*, 21 (1978) 1, 25-40.

27 Ludema, K. C., "A Review of Scuffing and Running-in of Lubricated Surfaces, With Asperities and Oxides in Perspective", *Wear*, 100 (1984), 315-331.

28 Park, K. B., and Ludema, K. C., "Evaluation of the Plasticity Index as a Scuffing Criterion", *Wear*, 175 (1994), 123-131.

29 Xue, O. J. and Ludema, K. C., "Plastic Failure Effects in Scuffing of Soft Metals", *Wear of Materials* (1983), 499-506.

30 Kim, K. and Ludema, K. C., "A Correlation Between Low Cycle Fatigue Properties and Scuffing Properties of 4340 Steel", *Transactions of the ASME, Journal of Tribology*, 117 (1995) 10, 617-621.

31 Somi Reddy, A., Pramila Bai, B. N., Murthy, K. S. S., and Biswas, S. K., "Wear and Seizure of Binary Al-Si Alloys", *Wear*, 171 (1994), 115-127.

32 Sheiretov, T., Yoon, H., and Cusano, C., "Scuffing Under Dry Sliding Conditions Part I-Experimental Studies", *STLE Tribology Transactions*, 41 (1998) 4, 435-446.

33 Sheiretov, T., Yoon, H., and Cusano, C., "Scuffing Under Dry Sliding Conditions Part II-Theoretical Studies", *STLE Tribology Transactions*, 41 (1998) 4, 447-458.

34 Subramanian C., "Some Considerations Towards the Design of a Wear Resistant Aluminum Alloy", *Wear*, 155 (1992), 193-205.

35 Czichos, H., "Failure Modes of Sliding Lubricated Concentrated Contacts", *Wear*, 28 (1974), 95-101.

36 Czichos, H., "Failure Criteria in Thin Film Lubrication: Investigation of the Different Stages of Film Failure", *Wear*, 36 (1976), 13-17.

37 Begelinger, A. and De Gee, W. J., "Thin Film Lubrication of Sliding Point Contacts of ANSI 52100 Steel", *Wear*, 28 (1974), 103-114.

38 Begelinger, A. and De Gee, A. W. J., "On the Mechanism of Lubricant Film Failure in Sliding Concentrated Steel Contacts", *Transactions of the ASME, Journal of Lubrication Technology*, 10 (1976), 575-579.

39 Begelinger, A. and De Gee, A. W. J., "Lubrication of Sliding Point Contacts of ANSI 52100 Steel - The Influence of Curvature", *Wear*, 36 (1976), 7-11.

40 Bollani, G., "Failure Criteria in Thin Film Lubrication With EP Additives", *Wear*, 36 (1976), 19-23.

41 Föhl, J. and Uetz, H., "Failure Criteria in Thin Film Lubrication - Influence of Temperature on Seizing, Wear and Reaction Layer Formation", *Wear*, 36 (1976), 25-32.

42 Nivatvongs, K., Cheng, H. S., Ovaert, T. C., and Wilson, W. R. D., "Influence of Surface Topography on Low-Speed Asperity Lubrication Breakdown and Scuffing", *Wear*, 143 (1991), 137-148.

43 Patching, M. J., Kweh, C. C., Evans, H. P., and Snidle, R. W., "Conditions for Scuffing Failure of Ground and Superfinished Steel Disks at High Sliding Speeds Using a Gas Turbine Engine Oil", *Transactions of the ASME, Journal of Tribology*, 117 (1995), 482-489.

44 Dyson, A., "Scuffing - a Review, Part 1", *Tribology International*, 8 (1975) 4, 77-87.

45 Dyson, A., "Scuffing - a Review, Part 2", *Tribology International*, 8 (1975) 6, 117-125.

46 Scott, D., Smith, A. I., Tait, J., and Tremain, G. R., "Materials and Metallurgical Aspects of Piston Ring Scuffing - A Literature Survey", *Wear*, 33 (1975), 293-315.

47 Gregory, J. C., "Thermal and Chemico-Thermal Treatments of Ferrous Materials to Reduce Wear, *Tribology International*, 3 (1970) 2, 73-83.

48 Tiwari, S. N., Pathak, J. P., and Malhotra, S. L., "Seizure Resistance of Leaded Aluminum Bearing Alloys", *Materials Science and Technology*, 1 (1985), 1040-1045.

49 Ni, X. and Cheng, H. S., "Seizure Resistance of Aluminum-Lead-Silicon Connecting Rod Bearings and Nodular Cast Iron Shafts", *STLE Tribology Transactions*, 39 (1996) 1, 121-129.

50 Ni, X. and Cheng, H. S., "Seizure Failure of Copper-Lead with Overlay and Aluminum-Tin Connecting Rod Bearings", *STLE Tribology Transactions*, 39 (1996) 1, 194-200.

51 Barber, G. C., Matthews, J. J. and Jaffry, S., "Wear and Scuff Resistance of Aluminum 390", *Lubrication Engineering*, 47 (1991), 423-430.

52 Bradley, E. F., "Improving Frictional Behavior with Surface Treatments", *Metals Engineering Quaterly*, 7 (1967) 2, 29-32.

53 Braendel, H. G., "Modern Ring Design Affecting Scuff Wear, Oil Control and Quick Seating in Heavy Duty Engines", *Revue-M mécanique*, 17 (1971) 1, 3-12.

54 Brown, W. L., "Development of Piston-Ring Coatings, SAE Technical Paper 690754, (1969).

55 Prasse, H. F., McCormick, H., E., and Anderson, R. D., "Automotive Piston Rings 1967 State of the Art", SAE Technical Paper 670019, (1967).

56 Prasse, H. F., McCormick, H., E., and Anderson, R. D., "Heavy Duty Piston Rings - 1968", SAE Technical Paper 680238, (1968).

57 Sheiretov, T. K., "Scuffing of Aluminum/Steel Contacts Under Dry Sliding Conditions, Ph.D. Thesis, Department of Mechanical and Industrial Engineering, University of Illinois at Urbana-Champaign, 1997.

58 Ludema, K. C., "Friction, Wear, Lubrication: A Textbook in Tribology", CRC Press, 1996

59 Quinn, T. F. J. and Winer, W. O., "An Experimental Study of the "Hot-Spots" Occurring During the Oxidational Wear of Tool Steel on Sapphire", *Transactions of the ASME, Journal of Tribology*, 109 (1987) 4, 315-320.

60 Hays, D. F. and Maki, E. R., "The Crowned Circular Slider Bearing: Analysis and Test", *Transactions of the ASME, Journal of Tribology*, (1972), 280-285.

61 Yoon, H. K., Sheiretov, T. K. and Cusano. C., "Tribological Evaluation of Some Aluminum-Based Materials in Lubricant/Refrigerant Mixtures", *Wear*, 218 (1998), 54-65.

62 Hotten, B. W., "Bidentate Organic Oxygen Compounds as Boundary Lubricants for Aluminum", *Lubrication Engineering*, 30 (1974), 398-403.

63 Laemmle, J. T. and Bohaychick, J., "Novel Substituted Malonic Diesters: Effectiveness of Bidentate Bonding of Additives on Aluminum Workpiece Surfaces", *Lubrication Engineering*, 43 (1986), 717-722.

64 Hironaka, S., and Sakurai, T., "The Effect of Pentaerythriol Partial Ester on the Wear of Aluminum", *Wear*, 50 (1978), 105-114.

65 Montgomery, R. S., "The Lubrication of Aluminum by Phtalic Esters", Wear, 9 (1966), 297-299.

66 Montgomery, R. S., "Chemical Effects on Wear in the Lubrication of Aluminum", *Wear*, 8 (1965), 289-302.

67 Kubo, K., Shimakawa, Y., and Kibukawa, M., "Study on the Load Carrying Mechanism of Sulphur-Phosphorous Type Lubricants", Proc. JSLE. Int. Tribology Conf. 8-10 July, 1985, Tokyo, Japan, Elsevier, 661-666.

68 Rigney, D. A., Chen, L. H., and Naylor, G. S., "Wear Processes in Sliding Systems", *Wear*, 100 (1984), 195-219.

69 Razavizadeh, K. and Eyre, T. S., "Oxidative Wear of Aluminum Alloys", *Wear*, 79 (1982), 325-333.

70 Jaeger, J. C., "Moving Sources of Heat and the Temperature of Sliding Contacts", *J. Proc. Roy. Soc. N.S.W.*, 76 (1942), 203-224.

71 Bell, J. C., Dyson, A., and Hadley, J. W., "The Effects of Rolling and Sliding Speeds on the Scuffing of Lubricated Steel Discs", *ASLE Transactions*, 18 (1975) 1, 62-73.

72 Bailey, M. W., and Cameron, A., "The Effects of Temperature and Metal Pairs on Scuffing", *ASLE Transactions*, 16 (1973) 2, 121-131.

73 Carper, H. J., and Ku, P. M., "Thermal and Scuffing Behavior of Disks in Sliding-Rolling Contact", *ASLE Transactions*, 18 (1975) 1, 39-47.

74 He, X., "Experimental and Analytical Investigation of the Seizure Process in Al-Si Alloy/Steel Tribocontacts", Ph.D. Thesis, Department of Mechanical Engineering, Northwestern University, 1998.

75 Johnson, R. R., Dow, T. A., and Zhang, Y. Y., "Thermoelastic Instability in Elliptic Contact Between Two Sliding Surfaces", *Transactions of the ASME, Journal of Tribology*, 110 (1988) 1, 80-86.

76 Lee, Y. and Ludema, K. C., "The Effects of Surface Roughening and Protective Film Formation on Scuff Initiation in Boundary Lubrication", *Transactions of the ASME, Journal of Tribology*, 113 (1991) 4, 295-302.

77 Stachowiak, G. W. and Batchelor, A. W., "Engineering Tribology", Tribology Series, 24, Elsevier, 1993.

78 Frewing, J. J., "The Heat Adsorption of Long Chain Compound and Their Effect on Boundary Lubrication", *Proc. Roy. Soc., London*, A 282 (1944), 270.

79 Shen, M. C., Cheng, H. S. and Stair, P. C., "Scuffing Failure in Heavily Loaded Slow Speed Conformal Sliding Contacts", *Transactions of the ASME, Journal of Tribology*, 113 (1991), 182-191.

80 Buckley, D. H., "Surface Effects in Adhesion, Friction, Wear, and Lubrication", Tribology Series, 5, Elsevier, 1981.

81 Ren, N. and Lee, S. C., "Contact Simulation of Three-Dimensional Rough Surfaces Using Moving Grid Method", *Transactions of the ASME, Journal of Tribology*, 115 (1993), 597-601.

82 Holm, R., "Electric Contacts. Theory and Applications", Springer-Verlag, New York, 1967.

83 Qui, L. and Cheng, H. S., "Temperature Rise Simulation of Three-Dimensional Rough Surfaces in Mixed Lubricated Contact", *Transactions of the ASME, Journal of Tribology*, 120 (1998), 310-318.

84 Carslaw, H. S. and Jaeger, J. C., "Conduction of Heat in Solids", Oxford Press, 2nd Edition, 1959.